Assessment of Anthropogenic Air Pollution Exposure in Urban Trees

Thesis for the Degree of Doctor of Philosophy (PhD)

by **Semonti Mukherjee**

Supervisor:

Dr. Edina Kundrát-Simon

UNIVERSITY OF DEBRECEN

Doctoral Council of Natural Sciences and Engineering

Juhász-Nagy Pál Doctoral School

Debrecen, 2026

Hereby I declare that I prepared this thesis within the Doctoral Council of Natural Sciences and Engineering, ***Juhász-Nagy Pál Doctoral School****, University of Debrecen in order to obtain a PhD Degree in Natural Sciences at Debrecen University. The results published in the thesis are not reported in any other PhD*

Debrecen,2026

……

Semonti Mukherjee

PhD candidate

Hereby, I confirm that ***Semonti Mukherjee*** *conducted his studies with my supervision within the Quantitative and Terrestrial Ecology Doctoral Program of* ***Juhász-Nagy Pál Doctoral School*** *between 2022 and 2026. The candidate's independent studies and research significantly contributed to the results published in the thesis.*

I also declare that the results published in the thesis are not reported in any other theses.

I support the acceptance of the thesis.

Debrecen, 2026.

……

Dr. Edina Kundrát-Simon

Thesis supervisor

Dissertation submitted in partial fulfillment of the requirements for the doctoral (PhD) degree in Environmental Sciences

Assessment of Anthropogenic Air Pollution Exposure in Urban Trees

Written by

Semonti Mukherjee

Prepared in the framework of Juhász-Nagy Pál Doctoral School of the University of Debrecen
(Quantitative and Terrestrial Ecology program)

Dissertation supervisor:

Dr. Edina Kundrát-Simon

The official opponents of the dissertation:

…..... …..

…..... …..

The evaluation board:

Chairperson: …..
…..
.....

members: …..

…..

…..... …..

…..... …..

The date of the dissertation defense:..... 2026

List of Abbreviations

AAC - Ascorbic Acid Concentration

ANOVA - Analysis of Variance

APTI - Air Pollution Tolerance Index

CEE - Central and Eastern European

Chl-*a* - Chlorophyll a

Chl-*b* - Chlorophyll b

ChlF - Chlorophyll Fluorescence

CO - Carbon Monoxide

COVID-19 - Coronavirus Disease 2019

Eq. - Equation

EU - European Union

G. biloba - *Ginkgo biloba*

GNDVI- Green Normalized Difference Vegetation Index

H. helix - *Hedera helix*

HSD - Honestly Significant Difference

MANOVA - Multivariate Analysis of Variance

MDC - Median Deviation from Control

NDVI - Normalized Difference Vegetation Index

NO - Nitric Oxide

NO_2 - Nitrogen Dioxide

NO_x - Nitrogen Oxides

O_3 - Ozone

PCA - Principal Component Analysis

PRI- Photochemical Reflectance Index

Pheo-*a* - Pheophytin a

Pheo-*b* - Pheophytin b

PIDR - Pigment Integrity-to-Dust Ratio

PM - Particulate Matter

$PM_{2.5}$ - Particulate Matter with aerodynamic diameter ≤ 2.5 µm

PM_{10} - Particulate Matter with aerodynamic diameter ≤ 10 µm

RDA - Redundancy Analysis

ROS - Reactive Oxygen Species

RWC - Relative Water Content

SD - Standard Deviation

SE - Standard Error

SO_2 - Sulfur Dioxide

UHI - Urban Heat Island

VIF - Variance Inflation Factor

VOC - Volatile Organic Compounds

WMO - World Meteorological Organization

Table Contents

1. Introduction

Over the past century, the world has been urbanised at an unparalleled rate. At present, more than half the Earth's population lives in cities, and this share is anticipated to reach 68% by 2050. Our (EEA, 2019). Given the current spatial patterns of urbanisation, this leads to enhanced anthropogenic emissions of gases, particles and vapours derived from various domestic heating, industrial processes and construction sites, contributing to complex air pollution mixtures that exert chronic biochemical stress on urban vegetation(Evangelopoulos et al., 2020; Gao & Bukovsky, 2023; Tsai et al., 2015; Zhang et al., 2022). As a result of this spatial concentration of emission sources and variable urban morphology, pollutant levels can vary significantly within just a few city blocks. Therefore, tree species on the same street may experience substantially different air quality. Plants function as passive biosensors, integrating airborne pollutants through gas exchange, transpiration, direct surface deposition of particulate matter, and stomatal uptake of gaseous contaminants, thereby accumulating a biochemical record of their exposure to pollution in leaf tissue (Mulgrew & Williams, 2000; Volkov & Ranatunga, 2006). Trees and other plants absorb pollutants and also store and record the effects of air pollution exposure in their epigenetic memory (He & Li, 2018). Polluting gases such as SO_2, NO_2, and O_3 enter tree leaves through stomatal openings and the cuticle, where they can disrupt the integrity of chloroplast membranes, leading to a loss of enzymatic balance and increased production of reactive oxygen species (Khomenko et al., 2021).

Dust settles on leaf surfaces, lowering reflectance, covering stomata, reducing stomatal area, and limiting the movement of gaseous pollutants into and out of stomata, hindering photosynthesis efficiency and gas exchange. Pollutants

can also be physically deposited on leaf tissue and even move into leaf tissue (defined as the apoplast of intercellular and sub-stomatal chambers and mesophyll tissues), including particulates that contain trace amounts of metals, organic pollutants, or other contaminants. Each of these acts transforms each leaf into an uninterrupted recorder of the environmental conditions surrounding the plant. Among plant characteristics, chlorophyll a and b (photosynthetic pigments) can be considered both the most sensitive to and the easiest to measure indicators of stress from air pollution. Chlorophyll *a* and *b* absorb light energy for the purpose of carbon fixation, while carotenoids help to disperse excess energy and reactive oxygen species (Qor-El-Aine et al., 2022).

While anthocyanins provide an antioxidant buffer, the appearance of pheophytins indicates chlorophyll's irreversible degradation. Each air pollutant has a specific biochemical signature. SO_2 and NOx inhibit chlorophyll synthesis, while ozone accelerates bleaching, leading to an increase in carotenoid concentration as a compensatory response. Particulate dust contributes to a decrease in overall pigment due to the obstruction of stomatal gas exchange (Han et al., 2024; Li et al., 2018; Mansfield, 1998). The kinetics of pigment transformations exhibit high reproducibility over the time frame of these changes; therefore, these changes can serve as mechanistic indicators that convey the nature of the chemical process and its associated biological costs to plants (Shah et al., 2019). The surface dust also contains evidence of emissions from different sources, including transportation, residential heating, and industrial activity. Thus, the differential response of individual pigments to specific pollutants makes their combined analysis a powerful diagnostic tool for assessing pollution type and intensity in urban environments (Bierza & Bierza, 2024).

Leaves are among the most stress-sensitive organs in plants; when exposed to environmental pollutants, they demonstrate the value of biomonitoring, as biological responses work with chemical measurements to determine pollution levels. They also slowly reflect fluctuations in atmospheric pollution levels, and changes occur long before they can be observed by humans. Over time, cumulative physiological responses create a living record of urban exposure and reveal how urban environmental conditions leave plants with physical and physiological symptoms of exposure (Ogunkunle et al., 2015). At the moment, plant sensor technology is mostly composed of independent observation techniques rather than a combined, comprehensive approach. For example, the Air Pollution Tolerance Index (APTI) (Singh et al., 1991b) integrates only four leaf parameters: ascorbic acid content, total chlorophyll, relative water content, and leaf extract pH , which is insufficient to adequately distinguish sensitive from tolerant plant species (Molnár et al., 2020a, 2020b).

These indices will identify symptoms of poor air quality, but they do not explain why these symptoms are present (Rai, 2016). These indices are flawed because they rely solely on individual measurements, making it impossible to determine how much pollution a plant experiences or whether it has physiologically adjusted to the stress of pollution over time (Banerjee et al., 2021). Real-time data on air quality do not provide much insight into whether a plant is impacted by air quality with regard to biologically based indicators, such as pigment loss or changes in pH, as these represent separate and distinct physiological processes. Stressors that are important for stomatal activity, such as dust accumulation, are commonly overlooked despite their extreme impact on stomatal activity, pigment balance, and leaf temperature in urban ecosystems (Rai, 2016).

Indices suffer from a lack of portability because species-specific baselines are used in APTI and the other systems; thus, their interpretation varies across locations and over time. For example, trees that are deemed “tolerant” in one geographical area may be interpreted as “sensitive” in another area. This is not due to changes in pollutant levels, but to changes in the physiology of those trees. Recent changes in pigmentation and hydration are reported by Tripathi & Nema (2023) and Varela et al. (2023). When a common baseline is provided, it may yield inconsistent output data, making it difficult to obtain an accurate set of regional biomonitoring data. In addition to the lack of a common method, the use of species-specific indices also breaks methodological continuity across studies, making it difficult to compare biomonitoring results across regions or time periods. The indices do not relate the effects of air pollution on leaf structure, nor do they show the degree of pollutant stress as a constant measure across the landscape scale.

Dust is considered one of many urban stressors and among the most significant; however, it is not addressed within APTI, despite its immense impact on stomatal function, temperature, and pigmentation stability. The realisation of these effects is supported by the volume of recent investigations across Europe, which continuously demonstrate the need for a standardised methodological framework that explicitly links chemical exposure, particulate load, and biological response (Ștefănuț et al., 2021).

The current limitations of indices highlight the need for an index that distinguishes between general plant stress and specifies the plant physiological processes/phenomena that drive the stress response to external stimuli. The following index recognises that various plant stress signals, such as pollutant exposure, dust accumulation, and pigment degradation, are interrelated and do not act independently. Pigment integrity-to-Dust Ratio (PIDR), developed as

part of this doctoral research is an example of how we can measure internal plant processes (pigment degradation) with external stress (a build-up of dust particles) in order to provide a new way to utilize biological indicators for biomonitoring of plant stress responses and also to support monitoring of changes in stimulation/biochemical activity related to changes in environmental stressors. Linking atmospheric science with plant physiology into a single spatially portable bioindicator framework that is proposed here as complementary to, not a replacement for, APTI.

2. Aims and hypotheses

This thesis reported urban air quality and plant-based biomonitoring from complementary perspectives, beginning with atmospheric pollution dynamics and progressing to plant physiological responses and the development of improved bioindicator approaches.

The effect of reduced mobility on air quality during the COVID-19 period was analysed in Debrecen, Hungary, from 2018 to 2022. Our study aims to investigate the effect of COVID-19 on the air quality of 2018–2022 in Debrecen city (Hungary) during the three periods, i.e., the pre-pandemic, pandemic, and post-pandemic periods, based on the concentration of PM_{10}. We studied the effect of lockdown on PM_{10} concentrations, and analysed the effects of meteorological conditions (wind speed and wind direction) on air pollutant concentrations.

The hypotheses were the following:

H1.1. We hypothesised that PM_{10} concentrations were significantly lower during the pandemic and post-pandemic periods than in the pre-pandemic period.

H1.2. Our second hypothesis was that lockdowns had a positive effect on PM_{10} concentrations; thus, PM_{10} concentrations were significantly lower during lockdown months than before and after the lockdown.

H1.3. We also hypothesised that weather conditions, such as wind speed and direction, significantly affect PM_{10} concentrations.

The seasonal dynamics of photosynthetic pigment concentrations were investigated in *G. biloba* leaves during the vegetation period from July to

October in an urban environment in Debrecen City, Hungary, to evaluate their suitability for urban air pollution biomonitoring. The first aim of this study was to determine how the physiological and bioindicator responses of these trees changed after planting, thereby establishing an important baseline for future urban biomonitoring efforts.

The hypotheses were:

H2.1. Our hypothesis suggests that these pigments exhibit pronounced seasonal variation, with a peak in chlorophyll concentration expected in mid-summer (July and August), and a subsequent decline in autumn (September and October).

H2.2. Concurrently, we expect an increase in pheophytin levels, which serve as indicators of chlorophyll degradation.

H2.3. We hypothesised that initial exposure to air pollutants would negatively impact chlorophyll and carotenoid production as a short-term stress response, with prolonged exposure leading to additional pigment loss and reduced tolerance to air pollution.

This study examines spatial and temporal changes in photosynthetic pigments in *G. biloba* leaves and introduces the Pigment Integrity-to-Dust Ratio (PIDR) as a new bioindicator of urban air pollution stress in Budapest, Hungary. PIDR incorporates (i) the chlorophyll to pheophytin ratio and (ii) dust deposition on leaves. We present PIDR as a conceptual framework and pilot case study for Budapest, applying it to *G. biloba* leaves from three sites in Budapest in 2023 and 2024.

The hypotheses were:

H3.1. We hypothesised that PIDR showed higher spatial contrast in stress than APTI.

H3.2. We hypothesised that PIDR indicated patterns of changes in physiological condition.

H3.3. We hypothesised that PIDR reflected pollutant-specific patterns.

We investigated the relationship between urban air pollution and vegetation by examining leaf dust deposition and physiological traits in the common *Hedera helix* L. Research on dust and pollution tolerance in *Hedera helix* sp. exists, but little addresses seasonal physiological responses in urban Central Europe, especially in Debrecen. Integrated assessments of physiological parameters and dust in green wall contexts remain largely unexplored.

The hypotheses were the following:

H4.1. We hypothesised that dust deposition on leaf surfaces would be higher in areas with higher traffic intensity than at a less-polluted control site.

H4.2. In addition, pigment content and APTI values were expected to reflect spatial variation in air pollution levels.

H4.3. Measurable leaf parameters were assumed to correlate with distance from the city centre.

H4.4. These relationships were expected to reflect spatial differences in the intensity of urban air pollution.

3. Literature Review

3.1 Main air pollutants

Factors contributing to air quality in Central and Eastern European cities include air circulation patterns, climate zones, transportation systems, and energy systems. From 2015 to 2025, cities throughout central and Eastern Europe, not limited to Budapest, Warsaw, Krakow, Bucharest, Prague, Cluj-Napoca, and Bratislava, generally had high levels of several air pollutants. These include $PM_{2.5}$ and PM_{10}, NO_2, SO_2, CO, and O_3 (Almeida et al., 2020; Bodor et al., 2020; Juda-Rezler et al., 2020). To understand their complex movement, it is necessary to examine their sources, seasonality, and atmospheric circulation. Winter home heating is a major reason why $PM_{2.5}$ levels are higher and chemically distinct during the cold season in many parts of Central and Eastern Europe, including Poland, Hungary, Romania, Slovakia, and parts of the Czech Republic (Almeida et al., 2020; Ferenczi, 2013; Juda-Rezler et al., 2020). These winter heating activities increase $PM_{2.5}$ levels because burning fuels releases organic carbon and elemental carbon particles. Some of these particles were formed in the combustion process itself, while others were created by physical and chemical processes later in the smoke plume and in the atmosphere. In winter, residential heating is an important source; in urban areas, traffic is a year-round source. NO_2 and CO emissions from vehicles are greatest during the morning and evening rush hour, when traffic is the heaviest. Traffic volume is not the only factor influencing levels of pollution. Similar to urban morphology's influence on urban ventilation and dilutions, urban morphology can also affect

concentrations to be higher at the location of emission source rather than be diluted, such as in the historical centers of Budapest and Bucharest where the dense urban fabric can lead to higher vehicle emission concentrations (Salma et al., 2020; Tsai et al., 2015). Not all pollutants have the same temporal behavior; for example, the pattern of a winter peak is still observed for SO_2 in Central and Eastern Europe, where coal is used for heating or industries (Almeida et al., 2020; Choi et al., 2015). For pollutants such as PM, NO_2, CO, and SO_2, it is usually easier to understand their sources, as they are closely linked to specific emission sources and seasonal anthropogenic activities. But in the case of O_3, it is not discharged into the atmosphere; it is formed through chemical reactions involving NO_X, VOCs and atmospheric temperature (Huszar et al., 2015, 2020). O_3 levels are typically higher in spring and summer because of increased sunlight and heat increase their formation.

3.2 Seasonal variation of air pollutants

As pollution levels in cities change with the seasons, measuring and understanding urban air pollution becomes difficult. Long-term studies in Central and Eastern Europe (CEE) indicate that winter levels of pollutants such as $PM_{2.5}$, PM_{10}, NO_2, SO_2, and CO are mostly driven by increases in heating emissions, temperature inversions, shallow boundary layers and inadequate atmospheric mixing. Weekly, daily and seasonal patterns also influence different temporal cycles, which led to this chemical mixture (Almeida et al., 2020; Bodor et al., 2020; Ziernicka-Wojtaszek et al., 2024). The atmosphere has a significant impact on whether these emissions are short-lived or persist for a long time. When stable, high-pressure conditions prevail, pollutants generally accumulate closer to the surface, often exceeding WHO recommendations. During summer, despite improved atmospheric dispersion

caused by strong vertical mixing and increased boundary layers, especially during heatwaves and stagnant weather, ozone levels rise due to high solar radiation. Pollution does not only vary by season but also changes throughout the week. PM concentrations can be higher on weekends than on weekdays if wind speeds are low. This is probably due to changes in human activities, such as variations in traffic flow, leisure activities, weekend construction, and road maintenance context, which can cause dust resuspension (Bodor et al., 2020). In general, people and human activities (such as traffic, heating, and industry) determine how much pollution is released. But weather conditions determine how serious a pollution event is and whether it becomes a severe episode. These conditions include atmospheric mixing, dilution, and chemical reactions, all of which play a substantial role. In other words, meteorology mostly controls the intensity and timing of pollution events rather than human activities. The most significant meteorological parameter, e.g., temperature, influences both emission rates and atmospheric reactions, whereas relative humidity is an important factor in secondary aerosol formation, particularly sulfate and nitrate in winter $PM_{2.5}$ (Ziernicka-Wojtaszek et al., 2024). Further, wind speed and direction influence the dispersion and stagnation of pollutants, which are closely associated with pollution intensity in CEE cities (Bodor et al., 2020; Zaręba & Danek, 2022). The dynamics of the atmospheric boundary layer are among the most critical determinants of urban pollutant accumulation, as a shallow boundary layer restricts vertical dispersion, leading to surface-level concentration peaks. This controls the volume of near-surface accumulation of pollutants (Foskinis et al., 2024; Huszar et al., 2020). Also, precipitation can quickly reduce PM concentrations by removing particles from the atmosphere.

Sometimes pollution is not locally generated. In spring and summer, dust storms from the Sahara can temporarily degrade air quality in cities by

carrying large amounts of coarse dust particles, leading to elevated PM_{10} levels often above normal levels (Loskot et al., 2024). When the Sahara dust arrives, the types of particles in the air change from fine urban particles to larger mineral-rich particles containing elements like calcium, silicon, and iron (Achilleos et al., 2016; Evgenieva et al., 2024) while decreasing the $PM_{2.5}/PM_{10}$ ratio. Since this dust originates outside the region and does not come from local sources, it is difficult to determine whether changes in pollution levels are caused by local emissions or by natural long-range transport. Transport of matter over long distances, such as in Saharan dust episodes, may complicate measurements of air quality, and impact atmospheric stability and temperature (Foskinis et al., 2024). In places with persistent air pollution problems, such as parts of Poland, Romania and Hungary (and most strongly in the winter months), there are settlement, construction and financial reasons. Houses, flats and other buildings are heated with coal and solid fuels (lignite, wood and other solid biomass materials or derived from the agricultural sector) . Another factor is the old vehicle flow, and because of the city's morphology, the pollutants are not dispersed as easily.

While weather conditions have a strong effect on the dispersion of air pollution, social and structural conditions may also play a role in the level of air pollution in Central and Eastern Europe. Many homes in Poland, Romania, and Hungary burn coal and other solid fuels, contributing to air pollution. Outdated vehicles also generate CEE air pollution. The morphology and ventilation of the city can influence the way such pollutants are transported and dispersed. This is especially true for the industrial regions of south Poland, north Romania, east Slovakia, and north Hungary, with localized pollution hotspots. Especially in border regions, transboundary transport of traffic – derived pollutants, principally NO_2, CO, and PM_{10} from a neighbouring country can be an issue, as shown during the COVID-19

lockdowns (Georgieva et al., 2021; Z. Shi et al., 2021). Though Traffic and NO_2 levels decreased in general, but pollution was not completely eliminated due to residual heating, which continues to produce pollution.

With reduced traffic during lockdowns, researchers observed a decrease in NO_2 concentrations across cities in the CEE region, with the largest reduction in Budapest. This supports the idea that vehicular sources are the primary contributors to NO_2 levels. Salma et al. (2020) claimed that although human activities do not elicit a unified response to air pollutants, some combinations of pollutants were associated with greater physiological stress in plants than others. This research thesis will investigate the role of pigment-based biomonitoring in understanding these combinations and their impact on plant physiology.

3.3 Bioindicators in Urban Air Quality Monitoring

Fixed real-time atmospheric monitoring instruments can measure pollutant levels at discrete points, but they cannot reflect total exposure or cumulative effects on a living organism over weeks, months, or even years. Instead, biomonitoring uses plants as sensors to identify pollutant exposure based on damage caused by cumulative exposure, rather than ambient pollution levels (Chaudhuri & Roy, 2024; Contardo et al., 2020; Mota et al., 2025). Plant selection for biomonitoring varies depending on the specific pollutants and the nature of their biological effects. Lichens and mosses are suitable for accumulating heavy metals (e.g., Hg, Pb, Cd) and nitrogen compounds because they directly extract contaminants from the air or from deposition. These organisms lack a cuticle and a root system, leading to direct interaction with air pollutants. (Abas et al., 2022; Bahinskyi et al., 2025; Niepsch et al.,

2023). For airborne particulate matter (PM_{10} and $PM_{2.5}$), species such as broadleaved trees (e.g., *Platanus, Tilia, Quercus*) with rough or hairy leaves and conifers (e.g., pines and spruce) have been investigated for particle accumulation. (Corada et al., 2021; Mukhopadhyay et al., 2024). In the case of gas-phase pollutants like ozone, sensitive plants, such as the tobacco variety *Nicotiana tabacum cv. Bel-W3* or poplars are used to diagnose oxidative stress via leaf symptomology, including chlorotic stipples, necrotic flecks, interveinal bleached streaks and premature senescence. (Heggestad, 1991). Broadleaved trees are recommended biomonitors for particulate matter accumulation because their large leaf surfaces effectively intercept particles from the atmosphere, can absorb gaseous pollutants through their stomata and exhibit distinct physiological, biochemical and structural responses to airborne pollution. Some plant responses include chlorophyll and carotenoid pigment degradation, altered activity of antioxidant enzymes (superoxide dismutase and glutathione reductase), and reduced water content, which allows linking pollution levels to quantifiable internal damage. (Cavazzin et al., 2024; Mukhopadhyay et al., 2024; Perri et al., 2024). Beyond vascular plant communities, microbes, including airborne bacterial and fungal species, have also been used as biomonitors of environmental chemical pollution, reflecting broader ecosystem health. (Pozdniakova et al., 2025).

Methods of biomonitoring have been distinguished as either passive or active. Passive biomonitoring uses organisms naturally present in a habitat over time to document pollution accumulated from local, long-term exposure (Chaudhuri & Roy, 2024; Gallego-Cartagena et al., 2021; Piazzetta et al., 2019). Examples may include molluscs present along stream banks, lichens growing on trees, or even grass blades exposed to street emissions. Active biomonitoring methods involve using transplanted living mosses, transplanted

potted plants, or other indicator species within sites being evaluated under similar controlled conditions (Grifoni et al., 2025; Świsłowski et al., 2022, 2024). Through this process, direct comparisons between sites are possible, even though these organisms were not native to the environments examined. Passive methods provide valid estimates of genuine environmental concentrations at an individual location. Active methods provide the best spatial consistency among compared sites (Gerdol et al., 2014; Niepsch et al., 2023).

Biomonitoring techniques evolved alongside advances in pollution analysis and plant ecophysiology. Thus, whereas early work relied solely on identifying indicator species in polluted zones versus reference sites and on estimating pollutant accumulation, more recent research measures sensitive physiological (pigment damage), biochemical stress (antioxidant activity, photosynthetic efficiency, activity of antioxidant enzyme) and DNA damage responses that unveil more deeply the kind of stress induced and the pollution level at which such damage is induced (Campos et al., 2024; Gómez-Ensastegui et al., 2025; Mota et al., 2025; Mukhopadhyay et al., 2024). The techniques have more recently been expanded through remote sensing, other georeferencing technologies, and citizen science (Abecasis et al., 2022; Gamelas et al., 2024).

Nevertheless, numerous methodological shortcomings prevent easy comparison between studies, including differences in species, exposure durations, sampling methods, and dependent variables (Chaudhuri & Roy, 2024; Gerdol et al., 2014; Świsłowski et al., 2022). Several environmental factors mask the biological effects of different pollutants, including varying micrometeorological patterns across the canopy and in the litter layer, specific past land-use of forest sites, soil variables such as nutrient levels or pH, and

varying past pollution exposure at each sampling site. The interactions among these different types of variables make it difficult to determine a true relationship between specific air pollutants and an organism's response (Campos et al., 2024; Gerdol et al., 2014; Niepsch et al., 2023; Sfetsas et al., 2025). Therefore, biomonitoring schemes will ideally incorporate atmospheric deposition, particle fallout and plant response within a clearly linked chain of evidence to address this difficulty.

3.4 Dust and pigments as bioindicators

Leaves are ideal for this, as they sit between the air and plant physiology, trapping particles, absorbing gases over time, and reflecting cumulative exposure rather than a single moment (Abriha-Molnár et al., 2024; J. Zhu & Xu, 2021; Molnár et al., 2020b). Among leaf-based indicators, the determination of dust deposition on leaf surfaces and leaf pigments is particularly important. The former shows external exposure, while the latter responds to physiological and internal stress (Bierza & Bierza, 2024; Molnár et al., 2020b; Talebzadeh & Valeo, 2022). Analysing dust deposition on leaf surfaces is a low-cost, practical way to estimate particulate exposure, especially for trees near a traffic site (Abriha-Molnár et al., 2024; Castanheiro et al., 2020; Molnár et al., 2020b). Trees with rough or hairy foliage trap more large particles easily. Though retention of particulate matter depends on leaf traits and weather, as traffic can resuspend dust while precipitation can wash accumulated dust away (Chiam et al., 2019; Corada et al., 2021; Lyu et al., 2023; J. Zhu & Xu, 2021). Dust can cause leaf shading, block stomata, and affect photosynthesis and gaseous exchange (Bierza & Bierza, 2024; J. Zhu & Xu, 2021). However, dust alone cannot show internal strain, so it is important to capture the physiological impact of trees through pigment changes.

Pigments help us understand what is happening inside the leaf. Pollution often lowers the concentrations of chlorophyll (*a*, *b*, and total) by damaging chloroplast function, while carotenoids and anthocyanins act as protective pigments, defending the leaves only up to mild stress, but they decrease under severe stress (Bessonova et al., 2020; Bierza & Bierza, 2024; Talebzadeh & Valeo, 2022). The breakdown of chlorophyll, followed by the increase in phaeophytin level, signifies that the leaf is strongly damaged. Because pigment levels change non-linearly, pigments may temporarily increase slightly under moderate stress, which is why they should be interpreted in relation to dust or pollutant exposure (Abriha-Molnár et al., 2024; Borowiak et al., 2018; Molnár et al., 2020b). Generally, pigment loss is mainly caused by oxidative stress in chloroplasts triggered by pollution. Dust can partially block stomata, limiting CO_2 entry into the leaf. Under strong light, this imbalance increases the production of harmful reactive oxygen species (ROS). Further gases, such as O_3 and nitrogen oxides (NO_x), enter through stomata, increasing ROS and RNS levels and leading to stress (Bierza & Bierza, 2024; J. Zhu et al., 2021; J. Zhu & Xu, 2021). The chloroplast structures (thylakoid membranes) and pigment-protein systems in the leaf are damaged by excessive levels of ROS. This accelerates chlorophyll breakdown and increases pheophytin formation, leading to chlorosis and necrosis (Bessonova et al., 2020; Bierza & Bierza, 2024; Borowiak et al., 2018). Consequently, dust from leaves and pigments together serve as good, inexpensive measures of urban air pollution, since both the presence of pollution (exposure) and how plants respond to it (biological response) can be captured by these indicators. (Bessonova et al., 2020; Bierza & Bierza, 2024; Borowiak et al., 2018). Some uncertainties remain because species respond differently, and other environmental stresses (drought, heat, etc.) can confound the effects of pollution. Using fewer samples hinders the ability to describe how pollution

changes over time. Differing research methods reduce comparability across studies. These challenges make it difficult to link specific pollutant combinations to changes in pigment compositions. To simplify interpretation, researchers use composition indices that combine measures into a single indicator (Bierza & Bierza, 2024; Corada et al., 2021; Molnár et al., 2020b). One of the plant-based biomonitoring indices is APTI, which combines four-leaf properties, such as ascorbic acid, chlorophyll, leaf pH, and relative water content (Singh et al., 1991b). Based on these parameters, we can assess a plant species' tolerance or sensitivity to air pollution (Devkota et al., 2022; Molnár et al., 2020b; Sahu et al., 2020). It gained popularity due to its cost-effectiveness and its categorisation of species as tolerant or sensitive for greenbelt planning or biomonitoring (Bhadauria et al., 2022; Devkota et al., 2022; Karmakar et al., 2021; Yadav & Pandey, 2020). However, APTI is strongly affected by season, leaf age, methods, and site conditions, and its parameters respond to non-pollution stress (heat, drought, and soil factors). The results of APTI are often difficult to compare, especially in cities where pollution varies widely from place to place (Bhadauria et al., 2022; Bharti et al., 2018; Tripathi & Nema, 2023). Hence, it is suggested that improved indices be developed that more directly link pollution exposure to physiological damage, incorporating pigment integrity alongside dust load. The earlier statement appears valid since both chlorophylls and carotenoids contribute significantly to oxidative and photosynthetic stress. Study after study has found a reduction in pigments due to high industrialised environments (Bierza & Bierza, 2024; Lhotská et al., 2022; Molnár et al., 2020b; Öncü et al., 2025).

Dust acts as an environmental stressor, affecting plant physiology, stomatal pores, light transmission, and metal absorption, while simultaneously serving as an indicator of ambient pollution, since the weight per unit area of dust

collected on leaves roughly corresponds to proximity to emitting sources. The developed method incorporates leaf pigment concentrations and dust loads on leaves to simultaneously represent pollutant effects and plant responses in a single index (Fusaro et al., 2021; Roy et al., 2024). Therefore, no indices that measure particulate load (e.g., dust load or pollution PM) alongside pigment degradation exist in a mechanism-based manner, allowing the measurement of external and internal factors in a comparable way. We propose the Pigment Integrity-to-Dust Ratio (PIDR) index to fulfil these conditions.

In that way, PIDR aims to be more process-specific than APTI, linking the biochemical mechanism of pollutant-induced chlorophyll degradation directly to its external driver (dust load), and to be more sensitive to fine-scale urban pollution patterns than APTI alone. Both component measurements - leaf dust load and pigment concentrations - are, moreover, technically straightforward and low- cost, making PIDR practically accessible for routine urban biomonitoring.

3.5 Rationale for the Selection of *Ginkgo biloba* and *Hedera helix* as Bioindicator Species

For the successful application of species in urban biomonitoring programs, species selection must consider three types of criteria (biological, ecological, and practical), ensuring each selected species functions as a living detector of atmospheric pollution (Chaudhuri & Roy, 2024; Karmakar et al., 2021). Here, two species, *Ginkgo biloba L*. And *Hedera helix L*. was chosen as the focal bioindicator species for two reasons.

3.5.1 Selection rationale for *Ginkgo biloba*

G. biloba L. was selected for six interconnected reasons: (i) It is widely planted in cities across central and eastern Europe (e.g., Debrecen and Budapest) as an ornamental deciduous tree. Thus, multi-site comparisons are possible without additional controlled plantations (Molnar et al., 2020a; Simon et al., 2021). (ii) As a phylogenetically ancient species (a 'living fossil' unchanged for over 200 million years), its physiological reactions to environmental pressures have been extensively researched and are reproducible (Tredici, 2000; Huh et al., 2019). (iii) Its broad, fan-shaped leaf morphology facilitates reproducible leaf area measurement and standardised gravimetric analysis of dust accumulation (Molnar et al., 2020b; Abriha-Molnar et al., 2024). (iv) It has well-documented sensitivities in its chlorophyll and carotenoid systems to airborne pollutants from traffic, such as NOx and PM_{10}. This sensitivity has strong seasonal patterns, which separate pollution effects from background seasonal phenological changes (Jurčević Šangut & Šamec, 2024; Kinoshita et al., 2021; Shi et al., 2012). (v) The use of *G. Biloba* as a bioindicator in several cities in Europe and Asia makes possible a consistent, city-comparative verification (Molnar et al., 2020a; Bao et al., 2015). (vi) As a deciduous species, its well-defined sequence of leaf production, expansion, mature growth, ageing, and abscission within the growing season provides a natural temporal axis for physiological processes to be studied during leaf growth and maturity (Lichtenthaler, 1996). In addition, trees of equal age, planted on the Debrecen transect in July 2022, were included to minimise variability caused by tree age (Tredici, 2000).

3.5.2 Selection rationale for *Hedera helix*

H. helix L. (common ivy) is a perennial evergreen climber that enables continuous 12-month air-quality monitoring, including all winter pollution episodes resulting from the use of biomass heaters, which cannot be detected by deciduous species. (Lee et al., 2021; Corada et al., 2021; Almeida et al., 2020).

For the purposes of the Debrecen study, *H. helix* offered a distinct advantage since it was planted on standardised steel mesh structures situated on all city buses and tram stops as part of a municipal initiative called "greening cities. 36 of these sampling sites were placed in standard steel mesh structures on urban bus and tram stops. These represent a passive air-quality monitoring system with broad spatial coverage across a large portion of the urban pollution gradient. *H. helix* is physiologically sensitive to various air pollutants, as has been well-documented by several urban studies, which noted that *H. helix* typically showed a lower APTI, suggesting it is more sensitive (Pandey et al., 2003; Chauhan et al., 2022; Kovats et al., 2021).

Its waxy surface makes particulate accumulation easy to measure and use (Weerakkody et al., 2017; Corada et al., 2021). This is important because this species is frequently used in urban parks and trees, facilitating comparisons of air quality measurements taken at various city locations (Weerakkody et al., 2017b). Its sensitivity, a reason for avoiding its use in areas requiring pollution tolerance, makes it so useful for providing a rapid signal of changes in air pollution that could be dangerous to human health (Lee et al., 2021). Both *G. biloba* and *H. helix* were chosen because they monitor pollution through two distinct, but related, measurements that neither organism alone would cover, but together they do provide comprehensive data: temporal dynamics

measured with deciduous plants, where a known index exists and changes through seasons to detect shifts in air pollution levels and spatial context with a species that is evergreen and widely planted in many urban parks, offering measurements at any given time of year and showing how pollution levels are affected by localized variations (Weerakkody et al., 2017b).

4. Materials and Methods

4.1 Studied Areas, Data and Sample Collection in Debrecen, Hungary

4.1.1 Topographical, climatic background

The second-largest city in Eastern Hungary, Debrecen, on the Great Hungarian Plain, is situated approximately 120 meters above sea level and experiences the Urban Heat Island (UHI) effect (Bottyán et al., 2005). The city's topography exhibits a consistent uniformity, characterised by the absence of notable elevation variations. The area is characterised by the alternation of four seasons, representative of the climatic conditions found in Central Europe. The mean annual temperature is 10 °C. The annual precipitation totals 549 mm, while the city experiences approximately 2000 hours of sunshine each year (László et al., 2016). Debrecen has a humid continental climate (Dfb, verging on Dfa) as per the Köppen-Geiger classification (Peel et al., 2007). The climate of Debrecen is predominantly dry continental, with periodic oceanic and Mediterranean influences (OMSZ). Unusually high temperatures persisted throughout the February 2020 lockdown, averaging 5°C, compared with the climatological mean of 0.5°C for the 1981–2010 period. The low temperatures were caused by cold fronts that brought an unusually dry Arctic air mass (March 21st, March 30th). On March 26th, dust from the desert area adjacent to the Aral Sea was transported by eastern winds to southern Hungary (Varga, 2020). Precipitation in April showed a sporadic pattern, falling on only a few days and totalling just under 20 mm nationwide, with the northwestern region receiving less than 5 mm. One of the things we typically see in April is heavy precipitation, averaging between 35mm and

40mm over the past few years. The first part of the rainfall shutdown period (March 31st through April 11th) in Hungary. Following this in May, many cold fronts passed through Hungary, resulting in cooler-than-normal temperatures; the mean May temperature was 14℃, and the average May temperature for this season was 16℃. The majority of the precipitation from these cold fronts was quite low, ranging from 20 to 50 mm. Additionally, as observed by the Hungarian Meteorological Service, Hungary was covered with Saharan dust between May 13th and 15th. Most of Hungary's urban areas are located on the sandy soils of the Nyírség region. In contrast, the southwestern and western regions of Hungary's soils exhibit a transition from medium to heavy clay. The typical wind direction is from the north-northwest. In addition to prevailing winds, long-range transport of Saharan dust can affect air quality in Debrecen, especially during certain months of the year. (Pásztor et al., 2016).

During the winter, stagnant air conditions are common in the area due to the basin effect created by the Carpathian Mountains, which allows pollutants to accumulate in Debrecen's atmosphere (Varga, 2020). As a result, PM_{10} levels often exceed the EEA's standards. Research indicates that about 75% of Hungary's annual particulate matter air pollution originates from transboundary sources, although local contributors still play a considerable role, especially in winter (Szoboszlai et al., 2009). Throughout the heating season, the 24-hour threshold for particle pollution is often surpassed.

4.1.2 Meteorological and Air Pollution Data

The Hungarian Meteorological Service provided meteorological and air pollution data for the three periods—the pre-pandemic, pandemic, and post-pandemic-based on PM_{10} concentrations to examine the impact of COVID-19

on air quality in Debrecen, Hungary, from 2018 to 2022. Data were collected from three air quality monitoring stations: Station 1 (S_1), Kalotaszeg tér; Station 2 (S_2), Hajnal Street; and Station 3 (S_3), Debrecen Klinika Campus. All of the studies use it to measure the city's levels of CO, NO, NO_2, NOx, PM_{10}, $PM_{2.5}$, and SO_2. Two weather stations, M_1: Macs Met (Agrometeorological Observatory of Debrecen) and M_2: International Airport of Debrecen (HMS) (Fig. 1), provided wind direction and speed data. To ensure precise and representative data, anemometers at these stations are mounted 10 meters above ground, in accordance with international standards. For daily, monthly, and annual studies, wind direction and speed were measured at 10-minute intervals and averaged.

4.1.3 Collection of Ginkgo biloba samples

G. biloba L. is a popular ornamental tree in urban environments. This ancient tree is considered a “living fossil” and dates back to the Permian period. *G biloba* is among the most investigated species for medicinal use and environmental tolerance, due to its resistance to pests and diseases. Seasonal variation in polyphenols and pigments has been shown to serve as a sensitive indicator of environmental fluctuations, especially in *G. biloba* (Jurčević Šangut & Šamec, 2024; Kinoshita et al., 2021*)*. Because of its resilient nature, it is an ideal species for biomonitoring in urban landscape studies. From the newly constructed Western bypass that surrounds the city centre of Debrecen, Hungary, *G. biloba* leaves were collected from trees along the bypass. (Fig. 1).

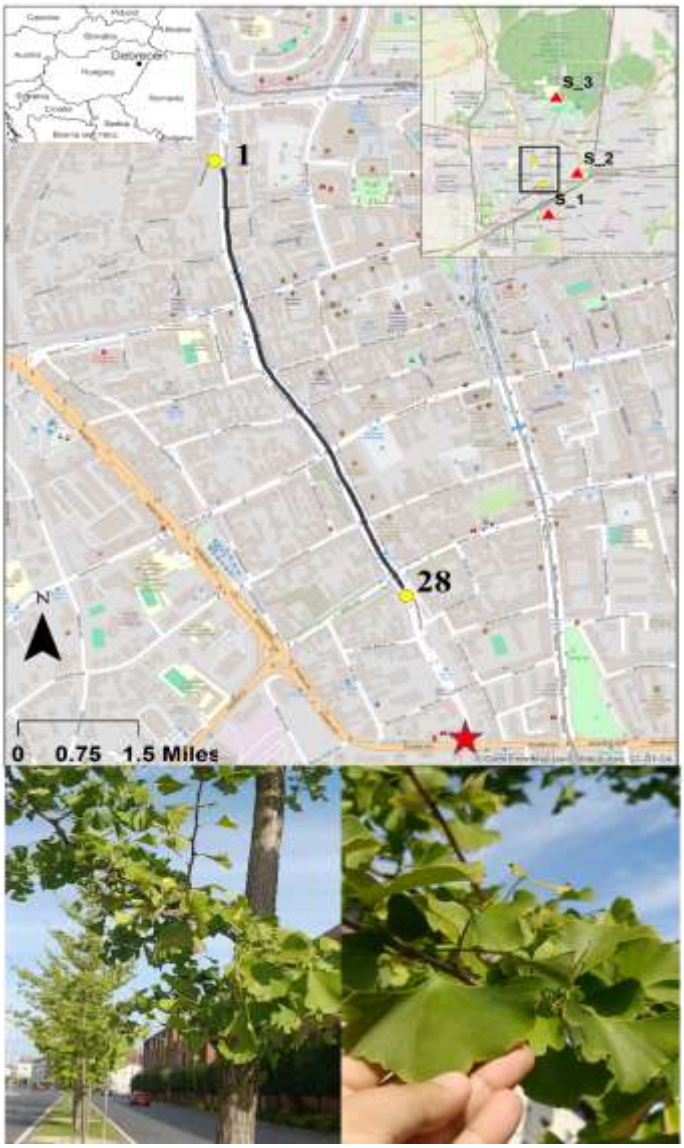

Fig. 1. Sampling layout in Debrecen city. A total of 28 trees were selected and sampled along the marked line. The red star marks the null point from which the distances of each sampling point were measured. The observation stations: Station 1, Kalotaszeg tér; Station 2, Hajnal Street; and Station 3, Debrecen Klinika Campus for monitoring air pollutants are indicated in the insert. The map was created using ArcMap version 10.4.

The leaf sampling involved 28 *G. biloba* specimens collected along a 1,200-meter linear transect in Debrecen, focusing on an intra-urban gradient of traffic influence. The 28 trees were spaced approximately 9.85 meters apart and selected to reflect varying traffic densities, especially near significant intersections and a railway station. All specimens were strategically positioned along the roadside to ensure uniform microclimatic conditions during evaluation of spatial variations in traffic-related air pollution. Given *G. biloba's* nonindigenous status and its role as an ornamental species, no age-matched controls from environments with lower pollution levels were available at the time of this study. The research employed variations in traffic intensity across geographic areas as a functional control mechanism. From July to October 2023, a total of 420-560 fully developed, healthy leaf samples were systematically collected monthly, comprising 15-20 samples from trees aged 1-2 years at the time of sampling (planted July 2022); nursery age prior to planting was not recorded. Samples were systematically collected from the upper and mid-canopy positions of each tree, at heights of about 1.5 to 2.5 meters above ground level. Leaf sampling was restricted to branches exposed to sunlight to minimise shading effects and maintain consistent light conditions among the subjects. Every tree was regarded as a distinct sampling unit for the purposes of statistical analysis. Samples were stored at −21°C for subsequent laboratory analysis.

4.1.4 Hedera helix sampling site

Leaves of *H. helix* samples were collected from ivy-covered steel mesh structures at 36 bus and tram stops in Debrecen (Fig. 2). Although 50 bus stops were originally planted within the framework of the project, at the time of

sampling, only 36 sites had sufficiently developed and intact ivy cover suitable for standardised leaf sampling. Sites with incomplete plant cover or maintenance-related disturbances were excluded. Consequently, we selected all bus and tram stops with established ivy growths of similar types to include in our analysis; those with similar characteristics were therefore included as well.

Fig. 2. Location of sampling sites and air pollution monitoring stations: Station 1 (S_1), Kalotaszeg tér; Station 2 (S_2), Hajnal Street; and Station 3 (S_3), Debrecen Klinika Campus. Two weather stations, M_1: Macs Met (Agrometeorological Observatory of Debrecen) and M_2: International Airport of Debrecen (HMS). The map was created using ArcMap version 10.4.

The control site was located in Debrecen-Jozsa (a suburban area of Debrecen), where traffic is lower and direct vehicle emissions are lower than at the inner-city study sites. The climate and horticulture maintenance practices were

similar to those in the other 3 sampling areas and the study area. Thus, although Debrecen-Jozsa cannot be deemed a pollution-free site, it will serve as an acceptable (i.e., low-exposure) reference site for this study, as it is also an urban regional node. From July 2023 until June 2024, samples will be collected each month during the first week (8.00-10.00 am) at each site, providing a composite biological sample for that site for that month. There is a limited amount of biomass at the sampling site, so the proposed use of 15 leaves for the analysis (due to multiple physiological and biochemical tests performed on the same sample) is an acceptable compromise between the number of leaves needed to perform the required analyses and minimising disturbances to the vegetation. The gathered samples were placed in labelled lab bags and transported to the laboratory for testing.

4.2 Studied Area and Sample Collection in Budapest, Hungary

The research was carried out using samples collected from three distinct locations in Budapest (Fig. 3). Each area reflecting varying degrees of traffic intensity: Rákóczi Avenue, characterised by high traffic (1.56 km in length, 35 m in width); Dembinszky Road, exhibiting moderate traffic (0.76 km in length, 17 m in width); and the Budatétény Rose Garden, which functioned as a control site low – traffic urban reference site, selected for its minimal direct vehicle emission exposure relative to the traffic - affected sites. The sampled *G. biloba* trees were established as field-grown roadside trees located directly along the roadside footway adjacent (approximately 1-3 m from the road edge) to the traffic corridor. The control site is located within a 2.5-hectare landscaped rose gene bank, characterised by minimal traffic impact and stable ecological conditions, thus serving as a low-stress reference environment.

Sampling occurred during two distinct seasonal periods: July and September in 2023, followed by September 2024, to capture both intra-annual and inter-annual variations. At each location, a selection of 10 mature, visually healthy *G. biloba* trees was made. Ten fully expanded leaves were collected from the lower third of the canopy (~2 m above ground) on the traffic-facing side of each tree, following established protocols to ensure standardisation of microenvironmental exposure. For each tree, five fully expanded leaves were used for pigment extraction, and three independent replicate extractions were performed. Samples were collected at the tree level to ensure statistical independence and to prevent pseudo-replication. All samples were collected during dry weather, with no rainfall on the day of sampling. They were promptly flash-frozen in liquid nitrogen and subsequently stored at -70°C until the time of biochemical analysis. Corresponding air pollution data were sourced from the nearest monitoring stations, specifically Teleki Square for the moderate-traffic site and Erzsébet Square for the high-traffic site. In the Control Zone (Budatétényi Rose Garden), background values were derived from the nearest suburban station, Budapest Budatétényi, due to the absence of a co-located monitoring device.

Fig 3. Map of the Budapest study area showing sampling and monitoring locations. The map was created using ArcMap version 10.4. Leaf samples of *Ginkgo biloba* were collected from three different sites: the control at Budatétényi Rose Garden (C), a site with moderate traffic in Dembinszky Street, and a site with high traffic in Rákóczi Avenue. Air pollutant data (CO, NO_2, O_3, PM_{10}, $PM_{2.5}$, SO_2) were obtained from nearby National Air Quality Monitoring Network stations: Budatétény Rose Garden (C), Station 1 (S1) in Teleki Square, and Station 2 (S2) in Erzsébet Square. These paired biological and atmospheric datasets provided the basis for stress classification and PIDR validation across the urban gradient.

4.3 Analysis of Deposited Dust

Leaf area was determined by scanning each leaf and analysing the images in ImageJ (Version 1.52a, Wayne Rasband, National Institutes of Health, USA). Each leaf was then washed in 250 mL of deionised water for 10 minutes on an

orbital shaker to dislodge the adsorbed particulate matter, followed by a second rinsing with 50 mL to ensure thorough recovery. The pooled 300 ml suspension was passed through a 150 µm mesh sieve/screen to remove larger debris, after which the filtrate was subjected to vacuum filtration using pre-weighed filter papers (5–8 µm retention; Munktell 392, Ahlstrom) (Fig. 4). Filters were then dried to constant weight (±0.1 mg / ±1 mg) for gravimetric determination of dust, following rigour in mass-difference protocols (Weerakkody et al., 2017a). Dust accumulation was normalised against leaf surface area and expressed as µg cm^{-2} (Szabó et al., 2023).

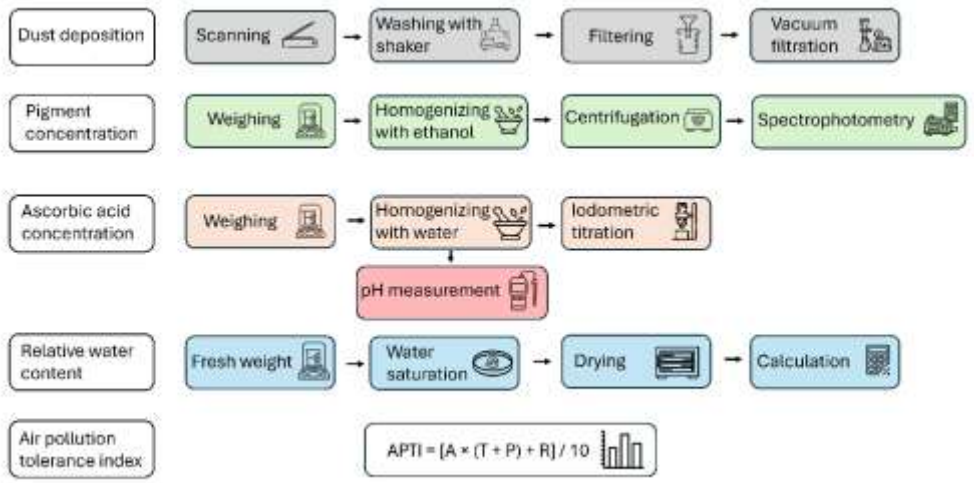

Fig. 4. Workflow diagram of laboratory methods used for the analysis of leaf-based air pollution indicators. The workflow diagram was made by The Noun Project (https://thenounproject.com).

4.4 Analysis of Pigments

Fresh leaves (20 mg fw) were homogenised by means of a grinding apparatus in 5 mL 96% ethanol for 4 min (2,500 RPM). Subsequently, the extract was

centrifuged, and the upper liquid phase was kept in the dark at 4°C for measurements. A UV/VIS spectrophotometer (BOECO S220) was used to measure the absorbance of the cleared extract in a 1-cm quartz cell in the presence of ethanol (absolute). Absorbances were measured at 470, 649, 665, and 750 nm following the method of Lichtenthaler et al. (1981). Chlorophyll and carotenoid concentrations were calculated by Equations 1-4 and reported as per gram fresh weight of leaf tissue. To determine the pheophytin concentration, the same ethanolic extract used previously was used. Absorbance readings were recorded prior to acidification at wavelengths 649, 665 and 750 nm. Then, one drop (50 µL) of 10M HCl (final concentration of approximately 0.1 M HCl) was introduced, and the pheophytin was generated by removing Mg^{2+} from all the chlorophyll. After 3 min, the absorbances were remeasured at wavelengths 655, 666 and 750 nm. Pheophytin concentration was calculated according to Vernon (1960). All operations were carried out under reduced light conditions to avoid the photodegradation of the pigments.

For statistical analyses, replicate values were averaged at the tree level, with each tree treated as a biological replicate. The equations used to calculate each pigment parameter are presented below (Eqs. 1-4); the corresponding workflow is illustrated in Fig. 4.

$$C_{\text{Chl-a}} = [13.36(A665 - A750) - 5.19(A649 - A750)] \times \frac{0.005}{m}$$

Equation: 1

$$C_{\text{Chl-b}} = [27.43(A649 - A750) - 8.12(A665 - A750)] \times \frac{0.005}{m}$$

Equation: 2

$$\text{Total Chlorophyll} = [5.24(A665 - A750) + 22.24(A649 - A750)] \times \frac{0.005}{m}$$

Equation: 3

In Eq. (1)

$C_{\text{Chl-}a}$: concentration in mg/g fresh mass

- $A_{665-750}$ is the absorbance at 665 nm minus the absorbance at 750 nm.
- $A_{649-750}$ is the absorbance at 649 nm minus the absorbance at 750 nm
- m is the fresh mass of the sample in grams.

In Eq. (2)

$C_{\text{Chl-}b}$: concentration in mg/g fresh mass

- $A_{665-750}$ is the absorbance at 665 nm minus the absorbance at 750 nm
- $A_{649-750}$ is the absorbance at 649 nm minus the absorbance at 750 nm
- m is the fresh mass of the sample in grams

In Eq. (3)

Total Chlorophyll: concentration in mg/g fresh mass

- $A_{665}-A_{750}$ is the absorbance at 665 nm minus the absorbance at 750 nm.
- $A_{649}-A_{750}$ is the absorbance at 649 nm minus the absorbance at 750 nm.
- m is the fresh mass of the sample in grams.

$$C_{\text{car}} = \frac{1000\,[A_{470} - A_{750}] - 2.13\,C_{\text{Chl-a}} - 97.64\,C_{\text{Chl-b}}}{209} \times \frac{0.005}{m}$$

Equation: 4

In Eq. (4)

- C_{car}: concentration in mg/g fresh mass
- $A_{470-750}$: A is the absorbance at 470 nm minus the absorbance at 750 nm.
- $C_{Chl\text{-}a}$: C is the chlorophyll-a concentration in milligrams (mg).
- $C_{Chl\text{-}b}$: C is the chlorophyll-b concentration in milligrams (mg).
- m is the fresh mass of the sample in grams

$$\text{Pheo-a} = [(20.15\,[A_{666} - A_{750}] - 5.87\,[A_{655} - A_{750}]) - (11.63\,[A_{665} - A_{750}] - 2.39\,[A_{649} - A_{750}])] \times \frac{0.005}{m} \quad \text{Equation: 5}$$

$$\text{Pheo-b} = [(31.9\,[A_{655} - A_{750}] - 13.4\,[A_{666} - A_{750}]) - (20.11\,[A_{649} - A_{750}] - 5.18\,[A_{665} - A_{750}])] \times \frac{0.005}{m} \quad \text{Equation: 6}$$

$$\text{Total-pheo} = [(6.75\,[A_{666} - A_{750}] + 26.03\,[A_{655} - A_{750}]) - (6.45\,[A_{665} - A_{750}] + 17.72\,[A_{649} - A_{750}])] \times \frac{0.005}{m} \quad \text{Equation:7}$$

In Eq (5), Eq (6), & Eq (7)

Pheo *a*, Pheo *b*, and Total pheo: concentration in mg/g fresh mass

- $A_{666-750}$: Absorbance at 666 nm minus absorbance at 750 nm.
- $A_{655-750}$: Absorbance at 655 nm minus absorbance at 750 nm.
- $A_{665-750}$: Absorbance at 665 nm minus absorbance at 750 nm.
- $A_{649-750}$: Absorbance at 649 nm minus absorbance at 750 nm.
- m is the fresh mass of the sample in grams.

4.5 Air Pollution Tolerance Index

The Air Pollution Tolerance Index (APTI) was calculated based on the concentration of chlorophyll and ascorbic acid and relative water contents of leaves, as well as the pH of leaf extracts (Fig. 5) (Singh et al., 1991; Molnár et al., 2020a; Simon et al., 2021)

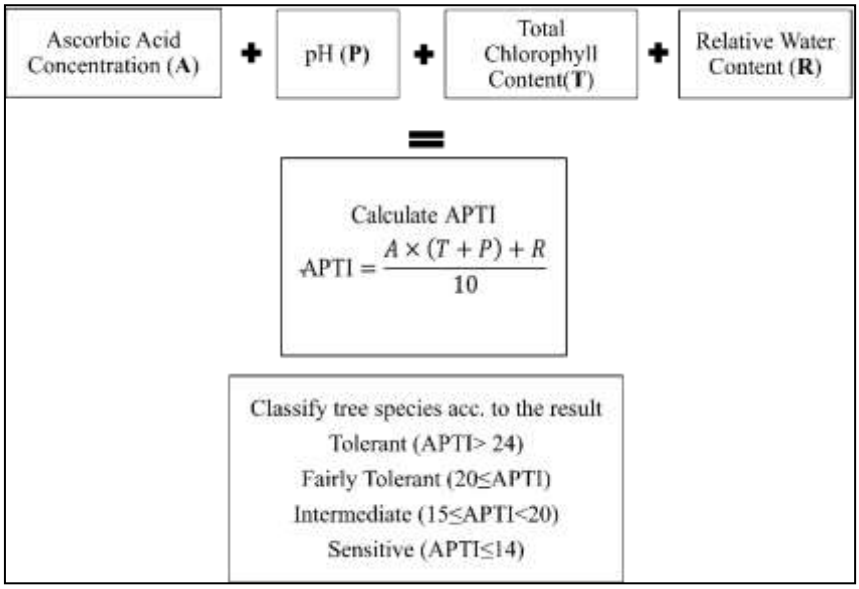

Fig. 5. Parameters of Air Pollution Tolerance Index calculation (APTI) (Singh et al., 1991)

4.6 PIDR Calculation for *G. biloba*

This study tested and introduced Pigment Integrity-to-Dust Ratio (PIDR) as a novel exploratory biomonitoring index, which combines two diagnostic aspects of leaf stress: (i) the balance between intact chlorophyll pigments (Chl-*a*, Chl-*b*) and their degradation products (Pheo-*a*, Pheo-*b*), and (ii) the accumulation of dust on the leaf surface. The process of averaging the two

pigment ratios balances the index while reducing the risk of bias from variations in any individual pigment. Pheophytin is a result of chlorophyll hydrolysis during leaf senescence or due to pollution stress, not an artefact of acidification. Leaves synthesise pheophytin during leaf senescence, following the degradation sequence chlorophyll > pheophytin > pheophorbide (Hörtensteiner et al., 2009; Matile et al., 1987). The spectrophotometer readings collected before acidification thus reflect chlorophyll degraded to pheophytin naturally under field conditions. After acidification, the spectrophotometer measures the total chlorophyll present, since acidification converts the remaining intact chlorophyll to pheophytin. The chlorophyll: pheophytin ratio computed from these two sets of measurements shows how much intact chlorophyll is present relative to chlorophyll that has been degraded to pheophytin and can serve as a measure of how much chlorophyll has broken down under the given stresses (Vernon, 1960). Adding dust load to the denominator gives PIDR, which measures pigment health compared to the amount of dust on the leaf. This connects changes in leaf pigment to dust buildup. The calculation of PIDR for *G. biloba* and morphologically similar broad-leaved species has been done as follows.

$$\text{PIDR } Ginkgo = \frac{\left(\frac{\text{Chl-a}}{\text{Pheo-a}} + \frac{\text{Chl-b}}{\text{Pheo-b}}\right)}{2 \times \text{Dust load } (\mu g/cm^{-2})} \quad \text{Equation: 8}$$

The values used for chlorophyll *a* (Chl-*a*) and *b* (Chl-*b*) were mg g^{-1} fresh weight. For pheophytin *a* (Pheo-*a*) and *b* (Pheo-*b*), concentrations were also given as mg g^{-1} fresh weight. Both the numerator and denominator values used in pigment-ratio computations have the same units; therefore, the ratios Chl-*a*/Pheo-*a* and Chl-*b*/Pheo-*b* are dimensionless. With pollution, when all Chl is broken down into pheophytin, the numerator (Chl-*a*/Pheo-*a* + Chl-*b*/Pheo-*b*) would theoretically approach 0 and under mild or prolonged pollution stress, it rises well above 2.0 in leaves from low – pollution reference sites, where

Chl far exceeds its degradation product, pheophytin. Dust load was the gravimetric measurement of dust particles divided by the leaf surface area (μg cm^{-2}). The PIDR has units of the dust load denominator, but in this study, PIDR is expressed as a fold change relative to the mean PIDR of high-traffic-exposed sites, compared with the median PIDR of the low-traffic reference site during the same period (Eq. 9), making the final index dimensionless. The averaging of the two pigment ratios also normalises the index and reduces the risk that any single pigment disproportionately influences it.

.4.6.1 Zone-level deviation analysis

PIDR values were presented as fold-change relative to the control-site median (M_t) for each sampling date to enable comparison between zones:

$$Fold\ Change_{i,t} = \mathrm{PIDRi,t} / \mathrm{M\,t} \quad \text{Equation: 9}$$

where *PIDR* refers to the raw value for each tree *(i)* at time *(t)*. Zone-level deviations were then summarised for each site (R, D, and Control) using both parametric (mean ± standard deviation, SD) and robust (median ± median deviation from control, MDC) statistics.

MDC was calculated as:

$$\mathrm{MDCt} = \mathrm{median}\left(\left|FoldChange_{i,t} - \mathrm{Median}\left(FoldChange_{t}\right)\right|\right) \quad \text{Equation: 10}$$

- i = individual tree sample
- t = sampling date
- *Fold Change*$_{(i,t)}$ = PIDR of tree i divided by the control-site median PIDR for date t
- median *(Fold Change)*$_t$ = median Fold Change for that date or zone

Both mean ± SD and median ± MDC were converted into percentage deviation from the control baseline to aid comparison across the zones:

$$\%\text{MDCt} = 100 \times \text{median}\left(\left|FoldChange_{i,t} - \text{Median}\left(FoldChange_{t}\right)\right|\right)$$

Equation:11

- i = individual tree sample
- t = sampling date
- $Fold\ Change_{(i,t)}$ = PIDR of tree i divided by the control-site median PIDR for date t
- median $(Fold\ Change)_t$ = median Fold Change for that date or zone

where value refers to the median of the fold change distribution for a given site. SD and MDC were scaled by 100 to allow direct comparison of variability across measures. While mean ± SD values were retained for reference, primary summaries used median ± MDC. This approach was chosen to better represent central tendency and reduce the influence of outliers, thus providing a clearer ecological interpretation of the main stress patterns.

4.6.2 Stress Classification

To create a stress classification, limits were set relative to the control group to maintain consistency across sites and dates. For each sampling period, the median PIDR for the MC site (the low-traffic reference) was used as the comparison reference, which varied by date. As low-stress status could vary during the study period (e.g., as the PIDR could fluctuate during winter due to

an abundance of stress periods), it was defined operationally in this investigation as the minimum possible stress level for the species and dataset. This was quantified as the median PIDR at the reference site during each specific sampling period, rather than a single constant ratio that would correspond to low stress. This baseline value for the reference site and sampling period is hereafter defined as the comparator baseline (b). Note that MC is not pollution - free and experiences various abiotic stresses, so MC represents only a relative, not an absolute, low-stress measurement.

PIDR values, which do not have a normal distribution, were adjusted using an inverse hyperbolic sine (asinh) transformation to make it easier to compare fold changes. For interpreting the entire PIDR range, a uniform analytical scale was used. The response is stable for values closer to zero and helps identify differences between larger values, lessening the impact of extreme values. Also, the asinh transformation fits ecological response patterns, showing gradual changes at lower pollution levels and sharper responses at higher stress levels.

Each individual measurement ($PIDR_i$) was then expressed as its deviation from this baseline:

$$\Delta i = \text{Asinh}(\text{PIDRi}) - \text{B} \quad \text{Equation:12}$$

Where $PIDR_i$ = raw PIDR value for sample i

Δi is the difference from the baseline.

A positive Δ_i means the leaf is close to or above the control (healthier), while a negative Δ_i means the leaf has lower pigment integrity (more stress)

The control-site median PIDR (M_C) was multiplied by fixed fractions (f = 1.0, 0.50, and 0.20) corresponding to varying levels of pigment loss to establish

stress thresholds. To ensure that all threshold values were comparable and expressed on the same scale, these scaled values were subsequently transformed using the same inverse hyperbolic sine (asinh) transformation as the sample data.

$$\mathrm{Tf} = \mathrm{asinh}(\mathrm{f} \times \mathrm{Mc}) - \mathrm{B} \quad \text{Equation:13}$$

where T_f = transformed threshold for each level.

Accordingly, stress categories were defined as:

- **Minimal to No Stress**: $\Delta_i \geq T_{1.0}$
- **Low stress:** $T_{0.50} < \Delta_i < T_{1.0}$
- **Moderate Stress:** $T_{0.20} < \Delta_i \leq T_{0.50}$
- **Severe Stress:** $\Delta_i \leq T_{0.20}$

To offer a paradigm that is both replicable and ecologically interpretable, stress thresholds were specified as fixed fractions of the control median PIDR (M_C). *Minimal to no stress* samples were defined as those that were at least as high as the control ($\geq 1.0 \times M_C$which represents the physiological condition of the low-traffic reference trees under comparable seasonal conditions. To capture slight deteriorations in pigment integrity that signify early physiological compensation while being above the functional midpoint, the band 0.50–<1.0 × M_C was named *Low Stress*. Studies by (Lichtenthaler, 1996; Trueba et al., 2019; Walker et al., 2018) indicate that a 50% decline in fluorescence or chlorophyll is often treated as a meaningful decline but not yet a severe level of physiological loss; for this reason, we used 0.50 (50% of MC) to mark Moderate Stress. Severe stress was defined using a lower cut-off of 0.20 (20%

of MC), reflecting findings that a 20-30% drop is typically associated with major damage to pigment pools and photosynthetic function (Trueba et al., 2019; Wykoff et al., 1998). In addition to providing a repeatable, ecologically significant classification across sample sites and dates, this proportional fold-of-control paradigm explicitly links stress intensity to pigment integrity loss relative to the low–traffic urban reference baseline.

4.7 Statistical Analysis

4.7.1 Statistical analysis of the effect of COVID-19

Statistical analyses were performed using IBM SPSS Statistics (version 21). The daily concentrations of PM_{10} were analysed to examine the effect of COVID-19 on air pollution levels. The PM_{10} concentrations were compared across the pre-pandemic, pandemic, and post-pandemic periods using a two-way analysis of variance (ANOVA). The PM_{10} concentration was used as the independent factor, stations and the three studied periods as the dependent factors. To study the effect of lockdowns on daily PM_{10} concentrations, we compared years with lockdowns in Hungary using a two-way ANOVA. The PM_{10} concentration was the independent factor, while the stations and the studied years were the fixed factors.

4.7.2 Statistical analysis in the case of G. biloba in Debrecen

Statistical analyses were also performed using IBM SPSS Statistics (version 21). Levene's test was used to analyse the equality of variances. Differences among months and studied areas were analysed with analysis of variance (ANOVA) and Tukey's pairwise comparisons test. A Pearson correlation test

was used to determine the correlation between pigment concentrations and air pollutants, and between pigment concentrations and the distance between sampling points. For the correlation analyses, monthly averages of air pollutant data from the three observation stations were used. Using Redundancy Analysis (RDA), we examined the relationships between pigment and air pollutant concentrations.

4.7.3 Statistical analysis in the case of G. biloba in Budapest

Statistical analyses were performed using IBM SPSS Statistics (version 21). Multivariate Analysis of Variance (MANOVA) was first applied to evaluate overall zone effects across the biochemical parameters (chlorophyll *a*, chlorophyll *b*, total chlorophyll, carotenoids, pheophytin, and dust deposition). One-way ANOVAs and Tukey's Honestly Significant Difference (HSD) tests were used to examine pairwise contrasts among three sites: the control (Budatétényi Rose Garden), a moderate-traffic area on Dembinszky Street, and a high-traffic location on Rákóczi Avenue, when MANOVA revealed significant differences. Levene's test was used to assess homogeneity of variances, and one-way ANOVA was used to examine temporal patterns across three sample dates: July 2023, September 2023, and September 2024. Instead of performing repeated measurements on the same tree, the study used cross-sectional comparisons of fresh leaf samples taken at each time point. The effectiveness of PIDR as a stress index was evaluated concerning multiple air pollutants, including CO, NO_2, O_3, PM_{10}, $PM_{2.5}$, and SO_2. The analysis involved computing Pearson correlation coefficients to assess the relationship between standardised PIDR values and pollutant concentrations at three distinct locations: a control site (Budatétényi Rose Garden), a site with moderate traffic (Teleki Square), and a site characterised by high traffic

(Erzsébet Square). Furthermore, distinct multiple regression models were constructed for each location to determine which pollutant had the greatest impact on PIDR variation. The relatively large standard deviations observed for some parameters reflect the biological heterogeneity expected among field-grown urban trees exposed to variable local microenvironmental conditions. The two strongest predictors were used in every case: for a high-traffic site, CO and $PM_{2.5}$; for a control site, O_3 and $PM_{2.5}$; and for a moderate-traffic site, O_3 and $PM_{2.5}$. To compare predictor strength, standardised coefficients (β) were used, and model fit was evaluated with R^2. Before interpreting model output, residual normality and collinearity (VIF < 5) were validated. Because of the limited number of sampling dates, the regression analyses were interpreted as exploratory rather than definitive

4.7.4 Statistical analysis in the case of H. helix in Debrecen

Statistical analyses were performed using IBM SPSS Statistics (version 21) for the Shapiro–Wilk test, Levene's test, ANOVA and Dunnett's test, using Canoco for Windows 4.5, used for PCA (Braak & Smilauer, 2002) and R software (version 4.1.2) by the R Foundation for Statistical Computing (2021) were used for correlation and regression analysis. Monthly data were aggregated into seasonal groups to reduce short-term temporal variability and to emphasise broader seasonal environmental patterns. Data distribution was assessed for normality using the Shapiro–Wilk test. The homogeneity of variances was tested with Levene's test. The concentrations of dust on leaf surfaces, pigments, and ascorbic acid, the relative water content, pH, and APTI of the studied areas were compared using a two-way ANOVA with one factor, the studied sites, and the other, the studied seasons. Differences from the control were tested using a paired Dunnett's test. Pearson correlation analysis

and regression analysis were performed between the measured physiological parameters (dust deposition on leaf surfaces, pigment concentrations, ascorbic acid content, relative water content, pH, and APTI) and the distance from the city centre, as well as with the air pollution data from the two monitoring stations in Debrecen city, including precipitation, temperature, and wind parameters. Correlations and regression analysis were performed with leaf dust deposition and leaf size. Principal component analysis (PCA) was performed to examine seasonal variation and parameter relationships.

5. Results

5.1 Restricted Mobility During COVID-19 Enhanced Debrecen, Hungary's Air Quality

5.1.1 Changes in PM_{10} Concentration During the Periods Before, During, and After the COVID-19 Pandemic

PM_{10} concentrations varied across pre-pandemic (before March 2020), pandemic March 2020 to February 2022 and post-pandemic (after March 2022) at all stations (Fig. 6). Significant differences in PM_{10} concentrations were observed between 2018 and 2019 at all stations (Station 1: $F = 231.289$, $p < 0.001$, Station 2: $F = 238.488$, $p < 0.001$, Station 3: $F = 39.293$, $p < 0.001$), with notable increased concentrations especially at Station 2 from the beginning of 2019.

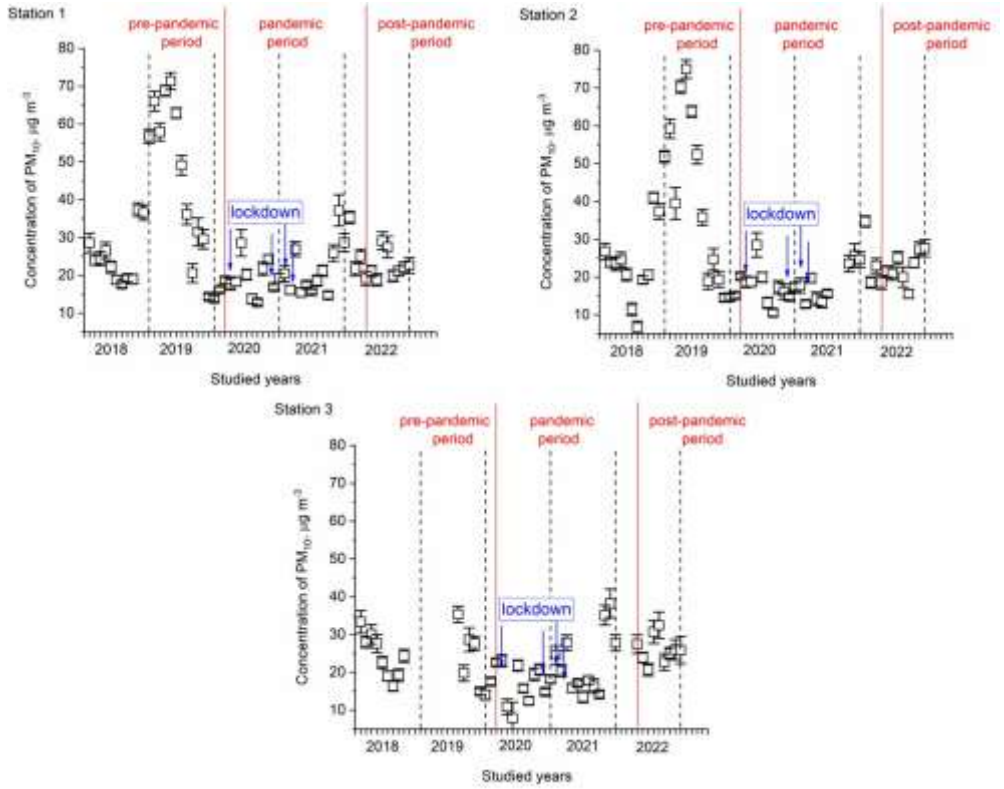

Fig. 6. Daily concentration of PM_{10} (mean ± SE) during the three studied periods (pre-pandemic, pandemic, and post-pandemic) in each month. Pre-pandemic period: before March 2020, pandemic period: March 2020–February 2022, post-pandemic period: after March 2022. Notations: blue arrows indicate the time of lockdowns.

The three stations differed during the pre-pandemic era, with different levels of exposure to traffic and other emissions. S1 and S2 were located at sites with moderate and heavy traffic exposure, respectively. S3 served as a background reference location and showed the lowest exposure to traffic emissions. S2 showed an exceptional peak of 41 ± 8 µg/m³ in January 2019 (which represented its peak monthly PM_{10} reading over the entire period), consistent with the high volume of traffic in S2. Road transport is the principal source of pollutants in the area, and there is no industrial activity in the neighbourhood

of any station. During the pandemic period, March 2020 to February 2022, PM_{10} remained at a stable low at both S2 and S3 in both 2020 and 2021, with a pandemic average of 22.6 µg/m³ at S2 and 20.3 µg/m³ at S3. These low concentrations can be attributed to a dramatic decrease in traffic and anthropogenic activities within the urban area. PM_{10} levels at S1 increased during spring 2021, with readings of 57 ± 11, 66 ± 14 and 58 ± 13 µg/m³ in March, April and May, respectively, contributing to its much higher average value during the pandemic period compared to the other two stations, despite the overall decline in road traffic. The unusually high readings observed at S1 can be explained by the influence of low wind speeds and a stable atmosphere during the second lockdown, which led to the accumulation of locally high pollution at the traffic hotspot of S2 (see Figure 6). Following the end of the lockdown phase in March 2022, S1 had again the highest average PM_{10} readings (31.0 µg/m³) driven by high spring readings (52 ± 9 and 49 ± 25 µg/m³ in March and April, respectively). The average post-pandemic readings at S2 (19.4 µg/m³) represented the lowest of the three stations. PM_{10} averages at S3 were found to be 23.9 µg/m³, which is higher than at S2, possibly reflecting the full return to activity at the Debrecen Klinika Campus after the restrictions were lifted during the pandemic. The growing differences between stations in the post-lockdown era are the consequence of the uneven recovery of traffic and localised emission sources in these three areas, as well as episodic inputs from agricultural burning and large-scale meteorological patterns in the region.

5.1.2 Impact of Lockdown Measures on PM_{10} Concentrations

The lockdown periods in Hungary commenced in March 2020 and concluded in March 2022, interspersed with multiple interruptions. Substantial

disparities were observed among years and stations when we analysed the identical months in each year (Table 1). Drastic declines were seen across all stations solely in January 2021.

Table 1. Daily PM_{10} concentration (mean ± SE) in the studied months during the lockdowns in Hungary in 2018–2022. The data with lockdowns in Hungary are indicated in bold. The lockdown periods were as follows: (i) from 11-03-2020 to 31-05-2020, (ii) from 01-11-2020 to 17-05-2021, (iii) from 01-11-2021 to 01-12-2021, and (iv) from 11-12-2021 to 06-03-2022. N.d. means data not detected.

Stations	Years	January	February	March	April	May	November	December
	2018	29 ± 14	24 ± 7	24 ± 10	26 ± 12	22 ± 9	36 ± 23	29 ± 13
	2019	37 ± 10	24 ± 6	23 ± 9	24 ± 11	21 ± 9	29 ± 18	25 ± 11
Station 1	2020	36 ± 15	30 ± 8	**30 ± 14**	**33 ± 17**	**23 ± 9**	**36 ± 20**	**28 ± 12**
	2021	*18 ± 7*	**38 ± 10**	**57 ± 11**	**66 ±14**	**58 ± 13**	**22 ± 10**	**25 ± 10**
	2022	*20 ± 12*	**19 ± 21**	**52 ± 9**	49 ± 25	39 ± 23	16 ± 10	22 ± 12
	2018	27 ± 12	13 ± 16	n.d.	8 ± 17	n.d.	2 ± 5	3 ± 9
	2019	41 ± 8	19 ± 11	32 ± 21	24 ± 14	14 ± 4	21 ± 8	19 ± 9
Station 2	2020	36 ± 12	19 ± 11	**24 ± 16**	**25 ± 12**	**15 ± 5**	**22 ± 8**	**21 ± 10**
	2021	**19 ± 7**	**28 ± 18**	**29 ± 18**	**21 ± 8**	**15 ± 5**	**24 ± 8**	**19 ± 9**
	2022	**18 ± 11**	**27 ± 17**	**20 ± 8**	14 ± 8	13 ± 4	25 ± 18	19 ± 8
	2018	33 ± 17	10 ± 22	20 ± 8	14 ± 8	11 ± 5	22 ± 12	18 ± 8
	2019	n.d.	15 ± 6	21 ± 8	15 ± 5	12 ± 6	32 ± 19	22 ± 12
Station 3	2020	35 ± 12	15 ± 7	**27 ± 11**	**16 ± 6**	**18 ± 4**	**25 ± 10**	**23 ± 12**
	2021	**11 ± 11**	**12 ± 12**	**20 ± 8**	**16 ± 10**	**13 ± 8**	**28 ± 11**	**25 ± 15**
	2022	**25 ± 14**	**25 ± 14**	**27 ± 11**	25 ± 2	17 ± 5	21 ± 13	27 ± 19

Particulate matter levels may have been consistently lower across the stations due to the overall reduction in pollution sources during lockdowns. In S1 and S2, the result was just marginally significant ($p = 0.077$), whereas the difference was insignificant in S1 and S3 ($p = 0.461$), suggesting that local effects, such as site-specific traffic and climate conditions, may have caused the monitoring sites to diverge as lockdowns continue. This implies that there may be different PM_{10} values at the two stations, possibly due to site-specific variations in lock-out, source differences, and regional effects on air pollutant dispersion. Because this is only marginally relevant, as it is the only trend observed at both monitoring stations (not observed in 2021, 2020, or 2019). Regional effects are increasingly affecting air quality at both sites as lockdowns continue.

5.1.3 Impact of Meteorological Parameters on PM_{10} Concentration

The relationship between PM_{10} levels and weather factors, such as wind direction and speed, was gathered from two weather stations: M1: International Airport of Debrecen (HMS) and M2: Macs Met (Agrometeorological Observatory of Debrecen).

The heat maps (Figs. 7 and 8) clearly illustrate the correlation between PM_{10} concentrations and wind factors. PM_{10} levels were consistent throughout the pre-pandemic period, with no statistically significant variations between the sites ($p > 0.05$). It is seen that, whereas regional climate patterns and persistent pollution sources have historically affected air quality, post-pandemic disparities have surfaced. PM_{10} levels remained stable during the pre-pandemic period, with no statistically significant differences among sites ($p > 0.05$). In addition to these regional climate and long-term air pollution sources,

the discrepancies observed after the pandemic are most pronounced between the high-traffic stations S1 and S2 and the background station S3, reflecting the uneven recovery of traffic emissions across monitoring locations. (Fig.6, Table 1). Because microclimate variables as well as localized sources were distinct at different stations, PM_{10} concentrations diverge noticeably after March 2020, where S1 shows much higher levels (18 ± 8 µg m^{-3}) compared to S3 (14 ± 13 µg m^{-3}); however, prior to March 2020, there is no significant inter-station variation in PM_{10} concentrations ($p > 0.05$). Dominant wind directions at both sites- N, NW and NE-that affect the dispersion and transport of PM_{10} confirm that the specific microclimate at each site is a primary driver of site-specific PM_{10} variations (Fig 7 -8).

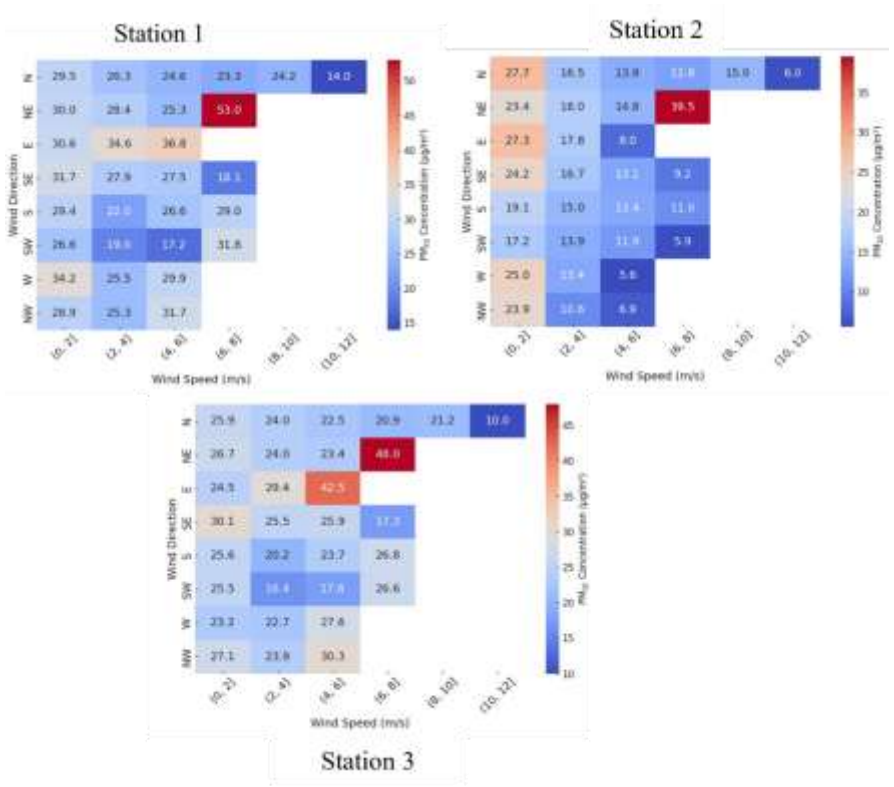

Fig. 7. Heat map of PM_{10} concentrations influenced by wind speed and wind direction at the stations.

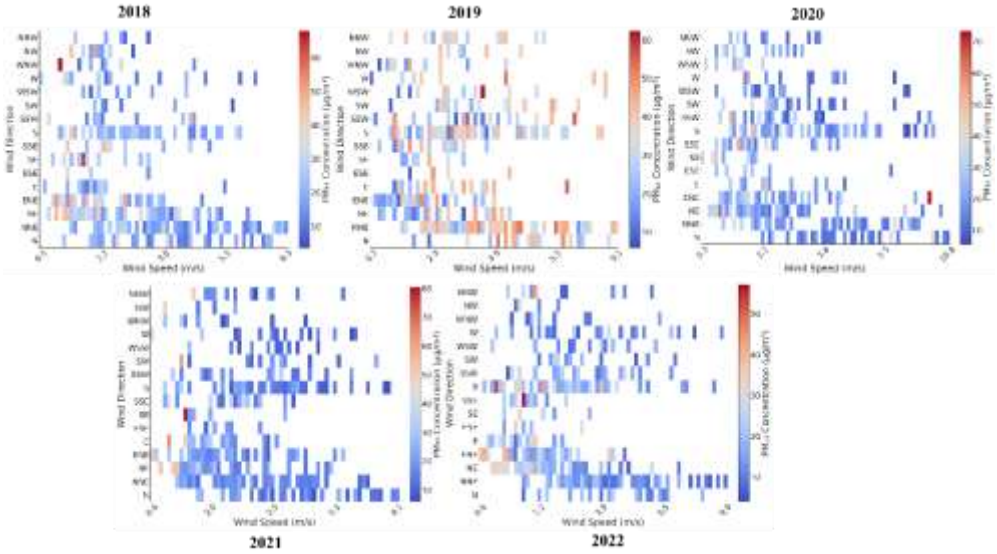

Fig. 8. The heat map illustrates the relationships among PM_{10} concentration (µg/m3), wind speed (m/s), and wind direction across the studied years. The colour gradient indicates the average daily PM_{10} concentration, highlighting how pollutant levels vary with wind speed and direction, aiding analysis of pollution dispersion patterns. This data is based on Metrological Station 1 and Metrological Station 2.

Furthermore, prevailing wind directions (N, NW, NE) significantly contributed to regional air quality variability, with N, NW, and NE associated with higher PM_{10} concentrations. This result underscores the likely influence of local emission sources or urban topography. While wind direction reflects the area's landscape and city layout, the persistent patterns recorded at M1 and M2 show that the meteorological data provide a solid basis for regional analysis. Moreover, combining wind direction data with PM_{10} concentrations at each station underscored its influence on regional and temporal fluctuations in air quality. Measuring available meteorological data may not accurately reflect site-specific microclimatic conditions, but the proximity of M2 International Airport of Debrecen (HMS) to the sampling sites and its

adherence to international measurement standards make it a reliable source for analysing patterns of pollutant transport and dispersion in this region.

5.2 Seasonal variation in leaf pigments of *G. biloba* resistance to air pollution in Debrecen City, Hungary

5.2.1 Seasonal trends in APTI

During the study period, individual trees' APTI scores ranged from 9.5 to 16, but the average monthly APTI values (± SE) remained below 15, indicating that *G. biloba* was susceptible to air pollution. A significant difference was found among months. The highest APTI was observed in October, and the lowest in July (Fig. 9). Based on the APTI values, significant differences in pH and ascorbic acid concentration were observed (Table 2).

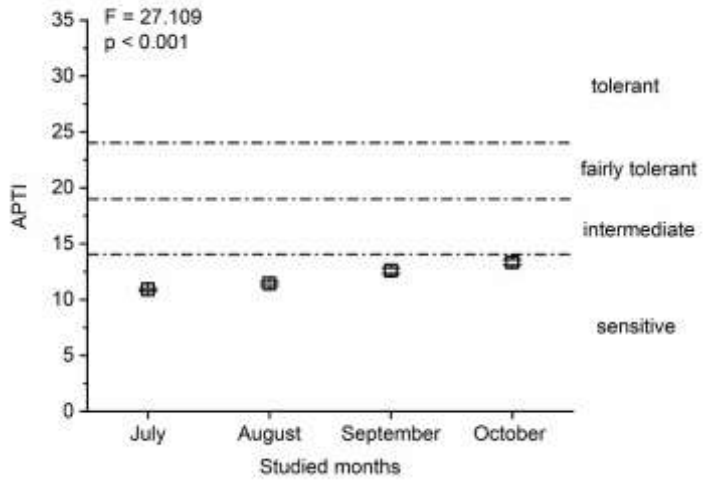

Fig. 9. APTI (mean ± SE) values based on the ascorbic acid and total chlorophyll concentrations, pH, and relative water content in *G. biloba* leaves during the studied months in urban areas in Debrecen city. (n= 15 - 20 samples

per tree × 28 trees × 4 months = 420 - 560 samples total per month, 28 trees were sampled in 2023)

Table 2. Values of the APTI parameters and significance differences among months of 2023 by using ANOVA (mean of:15 - 20 leaf samples per month per tree of 28 trees)

Parameters	Months	Mean ± SE	F	*p*
pH	July	3.52 ± 0.16	92.121	<0.001
	August	3.93 ± 0.32		
	September	4.46 ± 0.34		
	October	4.91 ± 0.46		
Total chlorophyll, mg g^{-1}	July	0.94 ± 0.47	2.479	0.065
	August	0.78 ± 0.47		
	September	0.81 ± 0.33		
	October	0.64 ± 0.31		
Ascorbic acid, mg g^{-1}	July	5.08 ± 1.84	11.918	<0.001
	August	5.94 ± 2.07		
	September	7.44 ± 2.57		
	October	8.34 ± 2.42		
Relative water content,%	July	86.43 ± 3.45	0.119	0.949
	August	86.97 ± 7.10		
	September	86.89 ± 4.31		
	October	87.21 ± 4.6 1		

5.2.2 Seasonal variations in pigment concentrations in G. biloba

Monthly data from July to October have been analysed, and a significant difference has been found among the months in Chl-*b* concentration. The mean concentration of Chl-*b* peaked in July and significantly declined in October (Fig. 10). A significant seasonal variation was also seen in the pheophytin concentration (Fig. 11).

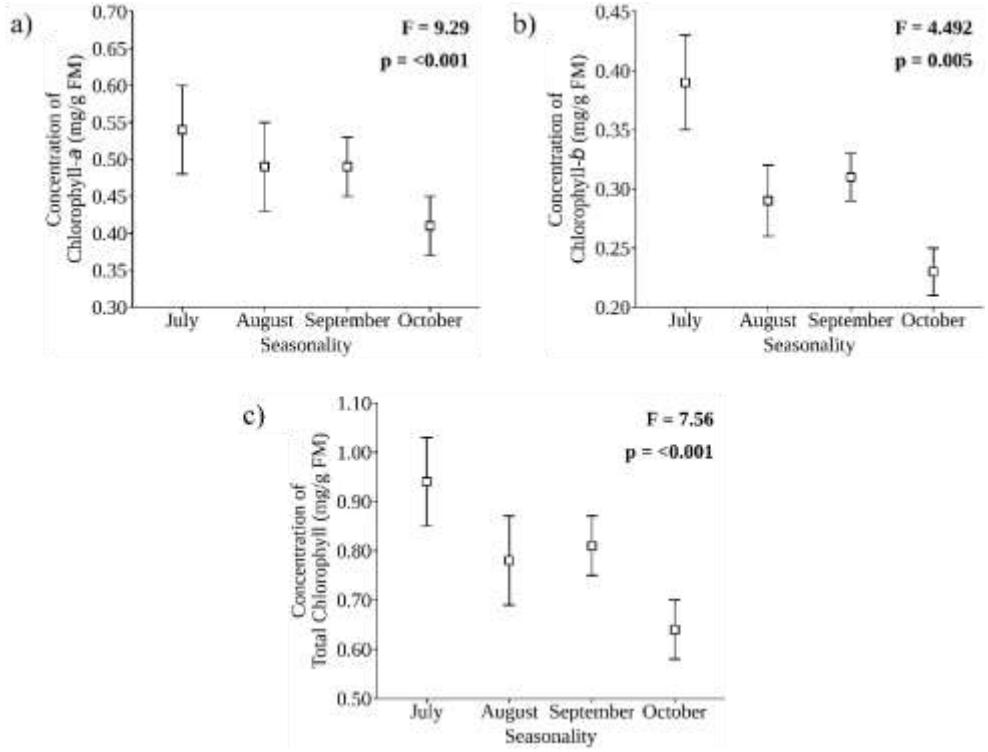

Fig. 10. Seasonal variability of (a) Chl-*a*, (b) Chl-*b* and (c) total Chl concentration (mean ± SE, mg/g fresh mass) in urban areas in Debrecen city.

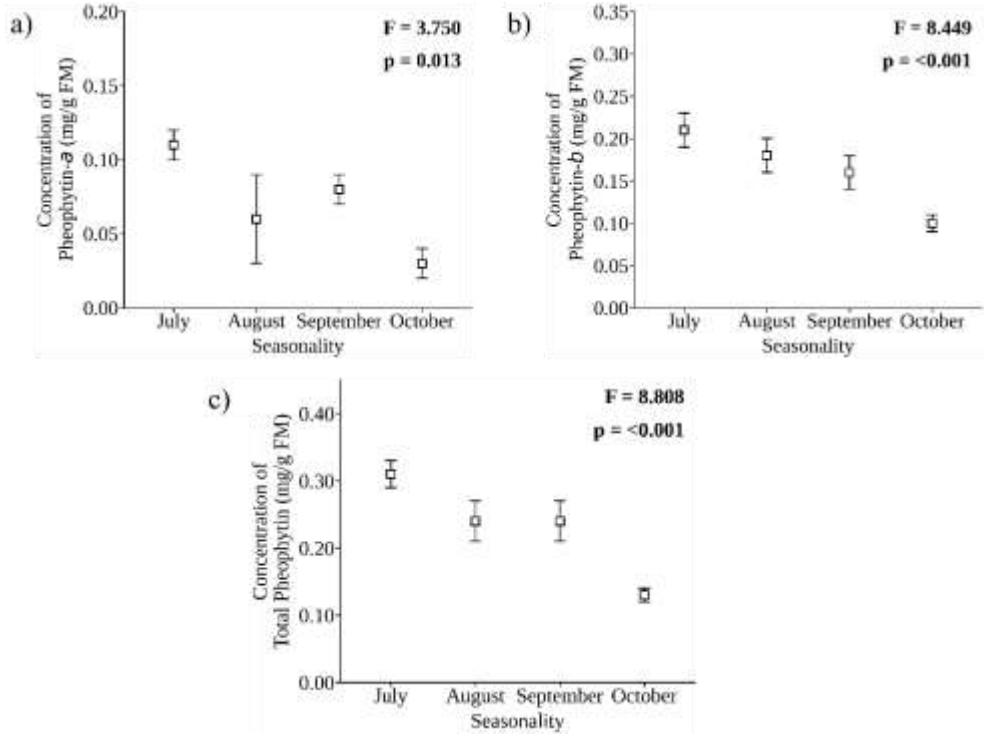

Figure. 11. Concentration of Pheo-*a* (a), Pheo-*b* (b), and total Pheo (c) (mean ± SE, mg/g fresh mass) during the studied months in urban areas in Debrecen city.

In July, the average Pheo-*a* concentration was 0.106 mg/g, which significantly declined to 0.06 mg/g in August, then increased to 0.08 mg/g in September, and further decreased to 0.03 mg/g in October (Fig. 11). The concentration of Pheo-*b* demonstrated similar pattern, initially starting at 0.21 mg/g in July, declining to 0.16 mg/g in September, and further dropping to 0.11 mg/g in October (Fig. 11). Here, chlorophyll and pheophytin concentrations were used as health indicators, calculated for 28 sampled trees each month except for August (n = 26) and October (n = 24), since anomalous negative pheophytin *a* (Pheo-*a*) measurements could be measured. Chl-*a* to Pheo-*a* ratios increased gradually from July (5.18 ± 0.28) through August (4.94 ± 0.45) to September (10.66 ± 2.50) and October (19.36 ± 4.31), whereas Chl-*a* concentration

decreased over the study months (0.544 → 0.376 mg g^{-1}). Pheophytin is a chlorophyll breakdown intermediate (Chlorophyll → Pheophytin → Pheophorbide → colourless catabolites) (Hörtensteiner et al., 2009; Matile et al., 1987). During the early stages of senescence (July and August), pheophytin accumulates as a byproduct of chlorophyll catabolism, leading to a relatively lower ratio, whereas with further senescence in the autumn months (September and October), the ratio is higher. Pheophytinase activity increased the rate of pheophytin breakdown to pheophorbide faster than its production, so that Pheo-*a* amounts decreased (0.107 → 0.038 mg g^{-1}) and consequently the Chl-*a* to Pheo-*a* ratio rose. Chl-*b* to Pheo-*b* ratios did follow a biological decline pattern (July: 1.82 ± 0.08, August: 1.61 ± 0.10, September: 2.27 ± 0.20, October: 2.23 ± 0.19). The results indicated that midsummer's thermal stress leads to the highest level of degradation (August), after which levels rose and remained stable again in autumn. This transient drop relative to the ratio at the beginning of the study might suggest that the stress induced by high temperature and irradiance is highest during the middle of summer and affects the catabolism of chlorophyll *b* more than chlorophyll *a*. Chl-*b* has been known to be sensitive to high irradiance and temperature stress in an urban environment (Lichtenthaler & Wellburn, 1983). Overall, Chl to total Pheo ratios also rose over the entire study period from July (2.92 ± 0.12) through August (2.78 ± 0.19) and September (3.93 ± 0.35) to October (4.68 ± 0.38). This was because total Pheo was mostly determined by Pheo-*a* in the early months of senescence, which sharply decreased in late summer. In general, ratio dynamics indicate that Chl-*a*/Pheo-*a* can reflect either rapid catabolism of pheophytin (late summer) or slow accumulation of the degradation product (early summer), and therefore either could indicate the damaging effects of pollution and senescence-related stress. (Vernon, 1960). Carotenoid concentrations varied slightly with the seasons, rising from a low level in July

(0.19 mg/g) to a peak in August (0.21 mg/g), then gradually declining in September (0.19 mg/g) and October (0.18 mg/g) (Fig. 12).

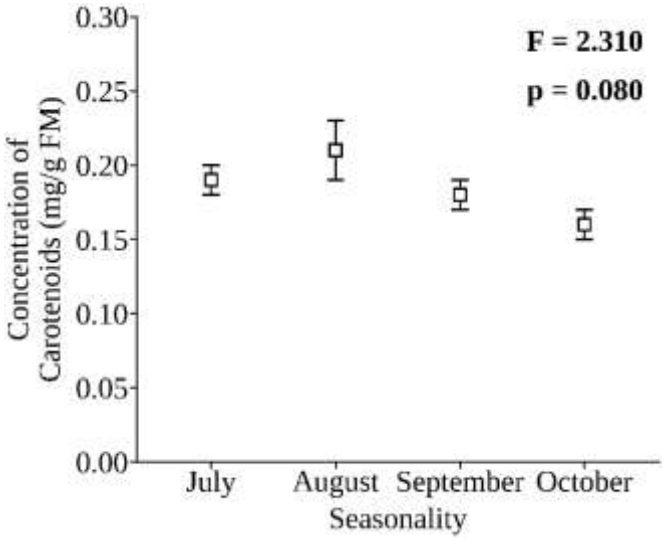

Fig. 12. Carotenoid concentration (mean ± SE, mg/g fresh mass) during the studied months in urban areas in Debrecen city.

These variations were not statistically significant, though. This overall stability demonstrated their continuous role in preventing oxidative damage to the photosynthetic system. However, statistical confirmation of substantial differences between months was not observed ($p = 0.080$).

5.2.3. Air pollutant levels

The examination of air pollutant levels at the three monitoring stations indicated significant regional variability across Debrecen city during the study period (Table 3).

Table 3. Air pollutant concentration (μ/m³) in Debrecen, Hungary

Air pollutants	Months				Results of ANOVA		EU air quality standards
	July	August	September	October	F	*p*	
CO	394 ± 142	422 ± 54	391 ± 73	458 ± 63	0.120	0.945	10
NO	0.2 ± 0.2	0.3 ± 0.3	0.5 ± 0.4	7.0 ± 4.8	1.949	0.200	n.d.
NO_2	2.2 ± 2.2	3.3 ± 3.3	4.5 ±3.7	18.1 ± 4.8	4.205	0.046	40
NO_x	2.6 ± 2.6	3.8 ± 3.8	5.3 ± 4.2	29.6 ± 12.0	3.661	0.063	n.d.
PM_{10}	16.3 ± 0.7	13.9 ± 3.3	13.3 ± 6.5	13.2 ± 6.6	0.087	0.965	40
$PM_{2.5}$	3.3 ± 3.3	3.2 ± 3.2	3.4 ± 3.4	3.6 ± 3.6	0.003	1.000	25
O_3	47 ± 23	45 ± 22	41 ± 20	32 ± 16	0.101	0.957	120
SO_2	0.6 ± 0.3	0.4 ± 0.4	0.4 ± 0.4	0.6 ± 0.6	0.057	0.981	n.d.

Notations: In the studied months, the results were summarised using ANOVA. The EU air quality standards (mean in 1-year period) unit was μg/m³ (https://environment.ec.europa.eu/topics/air/air-quality/eu-air-quality-standards_en). N.d. means data not reported. In the case of O_3, the reported data are the maximum daily 8-h mean.)

Monthly average levels of several air pollutants in each locality were estimated by combining all three observer samples into a single average measure. An extensive examination revealed that stations 1 and 2 were by far the highest in average concentration of NO_2, NO_X, CO, and PM_{10} throughout all months due to their locations in close proximity to the area studied and their exposure to a large amount of vehicle activity, while station 3 was located far away and measured much lower concentrations of all four pollutants. In fact, the average monthly levels measured at Station 1 were typically many times the other two stations, especially during September and October, making the geographic gradient most pronounced for the pollutants NO_2 and NO_X. Seasonal observations showed that the only air pollutant with significant monthly variability was NO_2. NO_2 would peak in October, with levels more

than 4 times those of previous months. No air pollutants exceeded maximum allowable standards. Geographical and temporal gradients are important for interpreting pigment concentration and APTI in *G. biloba* trees at different locations. To provide transparency and reproducibility, the monthly means ± SD for each pigment are provided in the Appendix table 1.

5.2.4. Spatial Variation in pigment concentration with distance from the pollution source

Distances were determined for each sampled tree throughout the linear urban transect outlined in Section 2.1, beginning at the main road intersection and varying along the corridor. Linear regression analysis was used to evaluate the relationship between distance from the main road intersection (Fig. 1, red star on the map) and concentrations of total chlorophyll, carotenoids, and pheophytins over the observed months. The regression lines for the July samples are illustrated in the Fig. 13.

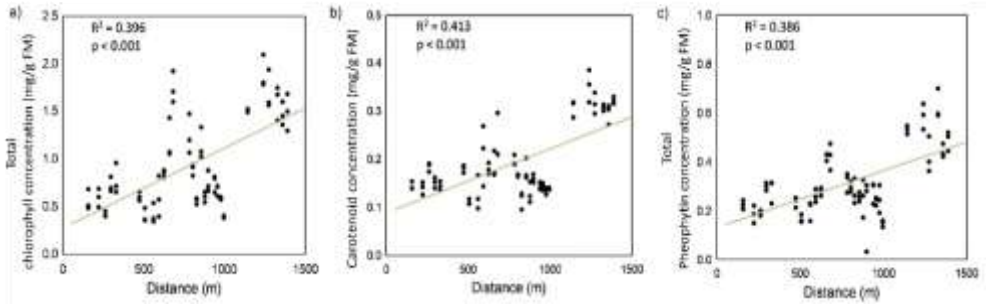

Fig. 13. Pigment concentrations (mg/g fresh mass) in leaves as a function of distance from the starting point of the sampling transect. Panels show: (a) total chlorophyll concentration, (b) carotenoid concentration, and (c) total pheophytin concentration. The leaf samples (indicated by black dots) were collected in July 2023. Solid lines denote the fitted linear regression models.

Significant positive correlations were observed between the total chlorophyll concentration of *G. biloba* leaves and distance in July ($R^2 = 0.396$, $p < 0.001$), August ($R^2 = 0.219$, $p < 0.001$), and September ($R^2 = 0.247$, $p < 0.001$). Correspondingly, strong positive correlations were observed between carotenoid concentration and distance in July ($R^2 = 0.413$, $p < 0.001$), August ($R^2 = 0.446$, $p < 0.001$), and September ($R^2 = 0.562$, $p < 0.001$). In July ($R^2 = 0.386$, $p < 0.001$), August ($R^2 = 0.260$, $p < 0.001$), September ($R^2 = 0.182$, $p < 0.001$), and October ($R^2 = 0.283$, $p < 0.001$), there were significant positive correlations between distance and the total pheophytin concentration.

5.2.5. Dependence of the pigment concentration on air pollution

The correlation between the pigments and air pollutant concentrations was studied using redundancy analysis (RDA, Fig. 14). The correlation between the first component (RDA1) and the second component (RDA2) was 0.994 and 0.135, respectively. RDA1 and RDA2 showed cumulative percentage

variations of 80.6% and 12.8%, respectively. Chl-*b* and the amounts of NOx, PM_{10}, and NO_2 showed negative relationships. The amounts of CO and total chlorophyll were negatively correlated. The concentrations of CO and Chl-*a* showed a negative connection.

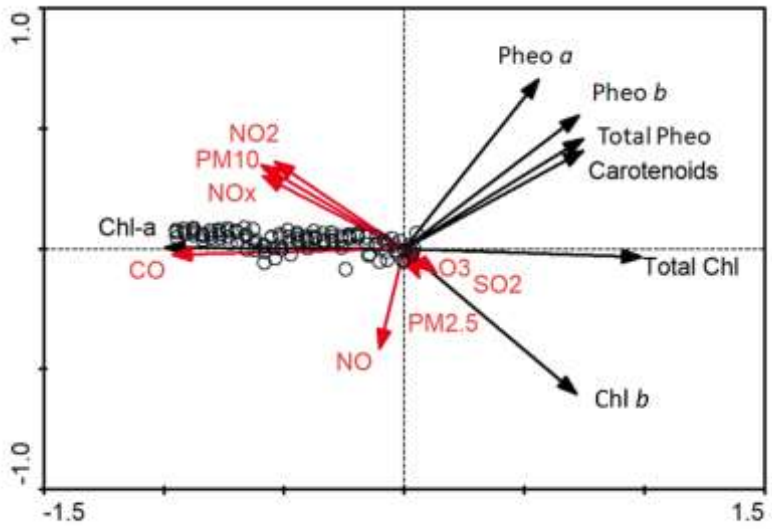

Fig. 14. Redundancy analysis biplot showing the interaction between air pollutants and pigment concentrations. Notations: black arrow – pigment concentration, red arrow – air pollutant concentration.

5.3 A comprehensive analysis of Pigment Integrity-to-Dust Ratio (PIDR) and Air Pollution Tolerance Index (APTI) as a bioindicator in urban trees

5.3.1 Site-Wise Variations in Biochemical Parameters

G. biloba leaves exhibited significant physiological and biochemical differences among the three sampling sites in Budapest. MANOVA results revealed significant disparities across the control site at Budatétényi Rose Garden, the moderate-traffic site at Dembinszky Street, and the high-traffic site at Rákóczi Avenue ($F = 5.52$, $p < 0.001$) (Table 4). Additionally, dust accumulation differed significantly ($F = 3.19$, $p = 0.003$), with the high-traffic location recording the highest loads, indicating the impact of increased vehicle emissions (Table 4). However, the choice of Budatétényi Rose Garden (control site) cannot be considered a healthy baseline because it is free of pollution; no urban site is entirely pollution-free, and the control trees themselves exhibited anomalous physiological values in September. It was selected for its distance from emission sources and the low frequency of car traffic. Control trees exhibited low relative water content (69.22% in September 2023 and 70.67% in September 2024). The pH of the extract of control tree leaf samples: 3.56, September 2023, 3.49, September 2024. Chl-*a* concentrations were the lowest for the control trees amongst the zones in September 2023 and 2024. These values most likely reflect the onset of natural senescence in *G. biloba*, a deciduous species. As senescence begins in September, a steady decline in RWC, total chlorophyll content, and pH is initiated and continues until senescence finishes and leaves are dropped. The senescence of *G. biloba* follows a typical pattern, and in temperate-zone urban conditions, it appears to be similar to that reported by Jurčević Šangut and Šamec (2024) and

Kinoshita et al. (2021). Because only four trees are in the control group, single-tree variance may influence the mean values and weaken the statistical comparison. For that reason, the word healthy is deliberately not used in this dissertation; the control site serves as a low-traffic reference point for comparison with pollution-sensitive trees, and all PIDR values based on September control data will be treated with caution.

Concentrations of chlorophyll *a* and *b* showed no apparent site-dependent patterns and did not follow a pollution gradient. In July 2023, moderate-traffic site trees exhibited the highest concentration of chlorophyll *a* (2.09 ± 0.53 mg g^{-1}), which was higher than that of the control site (1.95 ± 0.76 mg g^{-1}) and high-traffic site trees (1.40 ± 0.34 mg g^{-1}), contradicting our expectation. From 2023 to 2024, chlorophyll concentrations decreased at both traffic sites, most prominently at the moderate-traffic site (ΔChl-*a* = −0.57, ΔChl-*b* = −0.33) than the high-traffic site (ΔChl-*a* = −0.20, ΔChl-*b* = −0.13). This pattern supports cumulative pollution-induced chlorophyll degradation (Chl-*a*: $F = 9.29$, $p < 0.001$, Chl-*b*: $F = 5.55$, $p < 0.001$).

At the moderate-traffic site, total chlorophyll dropped dramatically (Δ = –0.90; $F = 7.56$, $p < 0.001$), indicating more severe pigment breakdown with continuous exposure. Carotenoid concentrations were significantly higher at the traffic-affected sites than at the control site ($F = 11.83$, $p < 0.001$). Both locations exhibited a decrease in levels from 2023 to 2024 (ΔD = –0.10; ΔR = –0.08) (Appendix Table 2). Pheophytin concentrations showed significant zone and time effects overall (Pheo-*a*: $F = 14.62$, $p < 0.001$; Pheo-*b*: $F = 8.06$, $p < 0.001$). However, Pheo-*a* at the moderate-traffic site in September 2023 (0.02 ± 0.06 mg g^{-1}) was substantially lower than at both the control site (0.10 ± 0.10 mg g^{-1}) and the high-traffic site (0.11 ± 0.07 mg g^{-1}), contrary to the expectation that more polluted sites accumulate more pheophytin

Both sites closest to traffic intersections scored higher on the APTI index than the control at every month included in the sampling ($F=3.12$, $p=0.003$). Between July 2023 and September 2024, the APTI index declined slightly at both traffic sites. The high-traffic site displayed a change (13.18→12.15) between the sampling months. Moderate-traffic site decline between the sample months of July and December. Between September 2023 and September 2024, the APTI index declined, with high traffic and marginal recovery observed at the moderate-traffic site. The pattern of reduction was most pronounced at the control site, and there were signs of recovery in APTI index measurements from September until the end of December.

Table 4 Results of APTI and pigment concentration and ANOVA analysis in the different sites (mean ± SD). Notation: Different superscript letters within the same sampling period indicate significant differences among sites according to Tukey's HSD test at $p < 0.05$.

Parameter	Sampling period	Studied sites			Results of ANOVA	
		High Traffic	Moderate Traffic	Control	F	P
APTI	Jul 2023	13.18 ± 1.46^{a}	12.39 ± 1.73^{a}	11.40 ± 1.34^{a}	3.12	0.003
	Sep 2023	12.62 ± 1.32^{a}	11.37 ± 3.77^{ab}	8.73 ± 6.10^{b}		
	Sep 2024	12.15 ± 1.72^{a}	11.44 ± 3.78^{ab}	8.16 ± 5.56^{b}		
Carotenoid, mg g^{-1} FM	Jul 2023	0.38 ± 0.07^{a}	0.48 ± 0.07^{a}	0.42 ± 0.14^{a}	11.8	<0.001
	Sep 2023	0.32 ± 0.05^{ab}	0.37 ± 0.12^{a}	0.22 ± 0.16^{b}		
	Sep 2024	0.25 ± 0.04^{a}	0.28 ± 0.14^{a}	0.23 ± 0.16^{a}		
Chlorophyll *a*, mg g^{-1} FM	Jul 2023	1.40 ± 0.34^{a}	2.09 ± 0.53^{b}	1.95 ± 0.76^{ab}	9.29	<0.001
	Sep 2023	1.24 ± 0.27^{ab}	1.79 ± 0.65^{b}	0.99 ± 0.76^{a}		
	Sep 2024	1.02 ± 0.27^{a}	1.20 ± 0.63^{a}	0.97 ± 0.77^{a}		
Chlorophyll *b*, mg g^{-1} FM	Jul 2023	0.77 ± 0.19^{a}	1.21 ± 0.36^{a}	1.17 ± 0.50^{a}	5.55	<0.001
	Sep 2023	0.72 ± 0.21^{ab}	1.11 ± 0.43^{b}	0.62 ± 0.50^{a}		
	Sep 2024	0.70 ± 0.21^{a}	0.89 ± 0.46^{a}	0.73 ± 0.57^{a}		
Total Chlorophyll, mg g^{-1} FM	Jul 2023	2.17 ± 0.53^{a}	3.30 ± 0.88^{b}	3.13 ± 1.25^{ab}	7.56	<0.001
	Sep 2023	1.96 ± 0.43^{ab}	2.90 ± 1.08^{b}	1.62 ± 1.26^{a}		
	Sep 2024	1.72 ± 0.48^{a}	2.08 ± 1.09^{a}	1.70 ± 1.33^{a}		
Pheophytin *a*, mg g^{-1} FM	Jul 2023	0.19 ± 0.05^{a}	0.24 ± 0.08^{a}	0.25 ± 0.11^{a}	14.6	<0.001
	Sep 2023	0.11 ± 0.07^{a}	0.02 ± 0.06^{a}	0.10 ± 0.10^{a}		
	Sep 2024	0.13 ± 0.03^{a}	0.07 ± 0.08^{a}	0.11 ± 0.10^{a}		
Pheophytin *b*, mg g^{-1} FM	Jul 2023	0.39 ± 0.08^{a}	0.50 ± 0.13^{a}	0.50 ± 0.23^{a}	5.36	<0.001
	Sep 2023	0.34 ± 0.07^{a}	0.35 ± 0.14^{a}	0.30 ± 0.25^{a}		
	Sep 2024	0.30 ± 0.05^{a}	0.28 ± 0.15^{a}	0.31 ± 0.23^{a}		
Total Pheophytin mg g^{-1} FM	Jul 2023	0.58 ± 0.13^{a}	0.74 ± 0.21^{a}	0.74 ± 0.34^{a}	8.06	<0.001
	Sep 2023	0.46 ± 0.12^{a}	0.37 ± 0.18^{a}	0.40 ± 0.34^{a}		
	Sep 2024	0.43 ± 0.08^{a}	0.35 ± 0.22^{a}	0.41 ± 0.33^{a}		

5.3.2 Pigment Integrity-to-Dust Ratio (PIDR)

In contrast to the control, temporal and spatial variations in PIDR-based stress classes were observed between the high-traffic site (Rákóczi) and the moderate-traffic site (Dembinszky) (Fig. 15). The distribution of individual leaves is reported to show within-site variability. PIDR stress-class proportions are summarised at the site level and sampling period (aggregated within individual trees), with the leaves nested within the trees (e.g., R1, R2). As a response, at high-traffic sites, there was a 20% rate of severe stress leaves, 36% low stress and 4% minimal to none, representing a 50% overall divergence from the control site reference median in that period. Moderate traffic sites exhibited a more polarised distribution, with 46.15% of samples in the moderate stress category and 38.46% in the low stress category, exhibiting an almost more significant divergence (53%) compared to high traffic sites, which indicates reduced resilience. There was a 47% discrepancy between the sample location at the high-traffic site and the reference site in September 2023, with PIDR predominantly classified as "low stress" (60%). Note that this did not reflect a decrease in biological stress from pollution, as the 2nd-3rd September 2023 saw a series of showers and thunderstorms in Budapest, according to historical data (Source: Historical Weather Data, http://weatherspark.com, 2023). Due to PIDR using the amount of dust on the leaf surface as the divisor, showers that wash away accumulated summer dust halve the measured dust, thereby increasing PIDR relative to the chlorophyll-to-phaeophytin signal, rather than signalling biological improvements. The September 2023 readings at high-traffic sites are therefore most likely due to rainfall and are best omitted for comparative, long-term interpretation of the PIDR value.

The moderate-traffic site in September 2023 showed a bimodal stress distribution: 31% of the samples fell into the severe stress category and 61.54% into the minimal-to-no stress category, resulting in a variance ratio relative to the reference median of 145% (PIDR = 2.51). This was also an artefact: Pheo-*a* values at this site for September 2023 approach zero (0.019 mg g^{-1}, below the lower detection limit of < 0.1 mg g^{-1}), which forces the ratio (Chl-*a*)/Pheo-*a* to be high, independent of the true plant condition. As indicated in Section 4.6, near-zero Pheo-*a* reflects degradation processes in a healthy population and is treated as a limitation when using ratios that are prone to inflation at the extremes (e.g., at or near 0). Therefore, this value is excluded from any PIDR calculation involving quantitative temporal values. This variation underscores physiological heterogeneity, possibly attributable to exposure to microenvironmental dust and pollution. At the high-traffic site, the proportion of leaves experiencing minimal-to-no stress decreased to 4% and shifted towards low (64%) and moderate (32%) stress in September 2024. This pattern reflects consistent instability in pigments and limited recovery potential. The moderate-traffic site, on the other hand, showed a more balanced stress distribution with an overall 80% deviance, despite being uncommon. Approximately 46% of the leaves had minimal-to-no stress, whereas 15% each had severe and moderate stress. Despite increased fluctuation, there is some consistency in the moderate-traffic area when compared to the prior year.

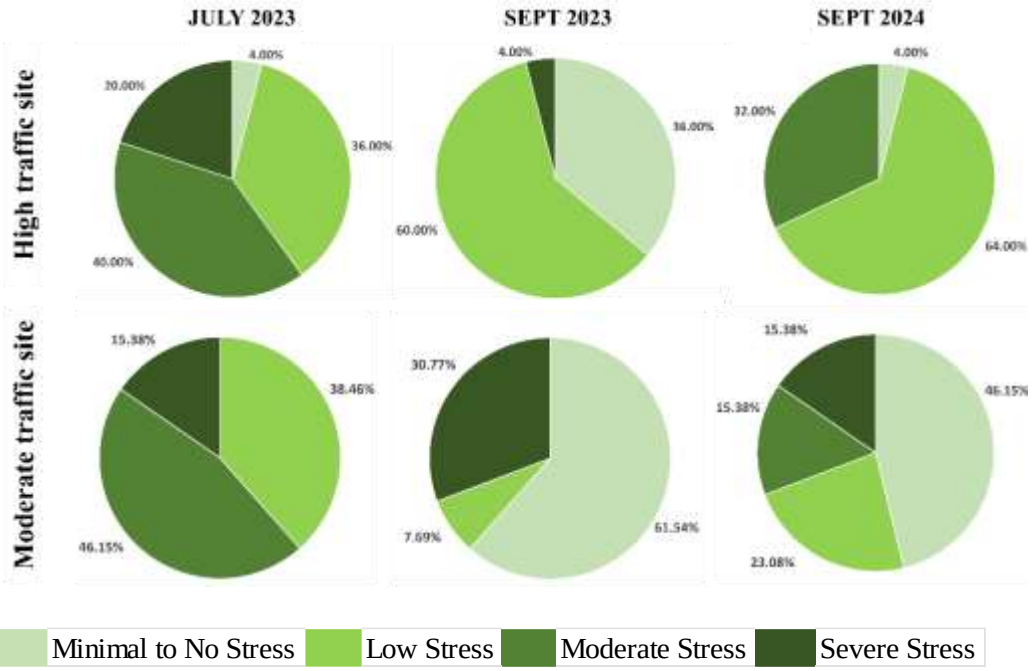

Fig. 15. Stress classifications of *G. biloba* leaves in moderate and high traffic sites and sampling dates July 2023, September 2023, and September 2024. Stress levels were classified as fixed fractions of the asinh-transformed control median: severe (≤0.20), moderate (0.20-0.50), low (0.50-1.0), and minimal-to-no stress (≥1.0×). Segment sizes indicate the proportion of samples in each group, emphasising regional and temporal differences in pigment stability. The moderate-traffic location had more stress signals that did not correlate linearly with traffic intensity, indicating local microenvironmental variation, pollutant and dust exposure, and physiological adjustment dynamics. This site contains higher PIDR classes, indicating stress response ranges.

5.3.3 Validation of PIDR through Air Pollutants

To evaluate PIDR's efficacy as a biochemical stress measure, it was compared to six major air pollutants (CO, NO_2, O_3, PM_{10}, $PM_{2.5}$ and SO_2) throughout three time periods: July 2023, September 2023, and September 2024 (Fig. 16) (Appendix Table 3). Raw PIDR values (Appendix Table 4). at the control site show a slight decline each period (2023 July PIDR = 1.70, 2023 September PIDR = 1.16, 2024 September PIDR = 1.08), which we attribute to the combined factors of a 49% decline in Chl-*a* (2023 July = 1.95 mg g^{-1}, 2023

September = 1.30 mg g^{-1}) due to natural seasonal senescence, coupled with a 127% accumulation of dust on foliage (2023 July = 3.41 µg cm^{-2}, 2023 September = 7.74 µg cm^{-2}), which reduces light transmission to the chloroplasts and progressively increases the dust load denominator of the PIDR formula, driving the gradual PIDR decline independently of pollution-induced pigment degradation. We believe that the higher value for the control site in the Z-score plot (Figure 16) is an artefact resulting from the single moderate traffic event (2023 September PIDR = 2.51) pulling the normalization of the overall control site values upwards and not reflecting the actual stress at the control site.

At the high-traffic location, CO was the dominant stressor in reducing PIDR. In September 2023, CO rose from 58.0 to 324.3 µg m^{-3} (+459%), and it fell to 193.4 µg m^{-3} by September 2024. Although CO diminished slightly, PIDR continued to fall to 0.522, paralleling a striking SO_2 rise from 2.43 to 25.43 µg m^{-3} (+946%). These two pollutants then acted as co-dominant stressors in year two, enhancing pigment loss due to cumulative stress. NO_2 at this location decreased from 27.7 in September 2023 to 12.7 µg m^{-3} by September 2024, so other stressors must be responsible for the continuing decline in PIDR.

In the moderate traffic location, NO_2 was greater in September 2023 (36.8 vs 27.7 µg m^{-3}) than in the high traffic volume location, indicating NO_2 was a more significant stressor at this site than at the high traffic volume site in September 2023. Unlike other particulate matter, NO_2 is a gaseous pollutant that is not removed by surface rainfall; hence, the moderate-traffic location exhibited a more genuine biological stress signal than the high-traffic location, despite both being exposed to the same September 2023 rainfall event. In September 2024, SO_2 rose sharply from 4.86 to 50.85 µg m^{-3} (+946%)-the greatest amount recorded among all sites in all time points. Together with NO_2

(25.5 µg m^{-3}), it contributed to a PIDR reduction to 0.109, the smallest PIDR recorded, again reinforcing long-term cumulative stress. Ozone followed the opposite gradient; the control location yielded the highest ozone levels (85.1 µg m^{-3}), followed by the moderate traffic location (76.6 µg m^{-3}) and the lowest was measured at the high traffic volume location (38.3 µg m^{-3}). Ozone concentrations were lowest at the high-traffic site, consistent with NO_x titration; traffic-generated nitric oxide (NO) reacts with O_3 to produce NO_2, simultaneously depleting ozone and elevating nitrogen dioxide concentrations at high-traffic locations. At traffic locations in September 2024, ozone and nitrogen oxides fell to undetectable levels due to both seasonal patterns and increased traffic levels. At the control site, PIDR decreased from 1.703 to 1.156 and then to 1.082 while NO_2 dropped precipitously to 4.76 µg m^{-3} in September 2024 and CO remained undetectable. This decrease in PIDR is not caused by air pollution but by leaf senescence over time, that is, a steady decline in Chl-*a* and a buildup of dust, as described previously.

A significant positive correlation between NO_2 and PIDR was observed at a high traffic site. Higher NO_2 levels were expected to indicate lower PIDR, since NO_2 is a stress factor, suggesting stressed trees. PIDR should decrease with increasing NO_2. In September 2023, the highest NO_2 reading was 27.69 µg m^{-3}, and the PIDR was 1.146. However, this is not an actual biological change: rainfall on September 2nd and September 3rd washed accumulated dust from the leaf sample foliage just before the September 2023 sampling. This rain meant less dust settled on the leaf surface, and therefore, the denominator in the PIDR was artificially reduced, inflating PIDR beyond the tree's actual stress levels. Therefore, the positive correlation found was a byproduct of rainfall events at the sampling site rather than indicative of NO_2 having stress-reducing properties (Appendix Table 4). The relationship between CO and PIDR was strongest at the high-traffic site and, as expected,

was negatively oriented, with r = -0.971, p = 0.155, and β = -0.80 (indicating that higher CO values were associated with lower PIDR values and a more stressed tree). We determined the $PM_{2.5}$ of all pollutants to be the single strongest predictor with a negative correlation with PIDR at the control site (β = -1.00) and thus higher background levels of pollution would mean lower PIDR and even the reference forest is being stressed by pollution, although the near-unit value should be viewed cautiously: as it is based on three temporal data points coupled with using Z-scores (which normalizes the variables and naturally inflation effect sizes more the stronger the relationship and is best seen here as an indicator of the direction than accuracy.

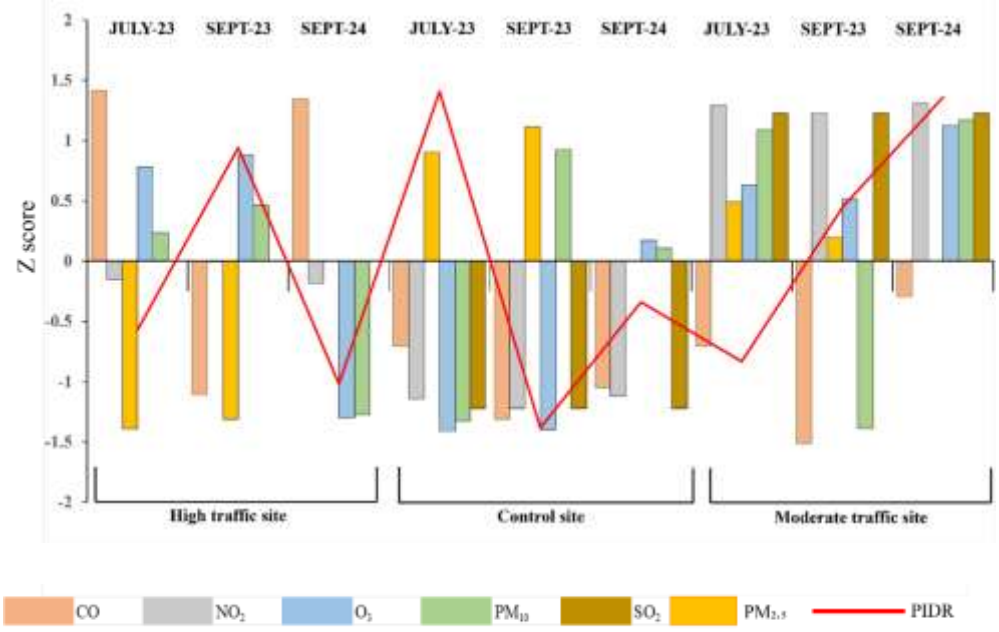

Fig. 16. Temporal trends in standardised air pollutant concentrations and PIDR across urban areas. Bar graphs illustrate the Z-scores of significant air pollutants throughout zones in different sites for three temporal intervals: July 2023, September 2023, and September 2024. The red line shows zone and time-specific PIDR changes. PIDR measures the temporal and spatial relationships between urban air pollution levels and plant physiological responses, highlighting site-specific and seasonal variations.

5.4 Assessment of air pollution tolerance of *H. helix* in urban areas of Debrecen city, Hungary

5.4.1 Differences in parameters among sites and seasons

Ascorbic acid concentration, chlorophyll and carotenoid concentration, and dust concentration on the leaf surface of *H. helix* varied significantly between sites and seasons (Appendix Table 5). Substantial variations in dust concentration were observed compared with the control. The disparities were favourable throughout the seasons, with the most significant effects noted in winter, and modest differences in both autumn and spring (Fig. 17).

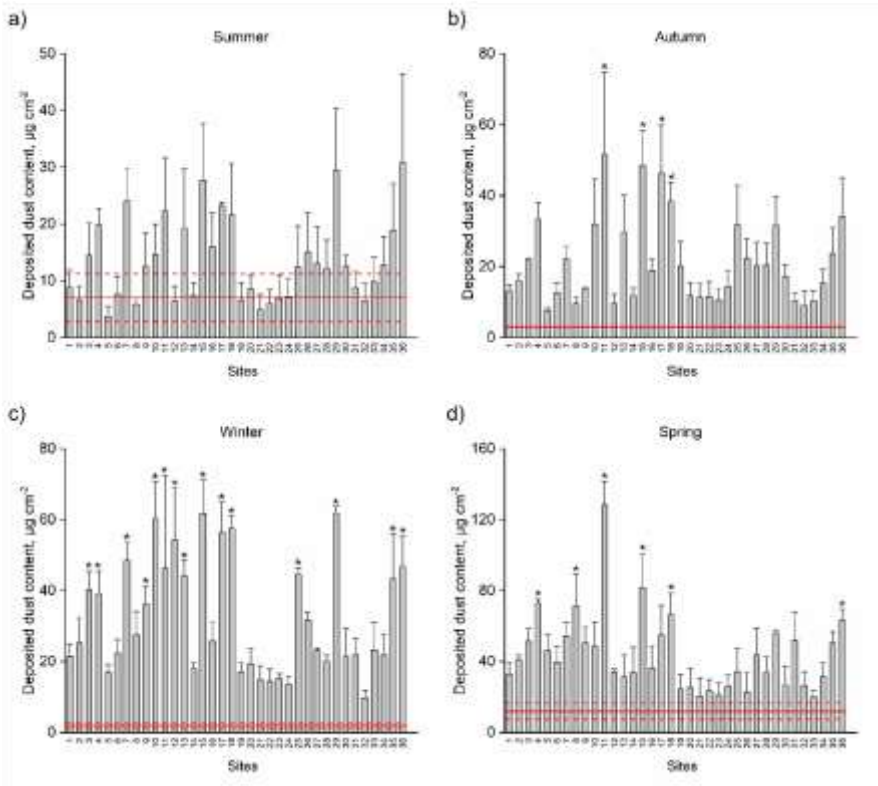

Fig. 17. Deposited dust concentration on leaf surfaces in summer (a), autumn (b), winter (c), and spring (d). Red lines indicate the mean ± standard error of the control, and significant differences ($p < 0.05$) from the control sample are marked with an asterisk.

Compared with the control, there were notable variations in chlorophyll concentration, but these were limited to a few locations during the summer, autumn, and spring seasons. The chlorophyll concentration varied around the control level throughout the seasons (Fig. 18).

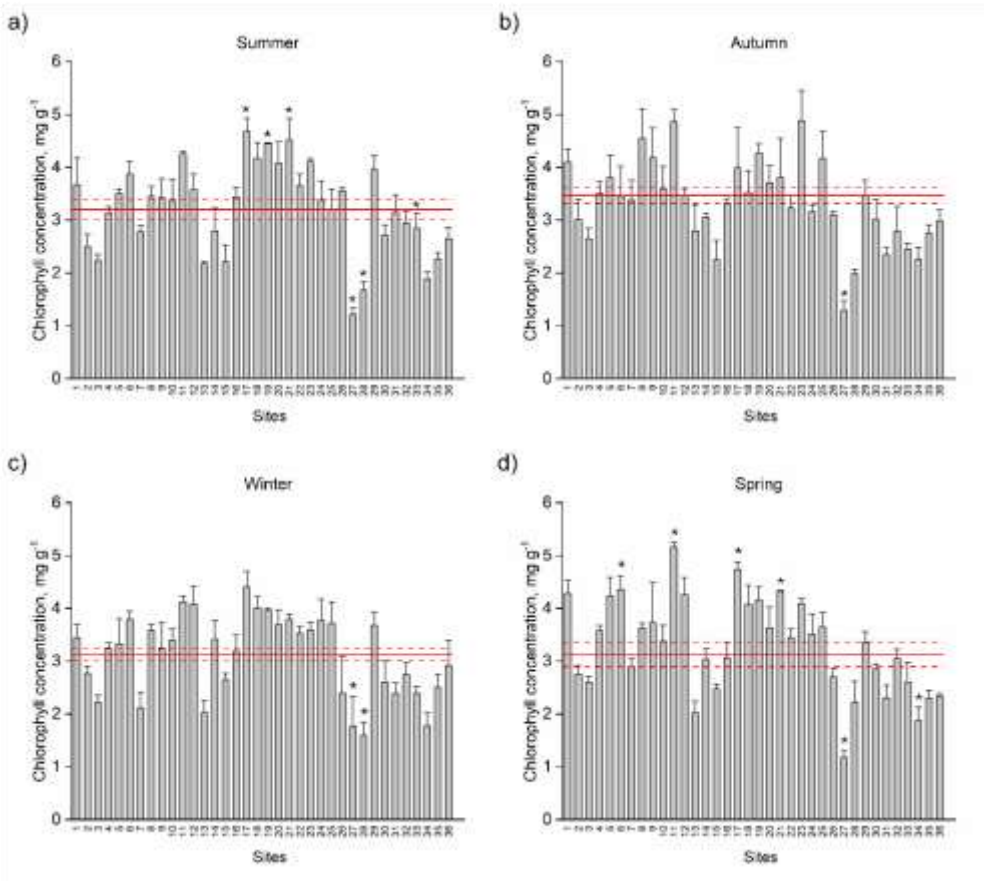

Fig. 18. Chlorophyll concentration of leaf samples in summer (a), autumn (b), winter (c), and spring (d). Red lines indicate the mean ± standard error of the control, and significant differences ($p < 0.05$) from the control sample are marked with an asterisk.

In autumn, winter, and spring, there were notable variations in carotenoid content as compared to the control. The carotenoid concentration varied

around the control level across seasons, although not significantly ($p < 0.05$) (Fig. 19).

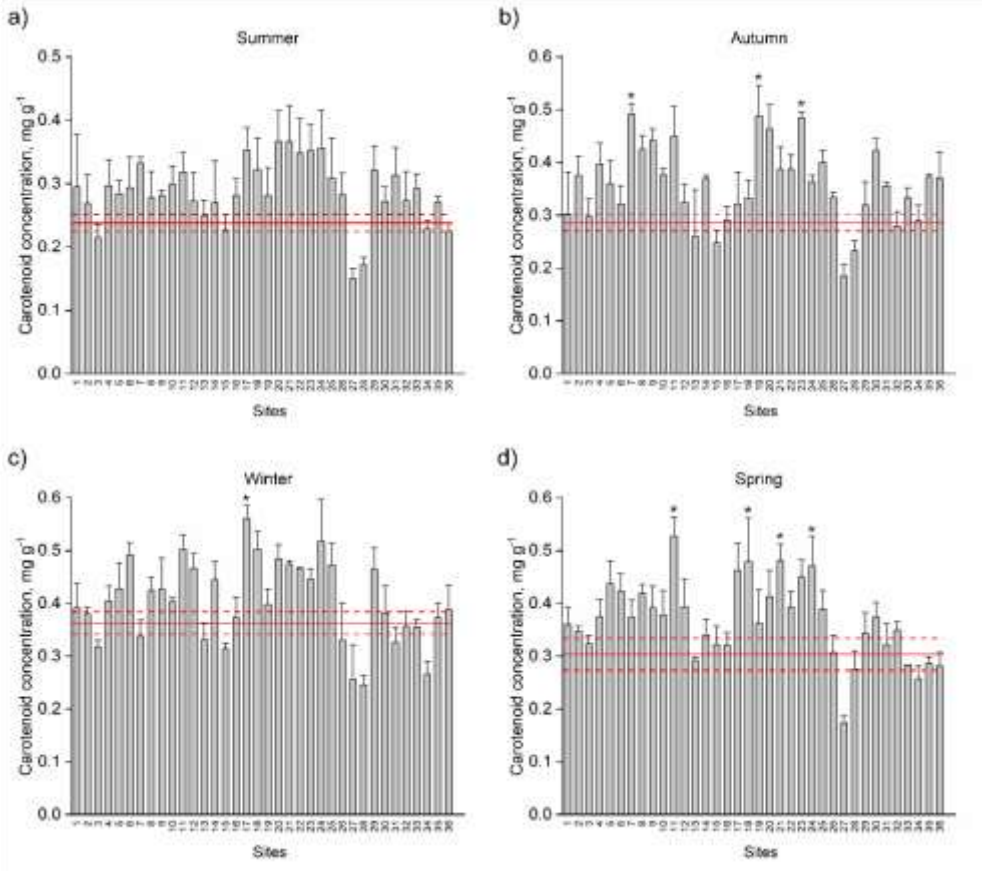

Fig. 19. Carotenoid concentration of leaf samples in summer (a), autumn (b), winter (c), and spring (d). Red lines indicate the mean ± standard error of the control, and significant differences ($p < 0.05$) from the control sample are marked with an asterisk.

Ascorbic acid concentrations differed significantly from the control only during the spring. The concentration of ascorbic acid varied around the control throughout the seasons, though not considerably ($p < 0.05$), except in autumn, when it exceeded the control at all locations (Fig. 20).

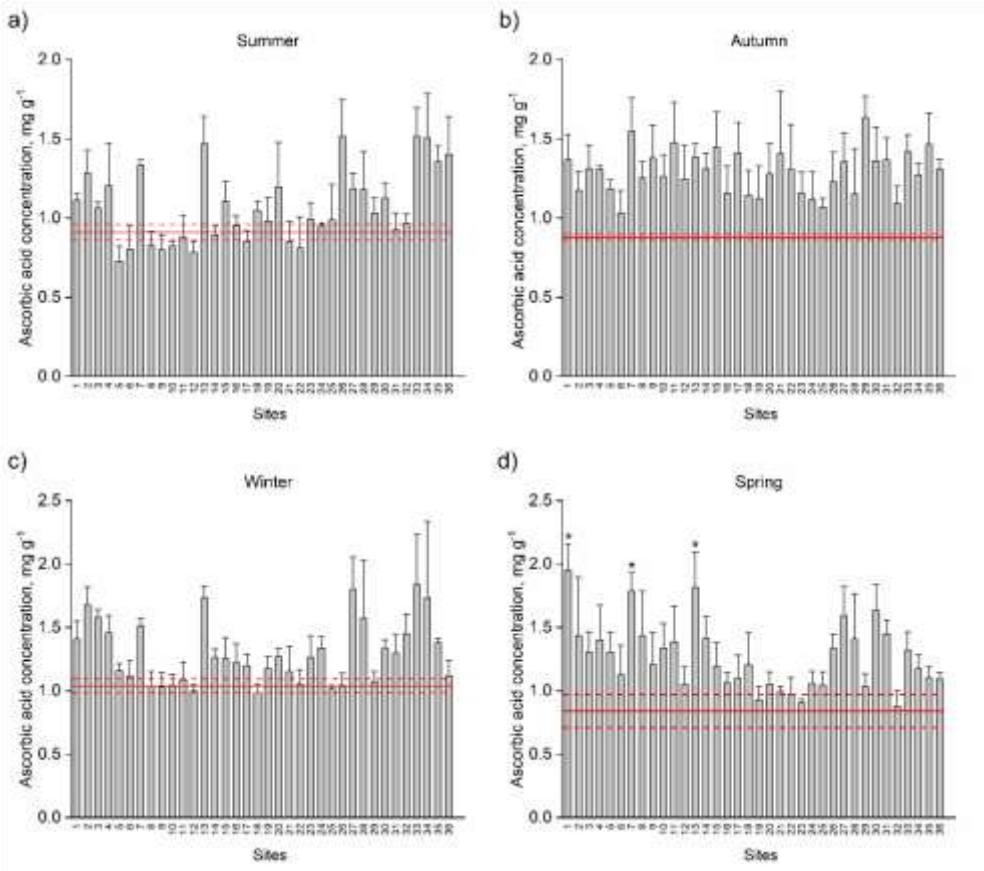

Fig. 20. Ascorbic acid concentration of leaf samples in summer (a), autumn (b), winter (c), and spring (d). Red lines indicate the mean ± standard error of the control, and significant differences ($p < 0.05$) from the control sample are marked with an asterisk.

5.4.2 Spatiality in the physiological parameters

The measured parameters (dust, chlorophyll, carotenoid, and ascorbic acid carotenoid concentration) showed a significant association with the distance from the city centre (Appendix Table 6). Regression analyses were conducted following the correlation analysis to investigate the spatial relationships between the assessed parameters and proximity to the city centre. Notable

spatial correlations were identified between distance and dust accumulation on leaf surfaces, as well as between distance and physiological indicators.

The accumulation of dust on leaf surfaces declined with increasing distance, showing significant correlations during the winter and spring seasons ($p < 0.01$). In contrast, the correlations observed in summer and autumn were weak and did not reach statistical significance (Fig. 21). Similarly, chlorophyll and carotenoid concentrations showed notable negative correlations with distance. Autumn, winter, and spring showed significant correlations with chlorophyll ($p < 0.05$), whereas autumn and spring showed significant correlations with carotenoid content ($p < 0.05$). Conversely, the concentration of ascorbic acid demonstrated a significant positive correlation with distance from the city centre, increasing with greater distance, especially during the winter season ($p = < 0.01$) (Table 5).

Table 5. Regression parameters for the relationship between distance from the city centre and measured physiological and environmental variables across seasons.

	Summer		Autumn		Winter		Spring	
	p	R^2	p	R^2	p	R^2	p	R^2
Dust	0.215	0.031	0.069	0.064	0.007*	0.192	0.001*	0.261
Chl	0.116	0.071	0.030*	0.131	0.047*	0.111	0.032*	0.128
Car	0.249	0.039	0.048*	0.110	0.069	0.094	0.038*	0.121
AAC	0.120	0.070	0.131	0.066	0.007*	0.195	0.257	0.038

Notations: Chl = concentration of Chlorophyll, Car = concentration of carotenoids, AAC = concentration of ascorbic acid.

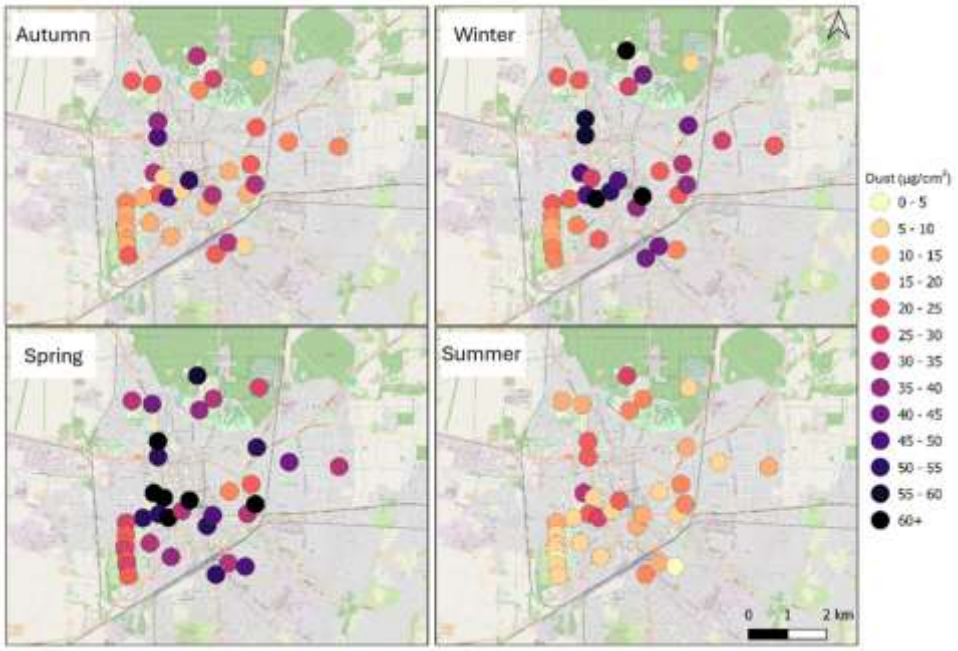

Fig. 21. Spatial distribution of particulate matter in the city

Leaf surface area and deposited dust showed a significant negative relationship ($p < 0.001$) across all seasons (Fig. 22). The linear regression accounted for a minimal percentage of the variance in each case, suggesting a limited predictive association.

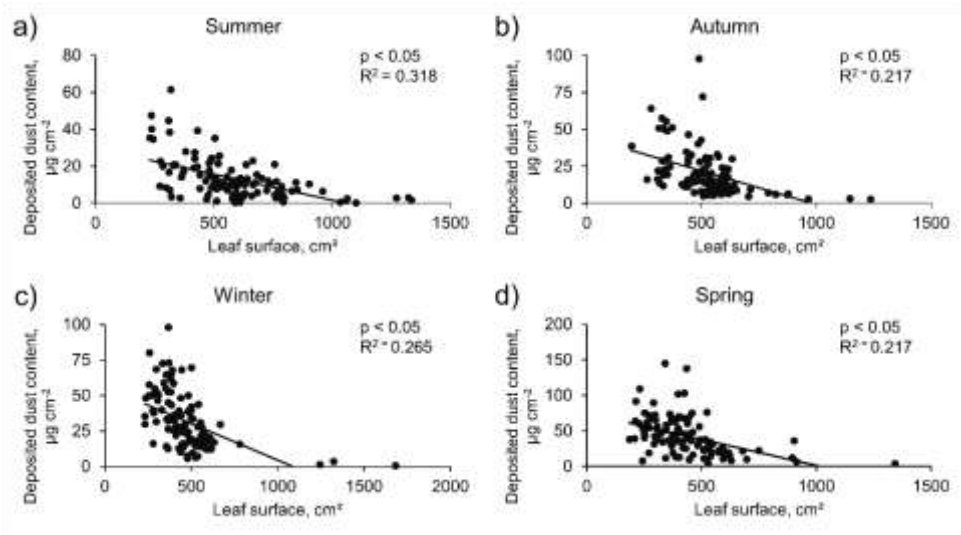

Fig. 22. Scatter plot with regression line between leaf surface and deposited dust content in a) summer, b) autumn, c) winter, and d) spring

5.4.3 Principal component analysis

Principal component analysis demonstrated distinct seasonal variations in the correlations between leaf surface dust deposition, pigment content, relative water content, pH, and ascorbic acid (Fig. 23; Appendix Table 7-10).

During the summer season, the initial two principal components accounted for 68.3% of the overall variance, with PC1 contributing 46.3% and PC2 contributing 22.0%. Principal Component 1 distinguished pigment-related variables, including chlorophyll and carotenoid, from dust, relative water content, and ascorbic acid. PC2 was predominantly characterised by an inverse correlation between dust and relative water content, with dust loading negatively associated and relative water content positively associated along this axis.

During the autumn season, the initial two components accounted for 55.5% of the overall variance. PC1 differentiated pigment variables from dust and ascorbic acid, whereas PC2 was predominantly defined by negative loadings on dust and ascorbic acid, alongside a positive loading on pH. Relative water content exerted a moderate influence on PC2 and was clearly distinct from dust.

In the winter, the first two components exhibited the maximum explained variance (71.9%). Principal Component 1 exhibited a significant correlation with chlorophyll and carotenoid, indicated by positive loadings, while ascorbic acid demonstrated a negative loading. PC2 was characterised by a strong correlation between dust and relative water content, with positive loadings, whereas pH showed loadings in the opposite direction.

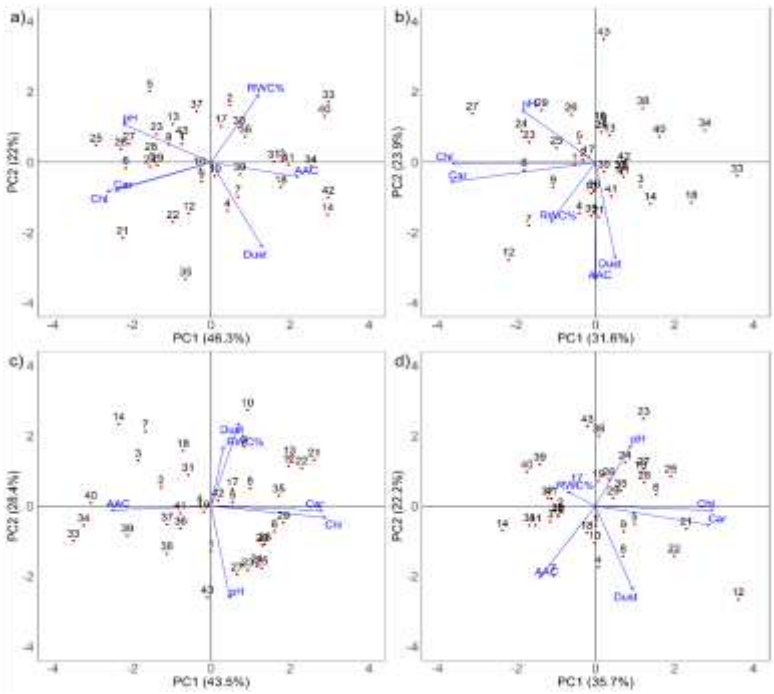

Fig. 23. PCA biplot of sample sites in a) Summer, b) Autumn, c) Winter, and d) Spring

5.4.4 Air Pollution Tolerance Index

The APTI values showed notable variation relative to the control in specific urban locations, with the peak incidence of impacted bus stops observed during the winter season (Fig.24). (Appendix Table 5). The APTI values ranged from 6.6 to 12.0 across all seasons, indicating *H. helix* is sensitive. The peak APTI values occurred during the winter season (Fig. 24). APTI showed notable seasonal variation. The post hoc Bonferroni analysis indicated no significant differences between summer and autumn, or between winter and spring. The observed values increased from summer to winter, then decreased in spring.

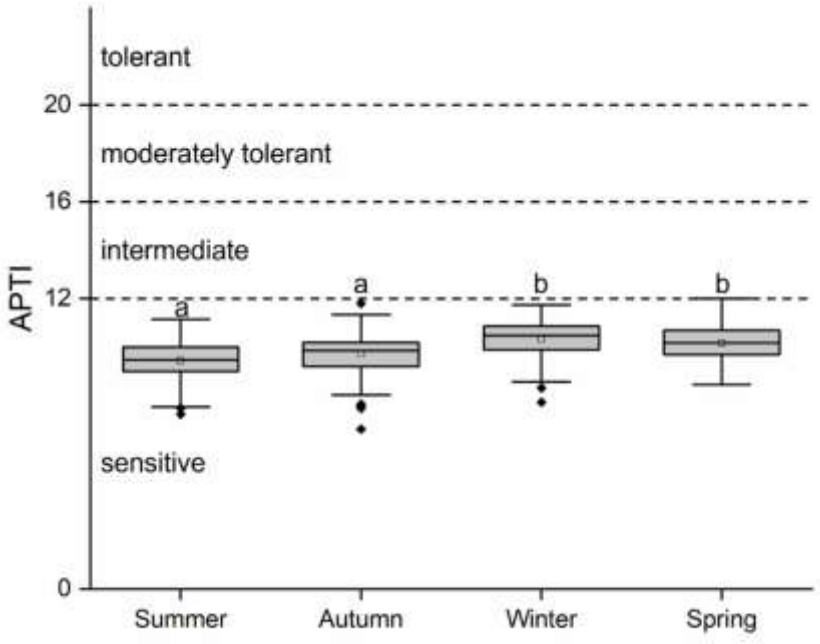

Fig. 24. APTI results for *H. helix* leaves across all seasons. The different letters above the boxplots indicate significant differences between the groups ($p < 0.05$). APTI Value Degree of Tolerance Reference by Singh et al. (1991).

5.4.5 Correlation with air pollutants and meteorological data

Carotenoid concentrations measured at different locations (Appendix Table 4) showed a positive correlation with carbon monoxide levels from meteorological and air pollution data (Appendix Table 10-12). Conversely, our findings indicate a negative correlation between positive correlation between carotenoid concentration and wind speed. The relationships observed between carotenoids and various air pollutants, including NO, NO_2, NOx, PM_{10}, $PM_{2.5}$, and SO_2, were either weak or inconsistent. While the remaining parameters exhibited weaker correlations with the values recorded at the stations than chlorophyll did, distinct patterns emerge: within the examined region, 31, dust, chlorophyll, and ascorbic acid all showed negative correlations with CO.

6. Discussion

6.1. Effects of COVID-19 on the level of air pollution

The annual average PM_{10} concentrations during the period prior to COVID-19 (2018-early 2020) varied across stations, reflecting their different locations relative to heavy traffic. Stations S1 and S2 were located in areas with higher traffic density, and concentrations were higher than at S3, the reference site with relatively less local traffic. During the COVID-19 pandemic, from March 2020 to February 2022, S2 and S3 concentrations were lower due to decreased urban mobility. At S1, however, PM_{10} concentrations rose during the second spring (March 2021, 57 ± 11 μg m^{-3}, April 2021, 66 ± 14 μg m^{-3}) after an initial decrease in March 2020 (Bodor et al., 2020; Varga, 2020), even though mobility continued to be reduced. Therefore, at individual urban sites, meteorology, not just emission reduction, can have a controlling impact on the trends of PM_{10} concentrations. Road traffic was the emission source at all three monitoring sites; the surrounding areas are devoid of substantial industrial activity. It must be noted that S3 (Debrecen Klinika Campus) operated almost normally during the lockdown phases, while most other workplaces were less active, which could explain why the reduction in PM_{10} related to the epidemic's lockdown measures was less pronounced than in S1 and S2. In spring 2021, S1 showed elevated PM_{10} levels due to light winds and a stable boundary layer during the second lockdown, which favoured the buildup of pollution near a major traffic junction and railway station (Bodor et al., 2020; Varga, 2020).

6.1.1 Meteorological modulation of PM_{10} dynamics

Our results show that wind speed, wind direction, and rainfall levels influenced PM_{10} levels measured at the stations in Debrecen, sometimes more than the effects of the lockdowns and reduced emissions. This is due to dry and warm conditions at the beginning of 2020 before the start of the restrictions, together with generally favourable N and NW winds that helped lower air pollution before movement restrictions were introduced and unfavourable atmospheric conditions in certain lockdown months, reducing the impact of lockdowns and reduced emissions (Bodor et al., 2020; Menut et al., 2020; Varga, 2020). Dominantly N, NW and NE wind directions for the meteorological station at M1 correlate with increased PM_{10} concentrations at both M1 and M2. Such wind conditions help transport regionally enhanced particulate pollution originating from the E, from agricultural activities, residential heating, and other activities, into the Debrecen urban area (Pásztor et al., 2016). Our observations stress the importance of considering meteorology in all analyses focusing on PM_{10} dynamics and the effectiveness of emission control interventions - in the short term with the COVID-19 lockdowns, but also in long-term air quality policymaking.

The pandemic-induced lockdowns produced varying PM_{10} levels across countries. Strict restrictions on movement led to a notable reduction in PM_{10} in Poland and Slovakia (Filonchyk et al., 2021), and S2 and S3 showed reductions consistent with some of those findings. Strictdowns resulted in 20%-40% reduction of BC in the most polluting countries in Europe and 11% BC reduction across Europe as a whole (Connerton et al., 2020; Evangeliou et al., 2021), but resulted in a range from a 40%-60% to zero reduction or even a 20%-30% reduction depending on meteorology, pollution source structure and stringency of lockdown measures (Bontempi et al., 2022; Dantas et al.,

2020; Zangari et al., 2020). Such a mixed global effect has also been demonstrated in Madrid and Milan (Baldasano, 2020; Collivignarelli et al., 2020), as well as in other regions (Rahman et al., 2021; Bray et al., 2021; Ropkins & Tate, 2021; Volta et al., 2022). Emissions dominate over meteorology in European cities, while in China, sources of pollution (agriculture, households, industry, power plants) had a greater impact on PM levels under restrictions than in European cities (Menut et al., 2020; Pei et al., 2020). Despite decreases in traffic, O_3 levels rose in European cities owing to reduced titration of ozone by NO_x, indicating that pollutants respond differently to reduced emissions (Barua & Nath, 2021).

The COVID-19 period demonstrated the strong dependence of anthropogenic emissions on urban PM_{10} levels, while also confirming the often-overriding influence of weather conditions at specific locations or during certain months. Plant-based biomonitoring represents an important complementary method because while instrumental monitoring measures short-term pollen loads (hours or days), photosynthetic pigments and pollen dust accumulation measure more prolonged (weeks to months) exposure to pollutants. In this sense, the biological indicators can provide a better picture of the chronic load of pollen and urban dirt pollution as a relevant aspect of physiological state for trees and therefore reduce reliance on time-dependent and episodic pollution measuring tools such as dust monitors and passive samplers which can only measure pollution over specific, short timeframes and can easily show large variations due to changing wind direction or other unpredictable meteorological variables (Chaudhuri & Roy, 2024; Molnár et al., 2020b).

6.2. Pigments as indicators

In Debrecen, the seasonal fluctuations in photosynthetic pigment concentrations of *G. biloba* leaves displayed a pattern of progressively increasing chloroplastic senescence typical of the autumnal development of this deciduous species. From July to October, Chl-*b* levels declined progressively, in correlation with reduced daytime length and lower ambient temperatures, signalling a reduction in the light-capturing ability of leaves as they aged (Kinoshita et al., 2021; Xie et al., 2019; Yang et al., 2010). Similarly, Chl-*a* and total chlorophyll concentrations declined over the study period, which can be attributed to the well-established degradation of chlorophylls during autumn senescence in deciduous plants (Lichtenthaler, 1996; Shi et al., 2012; Jurčević Šangut & Šamec, 2024). Carotenoid concentrations underwent much less pronounced changes between July and October compared to the chlorophylls. This resistance to decay can be understood in terms of the complementary roles that carotenoids fulfil as accessory pigments that expand the range of absorbed light and photoprotectors. Carotenoids play an important role in photoprotection; therefore, their protective function against the effects of active oxygen species continues to be critical even after photosynthetic pigment degradation proceeds further, which enhances overall oxidative susceptibility of the ageing leaves to further damage (Demmig-Adams & Adams, 1996; Sarijeva et al., 2007; Falcioni et al., 2023). A concurrent downward trend in ascorbic acid alongside chlorophyll and carotenoid concentrations suggested an increasing susceptibility of ageing *G. biloba* leaves to oxidative stress at the end of the 2022 growing season.

Pheophytin content was maximum in July and declined through October, reflecting early accumulation of this chlorophyll degradation intermediate during the onset of senescence, with rapid conversion to pheophorbide by pheophytinase in late fall (Hörtensteiner et al., 2009; Matile et al., 1987). The Chl-*a*/Pheo-*a* ratio increased from July (5.18 ± 0.28) to October (19.36 ± 4.3), representing the cumulative effect of chlorophyll degradation over that period. The relative increase in intact chlorophyll as senescence proceeds has a strong corresponding negative effect on pheophytin accumulation. This was consistent with an inverse relationship between total chlorophyll and pheophytin, as reported by Yang et al. (2010) and Shi et al. (2012) for the seasonal senescence of *G. biloba* leaves, and reinforced the use of pheophytin as a reliable marker of senescence-related stress. Along with the decline in chlorophyll, ascorbic acid levels also decreased, indicating that plants became increasingly vulnerable to oxidative stress, a finding that correlates with ascorbic acid's function as the major non-enzymatic antioxidant buffer in woody plants (Bilska et al., 2019; Menser, 1964).

The mean pigment values determined in this study may be interpreted in relation to comparable data in the existing scientific literature, with several key points regarding methodological variance. First, the mean concentration of 0.54 mg g^{-1} fw for Chl-*a* in Debrecen is less concentrated compared with those found by Lichtenthaler et al. (1981), who recorded values of 12.5 mg g^{-1} and Wang et al. (2023), who found 11.19 mg g^{-1}. However, this comparison is misleading due to disparities in methods e. g., extraction using ethanol, as performed herein, as opposed to the acetone usually preferred by previous studies by (Lichtenthaler, 1987; Wellburn, 1994), sample developmental stage (young 1-2-year-old urban ornamental trees were studied here, whereas older established plants were sampled by the authors above) and measurement units

(fresh-weight basis herein vs dry-weight basis for the latter authors) (Lichtenthaler, 1987; Wellburn, 1994). Second, the 0.39 mg g^{-1} fw mean Chl-*b* value detected in Debrecen falls within the range found by Xu et al. (2011) for young leaves of *G. Biloba* in the early summer (5.11 ± 1.84 mg g^{-1} fw) and Yang et al. (2010) for leaves collected in midsummer (4.3 ± 1.2 mg g^{-1} fw), suggesting that the plants sampled in the current study are in a physiological stage of growth. Kharbech et al. (2024) observed that Chl-*b* concentration declined noticeably as senescence advanced, and Shi et al. (2012) noted the decrease of Chl-*b* concentration under pollution. Both studies, including this one (Fig. 10), provided clear evidence that Chl-*b* levels decreased. Zhou et al. (2017) highlighted that factors such as light intensity and nutrients alter chlorophyll content differently across tree populations (Table 4) but, despite these disparities, provided no evidence of pollution-related effects on chlorophylls, with the standard Deviations indicating high variability within and between populations. Furthermore, the seasonal reduction in carotenoids is due to a decrease in the demand for these pigments to dissipate harmful levels of irradiance in autumn, as less UV radiation is present and the plant slows its processes. Elevated levels of carotenoids have long been thought to serve adaptive roles in response to intense irradiance and UV-B exposure (Sarijeva et al., 2007; Pandey et al., 2003; Demmig-Adams & Adams, 1996).

The relationship between abiotic factors and pigments provides insight into the physiological strategy of *G. biloba* under the stressors found in urban environments. In the early period, both Chl-*a* and CO showed significant negative correlations, and Chl-*b* showed strong negative correlations with NOx, PM_{10}, and NO_2. The chlorophyll-CO association in the sampled trees is probably due to the common occurrence of pollutants emitted from the street side and to the fact that CO correlates well with NO_2, NOx, and particulate matter. Therefore, CO does not directly affect pigment metabolism. Studies

investigating CO effects on chlorophyll metabolism in urban trees under ambient urban conditions have not found direct effects of CO on pigment synthesis, and these conclusions have been based on extrapolations from laboratory-scale studies on CO's interaction with *Arabidopsis* iron metabolism under controlled conditions (Kong et al., 2010).

CO exceedances increased in October, which may reflect increased traffic volumes associated with university studies commencing and other activities in the region near the railway station. Indeed, these findings support the finding that pollution is influenced by localised pollution sources, behaviour of traffic, differences in microenvironment (between stations) and other activities happening in urban settings, as found in the significant differences in NO_2, NOx and CO between the two sampling stations (Sæbø et al., 2012).

We observed lower average pigment content during most months at locations closest to the main traffic intersection (the pollution gradient origin). The distance to the pollution source in this study is considered a spatial proxy for the integrated gradients of traffic-related pollution, microclimate, and vegetation structure, rather than a direct influencing variable on its own (R_2=0.18-0.56). Therefore, we are associating the pollution gradient with the pigment content of moss samples, not a causal relationship based solely on distance. Furthermore, correlation strengths may be characterised as modest (R_2=0.18-0.56), given field-based studies with environmental variability as indicated by Rai (2016), Sæbø et al. (2012) and Singh et al. (1991).

The taller buildings around the roadside traffic count had already minimised the dispersal of traffic pollutants at that major interchange. The urban-canyon effect, in which tall, narrow buildings limit air movement and create a heat and pollutant trap, has been observed elsewhere in Europe (Tsai et al., 2015; Salma et al., 2020). In the first few days of exposure to minor pollution,

increases in chlorophyll concentration have been interpreted as a transient physiological adaptation rather than genuine tolerance (García-Sánchez et al., 2019). However, prolonged exposure to pollution stress triggers instability in chlorophyll and phaeophytins. It is therefore advisable to use chlorophyll as an indicator only if the exposure duration is consistent. According to recent literature, pollution stress, sulfur dioxide (SO_2) and particulate matter (especially $PM_{2.5}$ and PM_{10}) cause a breakdown in plant pigments and a reduction in chlorophyll and photosynthetic activity of several common urban plant species, including *G. biloba* (Bao et al., 2015; Kinoshita et al., 2021). For instance, Bao et al. (2015) concluded that the total amount of chlorophyll and the rate of photosynthesis of young trees of *Sophora japonica* declined logarithmically with an increasing amount of dust falling on them, and a large number of review papers concluded that PM air pollution is related to pigment degradation of many common urban plants (Kinoshita et al., 2021). Macro-morphological leaf properties, such as leaf area, perimeter, and width-to-length ratio, were recently highlighted as important selection criteria for identifying the most resilient urban bioindicators, and *G. biloba* meets these criteria (Rodríguez-Santamaría et al., 2022). From our study results, it is recommended that air quality monitoring in urban areas needs to be ongoing so as to protect urban trees, and it should support the hypothesis that SO_2 and PM_{10} are the principal air pollutants involved in pigment degradation among trees (Bao et al., 2015; Kinoshita et al., 2021).

Whereas the Debrecen findings relate specifically to leaf-level pigment and pollution-pigment relationships in a single season, the *G. biloba* study was conducted at different locations exhibiting different traffic levels and within the same growing season in two consecutive years, using Pigment Integrity-to-Dust Ratio (PIDR) for the first time as an urban pollution proxy. This study took place in an urban environment with differing levels of traffic: a busy city

centre location on Rákóczi Avenue, a medium-level road on Dembinszky Street, and the Budatétény Rose Garden as an undisturbed control. Shah et al. (2019) reported chlorophyll loss in roadside London plane trees due to sustained dust exposure over many years, while Bierza & Bierza (2024) observed strong relationships between dust content and urban-rural position in a Central European cityscape. Simon et al. (2011) reported that trace-metal-polluted urban dust affects pigment patterns and leaf physiological parameters in *Tilia cordata* trees. PIDR could result from oxidation stress, such as when O_3 (Agathokleous et al., 2023; Gottardini et al., 2014; Sheng & Zhu, 2019) and NOx pollutants lead to chlorophyll loss through demetallation and pheophytin accumulation or even mechanical stress, with dust coverage reducing the received irradiation and blockages in stomatal pathways intensifying local oxidative stress (Hirano et al., 1995; Kováts et al.,2021; Meravi et al.,2021; Shah et al., 2019). PIDR was found to be better than APTI at revealing spatial differences and temporal differences between sampling months (September) across all four investigated locations in the Budapest study. At the heavy-traffic sites, reduced PIDR was associated with greater NO_2 pollution (Table 4) because NOx pollutants inhibit photosynthesis (Sonti et al., 2021; Srivastava et al., 1975), reduce stomatal function (Agathokleous et al., 2020), and directly damage foliar processes (Sonti et al., 2021). Cotrozzi (2020) stated that SO_2 degradation begins with magnesium displacement from chlorophyll, as chlorophyll decreases and pheophytin increases, accompanied by reactive oxygen species-driven pigment destruction (Kharbech et al., 2024; Teng et al., 2021). Increased carotenoid concentration at the heavy-traffic site suggested photooxidative damage; previous work has confirmed that such concentrations rise under urban pollution exposure (Hubai et al., 2021; Mukhopadhyay et al., 2024). The temporal profile revealed distinct differences between September 2023 and 2024. PIDR found that plants on the

medium-traffic site had not only deteriorated (as revealed by APTI) but also partially recovered, whereas APTI simply mirrored a downward trend (Figure 15). Similar patterns have previously been observed in changes in chlorophyll content, carotenoid levels, and dust PM in several other urban tree species across different seasons (Moura et al., 2024; Sanusi & Livesley, 2020; Son et al., 2022).

Comparing PIDR with APTI, the indices proved more complementary than competitive. The APTI is a species index calculated from a sum of relative leaf water content, the amount of Ascorbic acid, Total Chl content and the overall pH level that produces classification in tolerance classes for each of the species in the respective sites (Molnár et al., 2020b), making it possible to differentiate tolerant species and even to compare ranking between different sites (Correa-Ochoa et al., 2022). However, the relative sensitivity to plant-pollutant biochemical interactions can be reduced by smaller differences, as these four parameters can be influenced by unrelated pollution sources, e.g., differences in microclimate, day-length cycles, and the phases of plant life and leaf development (Kováts et al., 2021). The comparison made by relating the pigment composition (chlorophyll and pheophytin) together and on the same site with the external factor of foliar dust can generate much more discriminative data in terms of site and time in this dataset (Agathokleous et al., 2023; Hasmik et al., 2021; Jolivet et al., 2016; Shah et al., 2019). In similar observations made on other species exposed to traffic-related aerosols, PM affected the chlorophyll integrity of *Betula pendula*, *Quercus robur* and *Tilia cordata* leaves from urban locations in Warsaw (Łukowski et al. 2020). Similarly, leaf wax and local traffic density proved crucial for scaling the deposited PM concentrations in urban trees in Vienna (Steinparzer et al., 2023). The robustness of such a method may be due to its inclusion of both the direct pollutant impact on leaf chemistry and the crucial environmental

filter, e.g., foliar dust accumulation in terms of the amount or composition of deposited dust particles. The current results strengthen the interpretation of PIDR as a better predictor of air pollutant damage compared with APTI under the scope of the present dataset (Correa-Ochoa et al., 2022) and potentially the basis of novel tools that will enable researchers to understand plant-air pollution processes more thoroughly (Łukowski et al., 2020; Zhu et al., 2021) as well as supporting policy concerning the planning of urban parks and green infrastructure in European cities (Weerakkody et al., 2017). This work may be considered a preliminary report on the first use of PIDR on two urban tree species (*G. biloba*, *H. helix*) at limited urban sites and during limited periods. The underlying mechanisms and theoretical framework are sound, but the generalisation of the threshold values currently used to define the different stress levels may be difficult for other species, climatic zones, or city planning frameworks. For that reason, PIDR should only be used after a thorough testing phase, including a large number of species, multiple cities and long time periods, as part of a standardised biomonitoring programme. As with all PIDR-based analyses in the present study, the time dimension in our dataset is restricted to two periods; hence, patterns of PM deposition and pigment changes reflect preliminary findings and require confirmation. This suggests using long-term sampling more regularly, mixed-effects models that account for possible temporal variation, and explicitly including weather as a variable that may affect results, potentially acting as a confounding factor. *G. biloba* is deciduous, so pigment extraction from the April-October period gives clear seasonal signals during the growing season. *H. helix* is evergreen and can monitor the environment year-round, making it useful for detecting pollution episodes triggered by the winter heating season, which is usually absent in deciduous species (Lee et al., 2021). In the analysis conducted on *H. helix* over 36 bus and tram stops located in Debrecen, some significant variations in

terms of deposited dust concentration, chlorophyll and carotenoid content (Fig 17-19) were detected between the control and the traffic-impacted urban sites, confirming that dust was concentrated more at polluted areas, supporting the previous assumptions about pollution impact coming from cars. Regression models also revealed that the higher the distance from the centre of the city during winter and spring (Fig. 22), the less deposited dust per sample, which is consistent with many similar studies made earlier both in Debrecen and other big European cities concerning particulate matter (e. g., Abriha-Molnár et al. 2024; Molnár et al., 2020b; Simon et al., 2011).

In the case of *H. Helix*, chlorophylls and carotenoids serve important functions in photosynthetic adaptation, light capture, and photoprotection, respectively (Lichtenthaler, 1987; Demmig-Adams & Adams, 1996), which explains why chlorophyll and carotenoids in this plant are positively associated across seasons and study areas. Coordinated regulation of both pigment groups across sites and seasons was confirmed by their consistently strong positive association. Nevertheless, pigment responses showed spatial variability without a consistent directional trend relative to the control, attributable to heterogeneous microclimate, vegetation structure, and pollution intensity across the 36 sampling sites (Negi & Varshney, 2003). Pollution usually decreases pigment concentrations (Joshi & Swami, 2007; Patidar et al., 2016), but levels are often higher in reference areas (Bibi et al., 2024) and increase transiently as a response to moderate stress (Abriha-Molnár et al., 2024; Mukherjee & Agrawal, 2016). So the broad patterns in the data may have reflected localized differences, regulated changes in photosynthesis and not only degradation. A notable negative association between leaf surface area and dust deposition was observed, consistent with aerodynamic boundary-layer effects whereby smaller leaves intercept a disproportionately large quantity of particulates (Xu et al., 2022). Ascorbic acid decreased in autumn versus spring

but increased at the urban site in spring (Fig. 21) and, in winter, it correlated negatively with leaf surface area and distance (Fig. 20) and positively with CO in the latter season as a mechanism to repair ROS damage and regulate cellular physiology (Kaur & Nagpal, 2017; Menser, 1964). Carotenoid concentration increased in correlation with the CO level, because CO has not been shown to affect carotenoids in any plant under field conditions, it must be that, in traffic-related pollution mixtures, it happened to coincide and influence other traffic-related components, as well as a temperature-induced boost in respiration related to the winter heating and the Urban Heat Island (UHI) phenomenon at and near cities (Bodor et al., 2020; Bilska et al., 2019; Lashkari et al., 2025).

Based on seasonally correlated traits and trait associations, we observed significant shifts in correlations, especially for pigment coordination, dust accumulation, relative water content, and antioxidant capacity across summer, autumn, winter, and spring. This suggests that the coordination and interactions of various physiological traits in *H. helix* were adjusted seasonally, not following a simple gradient in the relative importance of those factors, depending on the environmental conditions (Morais et al., 2022; Prusty et al., 2005). In summer, pigment content and relative water content were the most significant variables, while dust accumulation showed an inverse relation with relative water content. In winter, a positive correlation occurred between dust accumulation and relative water content. Ascorbic acid accumulation became decoupled from the dynamics of pigment accumulation in winter, repeating patterns of temperature-induced shifts in transpiration rate that affect relative water content, the plant's stress response, and antioxidant control (Bilska et al., 2019; Lashkari et al., 2025). Carotenoid content showed an inverse relationship with temperature (Adams, 2020; Kreslavski et al., 2013), suggesting that cooler environments might impose greater demands for photoprotection, while increased wind speed correlates with a higher

concentration of carotenoids, maybe due to wind speed influencing the displacement of urban air pollutants, resulting in greater deposition or as a result of wind causing mechanical stimulation that induces secondary metabolism (Florou et al., 2024; Porter et al., 2009; Šic Žlabur et al., 2021). So the results showed that the levels of antioxidants, pigment content, relative water content, and particle size change interact with one another throughout the urban seasons. Henceforth, *H. helix* did not respond uniformly to urban environmental conditions but adapted to specific seasonal conditions, leading to season-specific responses to pollution rather than a constant level of environmental stress. This confirms a seasonal adjustment in physiology to reflect the prevailing climate and pollutant levels during distinct seasons of the urban environment.

The APTI values of *H. helix* fell within the sensitive category (Singh et al. 1991, Fig. 24), indicating limited resistance to the polluted conditions in Budapest. There are only a few reports on APTI for this plant: Chauhan et al. (2022) found it to be moderately tolerant (10.92), but these results were collected under laboratory conditions (indoor), Pandey et al. (2003) show significant differences among climbing species concerning their tolerance, rose cultivars (like the ornamentals studied) are considered to be sensitive (low APTI) in Budapest (Nafula et al., 2025), deciduous species (e. g., *Acer platanoides*) differ about space and urban pollution tolerance as demonstrated by a study performed across various urban sites (Bibi et al., 2024). The physiological sensitivity of *H. helix* - which precludes its use for pollution-tolerant urban planting- is precisely what confers its value as a bioindicator: its responsiveness to environmental change makes it a reliable monitor of spatial and seasonal variability in urban air quality. As an evergreen species installed across an extensive network of Debrecen bus and tram stops, it

constitutes a highly practical tool for continuous, year-round city-wide biomonitoring.

7. Conclusion

A notable reduction in air pollutant concentrations was observed during the 2020 shutdown period compared with the baseline period of 2018–2022, during which we studied the effects of COVID-19 on particulate matter. Our results indicated that the severe weather events of 2020, occurring during a period of typical emissions (before the lockdown), led to a greater air quality improvement than the later reduction in emissions during unfavourable weather conditions. The average PM_{10} pollution in Debrecen during the first half of 2020 was significantly lower than in other years; however, this decline was due only to the winter months preceding the lockdown, whereas heightened PM_{10} levels were observed during the curfew. PM_{10} levels exhibited diverse patterns, typified by reductions, minor increases, or stability, contingent upon the precise sampling locations. These findings highlight the complexity of air pollution dynamics and underscore the need for continuous monitoring and targeted measures to mitigate adverse impacts on air quality and human health.

According to our data, the study demonstrates that *G. biloba* has reasonable qualities as a bioindicator for tracking pollutants associated with environmental changes, particularly airborne pollutants in metropolitan areas. All three APTI metrics (pH, ascorbic acid content, and relative water content) reached their highest levels in October, indicating an overall increase in contaminant resistance to *G. biloba*. However, the studies also suggest that *G. biloba* is more susceptible and sensitive at the end of July, as its APTI metrics were lowest then. The data further showed strong negative correlations between the Chl-*b* concentration with respect to NO_X, PM_{10}, and NO_2, as well as between the total chlorophyll concentration with respect to CO and between

Chl-*a* with CO. Based on our research, *G. biloba* pigments are useful tools for assessing the effects of urban air pollutants on plants and determining the quality of urban environments. We studied the effects of CO, SO_2, and PM, the main pollution sources, on pigment levels in plants and, therefore, on plant health. Therefore, our results are particularly applicable to local governments managing their municipalities' environments, and everyone will benefit from improved ongoing evaluations of urban environmental quality through these efforts.

Our results suggest that PIDR is a useful measure of pollution exposure for *G. biloba*. In this dataset, low levels of PIDR were associated with decreased total chlorophyll and increased pheophytin at sites with greater dust levels, whereas sites without dust showed more stable pigments. These findings relate to well-established physiological processes in which particulate matter reduces the ability of leaves to photosynthesise by blocking stomata, abrasion of leaf surfaces, and reduced light entering the leaf (Lee et al., 2021). In contrast, chlorophyll breakdown and pheophytin accumulation were accelerated by ozone and other oxidants. Hence, this approach established a clear relationship between particle deposition and pigment integrity.

As indicated by previous studies, vegetation index thresholds need to be recalibrated locally, as species with different adaptations to climate and urban structure than *Ginkgo* may exhibit different thresholds. In addition, a program of monthly or weekly monitoring would provide data on seasonal transitions and brief pollution events in order to improve PIDRs' adaptation and evaluation capabilities (Lhotská et al., 2022; Łukowski et al., 2020).

Bioindicators (such as metabolomic profiles of plant stress) will add another level of complexity and enable the use of biotic (microscale dispersion) and abiotic (urban climate models) data, together with PIDR datasets, for

forecasting. On a larger scale, data collected using remote sensing indicators (e.g., NDVI, PRI, GNDVI) will provide a means to relate leaf-level information to canopy-level tree information. Additionally, developing an instrument to measure pigments and dust will enable any citizen to contribute to real-time monitoring of trees and provide a framework for relating tree health to urban design and policy planning, as PIDR continues to evolve into a diagnostic/monitoring tool for multiple uses.

The research presented here demonstrates that urban environmental conditions, such as particulate matter deposition and meteorological variability, significantly influence leaf biochemical characteristics and, in turn, regulate physiological coordination across seasons. The results of the study also suggest that plant responses to urban pollution are not uniform across the landscape but are influenced by the combined effects of pollution gradients and seasonal climatic factors. Various associations identified between the biochemical parameters and the different environmental variables measured (i.e., carbon monoxide, temperature, and wind speed) illustrate the complexity of the interactions between atmospheric conditions and the regulation of plant metabolic processes. Based on these findings, it appears that plants' responses to oxidative stress and the dynamics of photoprotective pigments are critical for seasonal adjustments under urban conditions. Overall, the results of this research support the use of *H. helix* as a bioindicator of spatial and seasonal variability associated with urban air quality assessment.

Due to its physiologically sensitive nature, this plant species cannot be considered for pollution-tolerant planting; however, because of this trait, it is highly responsive to environmental changes and should be used in biomonitoring. As an evergreen plant and a common species in urban environments, *H. helix* is an excellent candidate for year-round air quality

assessment. Its potential for use in biomonitoring will be established with key species through additional geographic validation.

8. New Scientific Results

•PM_{10} levels indicated heterogeneous patterns characterised by variations including decreases, slight increases, or stability, contingent upon the specific sampling sites under consideration.

•The pigment composition of *G. biloba* exhibits a marked response to traffic-related air pollutant gradients. Our findings suggest that *G. biloba* can serve as a reliable and accurate bioindicator of long-term air quality in urban environments.

•This study tested the Pigment Integrity-to-Dust Ratio (PIDR) as a novel bioindicator that incorporates two key elements of plant stress: (i) the ratio of chlorophyll to its degradation products (pheophytins) and (ii) the quantity of dust deposited on the leaf surface.

•Our results demonstrated that PIDR is a reliable indicator of the response to physiological stress, based on pigment concentration changes and deposited dust concentration.

•We found that PIDR provides a more direct interpretation than APTI in this dataset, appearing as an advance to the current bioindicators, as it reflects complex stresses of urban environments.

•APTI values classified *H. helix* as an air pollution-sensitive species, with variations across sites and seasons.

•The concentrations of dust and pigments in the leaves decreased with increasing distance from the city centre, while the ascorbic acid content increased.

•These findings demonstrate that *H. helix* effectively reflects urban air pollution and environmental stress, supporting its use as a bioindicator in urban ecosystems. Its evergreen habit, particulate matter retention capacity, and sensitivity to environmental change make it a promising model for assessing spatial and seasonal variability in urban air quality.

9. Acknowledgement

I would want to begin by expressing my profound appreciation to God, the Almighty, for providing me with the fortitude and determination to finish my doctorate degree. To my parents, Ma and Baba: Your unwavering love and prayers have been a rock throughout this ordeal. God bless you and keep you both now and in the future. Dr. Edina Kundrát-Simon, my supervisor, has been there for me from the start and has been an incredible source of support and encouragement. I could not be more grateful. Additionally, I would like to thank Dr. Vanda Éva Abriha-Molnár, Dr Bianka Sipos, and Dina Bibi for their assistance during the fieldwork, as well as Prof. Dr Béla Tóthmérész and Juhász-Nagy Pál Doctoral School for the opportunity. Additionally, I would like to express my gratitude to the Tempus Foundation and the Stipendium Hungaricum for the opportunity and scholarship. And finally, Kushal, I am deeply grateful for your love and support; without you, none of this would have been possible.

10. Reference

Abas, A., Aiyub, K., & Awang, A. (2022). Biomonitoring Potentially Toxic Elements (PTEs) Using Lichen Transplant Usnea misaminensis: A Case Study from Malaysia. *Sustainability*, *14*(12), 7254. https://doi.org/10.3390/su14127254

Abecasis, L., Gamelas, C. A., Justino, A. R., Dionísio, I., Canha, N., Kertesz, Z., & Almeida, S. M. (2022). Spatial Distribution of Air Pollution, Hotspots and Sources in an Urban-Industrial Area in the Lisbon Metropolitan Area, Portugal—A Biomonitoring Approach. *International Journal of Environmental Research and Public Health*, *19*(3), 1364. https://doi.org/10.3390/ijerph19031364

Abriha-Molnár, V. É., Szabó, S., Magura, T., Tóthmérész, B., Abriha, D., Sipos, B., & Simon, E. (2024). Environmental impact assessment based on particulate matter, and chlorophyll content of urban trees. *Scientific Reports*, *14*(1), 19911. https://doi.org/10.1038/s41598-024-70664-4

Abubakar, L., Salemcity, A. J., Abass, O. K., & Olajuyin, A. M. (2021). The impacts of COVID-19 on environmental sustainability: A brief study in world context. *Bioresource Technology Reports*, *15*, 100713. https://doi.org/10.1016/j.biteb.2021.100713

Achilleos, S., Wolfson, J. M., Ferguson, S. T., Kang, C.-M., Hadjimitsis, D. G., Hadjicharalambous, M., Achilleos, C., Christodoulou, A., Nisanzti, A., Papoutsa, C., Themistocleous, K., Athanasatos, S., Perdikou, S., & Koutrakis, P. (2016). Spatial variability of fine and coarse particle composition and sources in Cyprus. *Atmospheric Research*, *169*, 255–270. https://doi.org/10.1016/j.atmosres.2015.10.005

Adams, M. D. (2020). Air pollution in Ontario, Canada during the COVID-19 State of Emergency. *Science of the Total Environment*, *742*, 140516.

Agarwal, A., Kaushik, A., Kumar, S., & Mishra, R. K. (2020). Comparative study on air quality status in Indian and Chinese cities before and during the COVID-19 lockdown period. *Air Quality, Atmosphere & Health*, *13*, 1167–1178.

Agathokleous, E., Kitao, M., & Koike, T. (2023). Testing phaeophytinization as an index of ozone stress in trees. *Journal of Forestry Research*, *34*(4), 1167–1174. https://doi.org/10.1007/s11676-022-01556-4

Alcaraz-Rocha, P., Puig-Fàbregas, J., Garrido, J. L., & Sobrino, C. (2023). Ocean acidification affects pigment concentration and photoprotection of marine phytoplankton. *Limnology and Oceanography*, *68*(4), 831–844. https://doi.org/10.1002/lno.12313

Almeida, S. M., Manousakas, M., Diapouli, E., Kertesz, Z., Samek, L., Hristova, E., Šega, K., Alvarez, R. P., Belis, C. A., & Eleftheriadis, K. (2020). Ambient particulate matter source apportionment using receptor modelling in European and Central Asia urban areas. *Environmental Pollution*, *266*, 115199. https://doi.org/10.1016/j.envpol.2020.115199

Bahinskyi, L., Świsłowski, P., Isinkaralar, O., Isinkaralar, K., & Rajfur, M. (2025). Low-Cost Monitoring of Airborne Heavy Metals Using Lichen Bioindicators: Insights from Opole, Southern Poland. *Atmosphere*, *16*(5), 576. https://doi.org/10.3390/atmos16050576

Baldasano, J. M. (2020). COVID-19 lockdown effects on air quality by NO_2 in the cities of Barcelona and Madrid (Spain). *Science of the Total Environment*, *741*, 140353.

Banerjee, S., Palit, D., & Banerjee, A. (2021). Variation of tree biochemical and physiological characters under different air pollution stresses. *Environmental Science and Pollution Research*, *28*(14), 17960–17980. https://doi.org/10.1007/s11356-020-11674-3

Bao, L., Ma, K., Zhang, S., Lin, L., & Qu, L. (2015). Urban dust load impact on gas-exchange parameters and growth of *Sophora japonica* L. seedlings. *Plant, Soil and Environment*, *61*(7), 309–315. https://doi.org/10.17221/215/2015-PSE

Barua, S., & Nath, S. D. (2021). The impact of COVID-19 on air pollution: Evidence from global data. *Journal of Cleaner Production*, *298*, 126755. https://doi.org/10.1016/j.jclepro.2021.126755

Beck, S., & Stengel, J. (2016). Mass spectrometric imaging of flavonoid glycosides and biflavonoids in *Ginkgo* biloba L. *Phytochemistry*, *130*, 201–206. https://doi.org/10.1016/j.phytochem.2016.05.005

Beckett, K. P., Freer-Smith, P. H., & Taylor, G. (1998). Urban woodlands: Their role in reducing the effects of particulate pollution. *Environmental Pollution*, *99*(3), 347–360. https://doi.org/10.1016/S0269-7491(98)00016-5

Bessonova, V. P., Chongova, A. S., & Sklyarenko, A. V. (2020). Influence of multicomponent contamination on the content of photosynthetic pigments in the leaves of woody plants commonly planted for greening of cities. *Biosystems Diversity*, *28*(2), 203–208. https://doi.org/10.15421/012026

Bhadauria, S., Dixit, A., & Singh, D. (2022). Estimation of air pollution tolerance and anticipated performance index of roadside plants along the national highway in a tropical urban city. *Environmental Monitoring and Assessment*, *194*(11), 808. https://doi.org/10.1007/s10661-022-10483-0

Bharti, S. K., Trivedi, A., & Kumar, N. (2018). Air pollution tolerance index of plants growing near an industrial site. *Urban Climate*, *24*, 820–829. https://doi.org/10.1016/j.uclim.2017.10.007

Bibi, D., Tőzsér, D., Sipos, B., Molnár, V. É., Simon, E., & Tóthmérész, B. (2024a). Complex study of air pollution based on tree species in Vienna. *Air Quality, Atmosphere & Health*, *17*(2), 417–424. https://doi.org/10.1007/s11869-023-01452-8

Bierza, K., & Bierza, W. (2024). The effect of industrial and urban dust pollution on the ecophysiology and leaf element concentration of *Tilia cordata Mill*. *Environmental Science and Pollution Research*, *31*(48), 58413–58429. https://doi.org/10.1007/s11356-024-34999-9

Bilska, K., Wojciechowska, N., Alipour, S., & Kalemba, E. M. (2019). Ascorbic Acid—The Little-Known Antioxidant in Woody Plants. *Antioxidants*, *8*(12), 645. https://doi.org/10.3390/antiox8120645

Bodor, Z., Bodor, K., Keresztesi, Á., & Szép, R. (2020). Major air pollutants seasonal variation analysis and long-range transport of PM_{10} in an urban environment with specific climate condition in Transylvania (Romania). *Environmental*

Science and Pollution Research, *27*(30), 38181–38199. https://doi.org/10.1007/s11356-020-09838-2

Bontempi, E., Carnevale, C., Cornelio, A., Volta, M., & Zanoletti, A. (2022). Analysis of the lockdown effects due to the COVID-19 on air pollution in Brescia (Lombardy). *Environmental Research*, *212*, 113193.

Borowiak, K., Budka, A., Hanć, A., Kayze, D., Lisiak, M., Zbierska, J., Barałkiewicz, D., Iwaniuk, D., & Łopatka, N. (2018). Relations between photosynthetic pigments, macro-element contents and selected trace elements accumulated in *Lolium Multiflorum* L. exposed to ambient air conditions. *Acta Biologica Cracoviensia s. Botanica*, 35–44. https://doi.org/10.24425/118043

Bottyán, Z., Kircsi, A., Szegedi, S., & Unger, J. (2005). The relationship between built-up areas and the spatial development of the mean maximum urban heat island in Debrecen, Hungary. *International Journal of Climatology*, *25*(3), 405–418. https://doi.org/10.1002/joc.1138

Braak, C. J. F. ter, & Smilauer, P. (2002). *CANOCO Reference Manual and CanoDraw for Windows User's Guide: Software for Canonical Community Ordination (version 4.5)*. https://research.wur.nl/en/publications/canoco-reference-manual-and-canodraw-for-windows-users-guide-soft/

Bray, C. D., Nahas, A., Battye, W. H., & Aneja, V. P. (2021). Impact of lockdown during the COVID-19 outbreak on multi-scale air quality. *Atmospheric Environment*, *254*, 118386. https://doi.org/10.1016/j.atmosenv.2021.118386

Campos, C. F., Santos, V. S. V., Campos Júnior, E. O. D., Da Costa Estrela, D., Pires, L. P., Meza Bravo, J. V., & Pereira, B. B. (2024). Assessment of genotoxicity of air pollution in urban areas using an integrated model of passive biomonitoring. *Environmental Pollution*, *355*, 124219. https://doi.org/10.1016/j.envpol.2024.124219

Castanheiro, A., Hofman, J., Nuyts, G., Joosen, S., Spassov, S., Blust, R., Lenaerts, S., De Wael, K., & Samson, R. (2020). Leaf accumulation of atmospheric dust: Biomagnetic, morphological and elemental evaluation using SEM, ED-XRF and HR-ICP-MS. *Atmospheric Environment*, *221*, 117082. https://doi.org/10.1016/j.atmosenv.2019.117082

Cavazzin, B., MacDonell, C., Green, N., & Rothwell, J. J. (2024). Air pollution biomonitoring in an urban-industrial setting (Taranto, Italy) using Mediterranean plant species. *Atmospheric Pollution Research*, *15*(6), 102105. https://doi.org/10.1016/j.apr.2024.102105

Chaudhuri, S., & Roy, M. (2023). Global ambient air quality monitoring: Can mosses help? A systematic meta-analysis of literature about passive moss biomonitoring. *Environment, Development and Sustainability*, *26*(3), 5735–5773. https://doi.org/10.1007/s10668-023-03043-0

Chauhan, S., Manisha, ., Bhargava, B., Kandpal, K., & Kumar, A. (2022). Analyzing Preferred Indoor Ornamental Potted Plants for Their Air Pollution Tolerance Ability. *Polish Journal of Environmental Studies*, *31*(3), 2019–2027. https://doi.org/10.15244/pjoes/140291

Chiam, Z., Song, X. P., Lai, H. R., & Tan, H. T. W. (2019). Particulate matter mitigation via plants: Understanding complex relationships with leaf traits.

Science of The Total Environment, *688*, 398–408. https://doi.org/10.1016/j.scitotenv.2019.06.263

Choi, H., Melly, S., & Spengler, J. (2015). Intraurban and Longitudinal Variability of Classical Pollutants in Kraków, Poland, 2000–2010. *International Journal of Environmental Research and Public Health*, *12*(5), 4967–4991. https://doi.org/10.3390/ijerph120504967

Collivignarelli, M. C., Abbà, A., Bertanza, G., Pedrazzani, R., Ricciardi, P., & Miino, M. C. (2020). Lockdown for CoViD-2019 in Milan: What are the effects on air quality? *Science of the Total Environment*, *732*, 139280.

Connerton, P., Vicente de Assunção, J., Maura de Miranda, R., Dorothée Slovic, A., José Pérez-Martínez, P., & Ribeiro, H. (2020). Air quality during COVID-19 in four megacities: Lessons and challenges for public health. *International Journal of Environmental Research and Public Health*, *17*(14), 5067.

Contardo, T., Vannini, A., Sharma, K., Giordani, P., & Loppi, S. (2020). Disentangling sources of trace element air pollution in complex urban areas by lichen biomonitoring. A case study in Milan (Italy). *Chemosphere*, *256*, 127155. https://doi.org/10.1016/j.chemosphere.2020.127155

Corada, K., Woodward, H., Alaraj, H., Collins, C. M., & De Nazelle, A. (2021). A systematic review of the leaf traits considered to contribute to removal of airborne particulate matter pollution in urban areas. *Environmental Pollution*, *269*, 116104. https://doi.org/10.1016/j.envpol.2020.116104

Corpus-Mendoza, A. N., Ruiz-Segoviano, H. S., Rodríguez-Contreras, S. F., Yañez-Dávila, D., & Hernández-Granados, A. (2021). Decrease of mobility, electricity demand, and NO2 emissions on COVID-19 times and their feedback on prevention measures. *The Science of the Total Environment*, *760*, 143382. https://doi.org/10.1016/j.scitotenv.2020.143382

Correa-Ochoa, M., Mejia-Sepulveda, J., Saldarriaga-Molina, J., Castro-Jiménez, C., & Aguiar-Gil, D. (2022). Evaluation of air pollution tolerance index and anticipated performance index of six plant species, in an urban tropical valley: Medellin, Colombia. *Environmental Science and Pollution Research*, *29*(5), 7952–7971. https://doi.org/10.1007/s11356-021-16037-0

Cotrozzi, L. (2020). The use of spectroscopy to assess photosynthetic traits and their involvement in the response of woody plants to air pollutants. *Plants*, *9*(9), 1074. https://doi.org/10.3390/plants9091074

Dahech, S., Abdmouleh, M. A., & Lagmiri, S. (2022). Spatiotemporal variation of air quality (PM and NO_2) in southern Paris during COVID-19 lockdown periods. *Atmosphere*, *13*(2), 289.

Dantas, G., Siciliano, B., França, B. B., da Silva, C. M., & Arbilla, G. (2020). The impact of COVID-19 partial lockdown on the air quality of the city of Rio de Janeiro, Brazil. *Science of the Total Environment*, *729*, 139085.

Demmig-Adams, B., & Adams, W. W. (1996). The role of xanthophyll cycle carotenoids in the protection of photosynthesis. *Trends in Plant Science*, *1*(1), 21–26. https://doi.org/10.1016/S1360-1385(96)80019-7

Del Tredici, P. (2000). The evolution, ecology, and cultivation of *Ginkgo biloba*. In T. van Beek (Ed.), *Ginkgo biloba* (pp. 7–24). Harwood Academic.

Devkota, A., Sapkota, S., & Dhyani, S. (2022). Assessing the air pollution tolerance index and anticipated performance index of roadside plant species for biomonitoring environmental health. *Pollution Research*, 874–883. https://doi.org/10.53550/PR.2022.v41i03.016

EEA, E. (2019). Air quality in Europe—2019 report. *European Environment Agency*.

Evangeliou, N., Platt, S. M., Eckhardt, S., Myhre, C. L., Laj, P., Alados-Arboledas, L., Backman, J., Brem, B. T., Fiebig, M., & Flentje, H. (2021). Changes in black carbon emissions over Europe due to COVID-19 lockdowns. *Atmospheric Chemistry and Physics*, *21*, 2675–2692.

Evangelopoulos, D., Perez-Velasco, R., Walton, H., Gumy, S., Williams, M., Kelly, F. J., & Künzli, N. (2020). The role of burden of disease assessment in tracking progress towards achieving WHO global air quality guidelines. *International Journal of Public Health*, *65*(8), 1455–1465. https://doi.org/10.1007/s00038-020-01479-z

Evgenieva, T., Vakareeva, E., Gurdev, L., & Dreischuh, T. (2024). Identification of Saharan-Dust Intrusions over Sofia, Bulgaria, Using Near-Ground PM10 and PM2.5 Mass Concentration Measurements. *Aerosol and Air Quality Research*, *24*(6), 230304. https://doi.org/10.4209/aaqr.230304

Falcioni, R., Antunes, W. C., Demattê, J. A. M., & Nanni, M. R. (2023). Biophysical, Biochemical, and Photochemical Analyses Using Reflectance Hyperspectroscopy and Chlorophyll a Fluorescence Kinetics in Variegated Leaves. *Biology*, *12*(5), 704. https://doi.org/10.3390/biology12050704

Ferenczi, Z. (2013). Predictability analysis of the $PM_{2.5}$ and PM_{10} concentration in Budapest. *Id\Hojárás*, *117*(4), 359–375.

Filonchyk, M., Hurynovich, V., & Yan, H. (2021). Impact of the COVID-19 lockdown on air quality in Poland, Eastern Europe. *Environmental Research*, *198*, 110454.

Florou, E., Politi, A., Andreadaki, E., Vrakas, K., Spaliara, H., Neli, A., Koulopoulou, C. E., Koulopoulos, A., Bantis, F., & Zervoudakis, G. (2024). When Light Is Crucial, but Wind Is Rather Trivial: A Basil Case Study. *Plants*, *13*(22), 3221. https://doi.org/10.3390/plants13223221

Foskinis, R., Gini, M. I., Kokkalis, P., Diapouli, E., Vratolis, S., Granakis, K., Zografou, O., Komppula, M., Vakkari, V., Nenes, A., Papayannis, A., & Eleftheriadis, K. (2024). On the relation between the planetary boundary layer height and in situ surface observations of atmospheric aerosol pollutants during spring in an urban area. *Atmospheric Research*, *308*, 107543. https://doi.org/10.1016/j.atmosres.2024.107543

Freitas, E. D., Ibarra-Espinosa, S. A., Gavidia-Calderón, M. E., Rehbein, A., Abou Rafee, S. A., Martins, J. A., Martins, L. D., Santos, U. P., Ning, M. F., & Andrade, M. F. (2020). *Mobility restrictions and air quality under COVID-19 pandemic in São Paulo, Brazil*. https://www.preprints.org/manuscript/202004.0515

Fusaro, L., Salvatori, E., Winkler, A., Frezzini, M. A., De Santis, E., Sagnotti, L., Canepari, S., & Manes, F. (2021). Urban trees for biomonitoring atmospheric particulate matter: An integrated approach combining plant functional traits,

magnetic and chemical properties. *Ecological Indicators*, *126*, 107707. https://doi.org/10.1016/j.ecolind.2021.107707

Gallego-Cartagena, E., Morillas, H., Carrero, J. A., Madariaga, J. M., & Maguregui, M. (2021). Naturally growing grimmiaceae family mosses as passive biomonitors of heavy metals pollution in urban-industrial atmospheres from the Bilbao Metropolitan area. *Chemosphere*, *263*, 128190. https://doi.org/10.1016/j.chemosphere.2020.128190

Gamelas, C. A., Canha, N., Justino, A. R., Nunes, A., Nunes, S., Dionísio, I., Kertesz, Z., & Almeida, S. M. (2024). Strawberry Plant as a Biomonitor of Trace Metal Air Pollution—A Citizen Science Approach in an Urban-Industrial Area near Lisbon, Portugal. *Plants*, *13*(24), 3587. https://doi.org/10.3390/plants13243587

Gao, J., & Bukovsky, M. S. (2023). Urban land patterns can moderate population exposures to climate extremes over the 21st century. *Nature Communications*, *14*(1), 6536. https://doi.org/10.1038/s41467-023-42084-x

García-Sánchez, I. E., Barradas, V. L., Ponce De León Hill, C. A., Esperón-Rodríguez, M., Rosas Pérez, I., & Ballinas, M. (2019). Effect of heavy metals and environmental variables on the assimilation of CO_2 and stomatal conductance of *Ligustrum lucidum*, an urban tree from Mexico City. *Urban Forestry & Urban Greening*, *42*, 72–81. https://doi.org/10.1016/j.ufug.2019.05.002

Georgieva, E., Syrakov, D., Atanassov, D., Spassova, T., Dimitrova, M., Prodanova, M., Veleva, B., Kirova, H., Neykova, N., Neykova, R., Hristova, E., & Petrov, A. (2021). Use of Satellite Data for Air Pollution Modeling in Bulgaria. *Earth*, *2*(3), 586–604. https://doi.org/10.3390/earth2030034

Gerdol, R., Marchesini, R., Iacumin, P., & Brancaleoni, L. (2014). Monitoring temporal trends of air pollution in an urban area using mosses and lichens as biomonitors. *Chemosphere*, *108*, 388–395. https://doi.org/10.1016/j.chemosphere.2014.02.035

Gómez-Ensastegui, C., Avila-Pérez, P., García-Rivas, J. L., Barrera-Díaz, C. E., Ortiz-Oliveros, H. B., & Martínez-Gallegos, S. (2025). Evaluation of an aquatic liverwort and terrestrial moss as biomonitors of heavy metals associated with particulate matter. *Scientific Reports*, *15*(1), 4127. https://doi.org/10.1038/s41598-025-88348-y

Gottardini, E., Cristofori, A., Cristofolini, F., Nali, C., Pellegrini, E., Bussotti, F., & Ferretti, M. (2014). Chlorophyll-related indicators are linked to visible ozone symptoms: Evidence from a field study on native *Viburnum lantana* L. plants in northern Italy. *Ecological Indicators*, *39*, 65–74. https://doi.org/10.1016/j.ecolind.2013.11.021

Grifoni, L., Jafarova, M., La Colla, N. S., Aherne, J., Raulli, A., & Loppi, S. (2025). Comparison of Lichen and Moss Transplants for Monitoring the Deposition of Airborne Microfibers. *Sustainability*, *17*(2), 537. https://doi.org/10.3390/su17020537

Guevara, M., Jorba, O., Soret, A., Petetin, H., Bowdalo, D., Serradell, K., Tena, C., Denier van der Gon, H., Kuenen, J., Peuch, V.-H., & Pérez García-Pando, C. (2021). Time-resolved emission reductions for atmospheric chemistry

modelling in Europe during the COVID-19 lockdowns. *Atmospheric Chemistry and Physics*, *21*(2), 773–797. https://doi.org/10.5194/acp-21-773-2021

Han, M., Lu, R., Han, M., Yang, X., Du, F., Chen, X., Huang, S., Luo, S., & Han, D. (2024). Anthocyanin Accumulation and Chlorophyll Degradation Lead to the Formation of Colourful Leaves of Syringa oblata in Autumn. *Acta Botanica Brasilica*, *38*, e20230226. https://doi.org/10.1590/1677-941x-abb-2023-0226

Hasmik, H., Tepanosyan, G., Gevorgyan, A., Baldacchini, C., & Sahakyan, L. (2021). Similarities and differences of potentially toxic elements contents in leaves of *Fraxinus excelsior* L. and *Platanus orientalis* L. in an urban environment. *Urban Forestry & Urban Greening*, *65*, 127359. https://doi.org/10.1016/j.ufug.2021.127359

He, Y., & Li, Z. (2018). Epigenetic Environmental Memories in Plants: Establishment, Maintenance, and Reprogramming. *Trends in Genetics*, *34*(11), 856–866. https://doi.org/10.1016/j.tig.2018.07.006

Heggestad, H. E. (1991). Origin of Bel-W3, Bel-C and Bel-B tobacco varieties and their use as indicators of ozone. *Environmental Pollution*, *74*(4), 264–291. https://doi.org/10.1016/0269-7491(91)90076-9

Hirano, T., Kiyota, M., & Aiga, I. (1995). Physical effects of dust on leaf physiology of cucumber and kidney bean plants. *Environmental Pollution*, *89*(3), 255–261. https://doi.org/10.1016/0269-7491(94)00075-O

Huh, M. K. (2019). Genetic diversity and population structure of *Ginkgo biloba* L. in Korea. *Journal of Asia-Pacific Biodiversity*, *12*(3), 342–348. https://doi.org/10.1016/j.japb.2019.03.012

Hörtensteiner, S., Vicentini, F., & Matile, P. (2009). Pheophytin pheophorbide hydrolase (pheophytinase) is involved in chlorophyll breakdown during leaf senescence in Arabidopsis. *The Plant Cel*l, 21(3), 767–785. https://doi.org/10.1105/tpc.108.064089

Hubai, K., Kováts, N., & Teke, G. (2021). Effects of urban atmospheric particulate matter on higher plants using Lycopersicon esculentum as model species. *SN Applied Sciences*, *3*(9), 770. https://doi.org/10.1007/s42452-021-04745-8

Huszar, P., Belda, M., & Halenka, T. (2015). *On the long term impact of emissions from central European cities on regional air-quality*. https://doi.org/10.5194/acpd-15-32101-2015

Huszar, P., Karlický, J., Ďoubalová, J., Nováková, T., Šindelářová, K., Švábik, F., Belda, M., Halenka, T., & Žák, M. (2020). *The impact of urban land-surface on extreme air pollution over central Europe*. https://doi.org/10.5194/acp-2020-399

Jolivet, Y., Bagard, M., Cabané, M., Vaultier, M.-N., Gandin, A., Afif, D., Dizengremel, P., & Le Thiec, D. (2016). Deciphering the ozone-induced changes in cellular processes: A prerequisite for ozone risk assessment at the tree and forest levels. *Annals of Forest Science*, *73*(4), 923–943. https://doi.org/10.1007/s13595-016-0580-3

Joshi, P. C., & Swami, A. (2007). Physiological responses of some tree species under roadside automobile pollution stress around city of Haridwar, India. *The*

Environmentalist, *27*(3), 365–374. https://doi.org/10.1007/s10669-007-9049-0

Juda-Rezler, K., Reizer, M., Maciejewska, K., Błaszczak, B., & Klejnowski, K. (2020). Characterization of atmospheric $PM_{2.5}$ sources at a Central European urban background site. *Science of The Total Environment*, *713*, 136729. https://doi.org/10.1016/j.scitotenv.2020.136729

Jurčević Šangut, I., & Šamec, D. (2024). Seasonal Variation of Polyphenols and Pigments in *Ginkgo* (*Ginkgo biloba* L.) Leaves: Focus on 3′,8″-Biflavones. *Plants*, *13*(21), 3044. https://doi.org/10.3390/plants13213044

Karmakar, D., Deb, K., & Padhy, P. K. (2021). Ecophysiological responses of tree species due to air pollution for biomonitoring of environmental health in urban area. *Urban Climate*, *35*, 100741. https://doi.org/10.1016/j.uclim.2020.100741

Kaur, M., & Nagpal, A. K. (2017). Evaluation of air pollution tolerance index and anticipated performance index of plants and their application in development of green space along the urban areas. *Environmental Science and Pollution Research*, *24*(23), 18881–18895. https://doi.org/10.1007/s11356-017-9500-9

Kharbech, O., Mahjoubi, Y., Boutar, M., Djebali, W., & Chaoui, A. (2024). Up-regulation of nitrogen metabolism and chlorophyll biosynthesis by hydrogen sulfide improved photosystem photochemistry and gas exchange in chromium-contaminated bean (*Phaseolus vulgaris* L.) plants. *Plant Physiology and Biochemistry*, *217*, 109211. https://doi.org/10.1016/j.plaphy.2024.109211

Khomenko, S., Cirach, M., Pereira-Barboza, E., Mueller, N., Barrera-Gómez, J., Rojas-Rueda, D., De Hoogh, K., Hoek, G., & Nieuwenhuijsen, M. (2021). Premature mortality due to air pollution in European cities: A health impact assessment. *The Lancet Planetary Health*, *5*(3), e121–e134. https://doi.org/10.1016/S2542-5196(20)30272-2

Kinoshita, T., Kume, A., & Hanba, Y. T. (2021). Seasonal variations in photosynthetic functions of the urban landscape tree species *Ginkgo biloba*: Photoperiod is a key trait. *Trees*, *35*(1), 273–285. https://doi.org/10.1007/s00468-020-02033-3

Kong, W. W., Zhang, L. P., Guo, K., Liu, Z. P., & Yang, Z. M. (2010). Carbon monoxide improves adaptation of *Arabidopsis* to iron deficiency. *Plant Biotechnology Journal*, *8*(1), 88–99. https://doi.org/10.1111/j.1467-7652.2009.00469.x

Kovács, K. D. (2022). Nighttime light emissions explain the decline in NO_2 during a COVID-19-induced total lockdown in France. *Geographia Technica*, *17*(1/2022), 104–115.

Kováts, N., Hubai, K., Diósi, D., Sainnokhoi, T.-A., Hoffer, A., Tóth, Á., & Teke, G. (2021). Sensitivity of typical European roadside plants to atmospheric particulate matter. *Ecological Indicators*, *124*, 107428. https://doi.org/10.1016/j.ecolind.2021.107428

Kreslavski, V. D., Shirshikova, G. N., Lyubimov, V. Yu., Shmarev, A. N., Boutanaev, A. M., Kosobryukhov, A. A., Schmitt, F.-J., Friedrich, T., & Allakhverdiev, S. I. (2013). Effect of preillumination with red light on photosynthetic

parameters and oxidant-/antioxidant balance in *Arabidopsis thaliana* in response to UV-A. *Journal of Photochemistry and Photobiology B: Biology*, *127*, 229–236. https://doi.org/10.1016/j.jphotobiol.2013.08.008

Lashkari, A., Saadati, S., & Saffari, V. R. (2025). Methyl jasmonate and ascorbic acid enhance salinity tolerance in pot marigold (*Calendula officinalis* L.) through improved morphophysiological and biochemical traits. *Scientific Reports*, *15*(1), 30434. https://doi.org/10.1038/s41598-025-16597-y

László, E., Bottyán, Zs., & Szegedi, S. (2016). Long-term changes of meteorological conditions of urban heat island development in the region of Debrecen, Hungary. *Theoretical and Applied Climatology*, *124*(1–2), 365–373. https://doi.org/10.1007/s00704-015-1427-9

Lee, J. K., Kim, D. Y., Park, S. H., Woo, S. Y., Nie, H., & Kim, S. H. (2021). Particulate Matter (PM) Adsorption and Leaf Characteristics of Ornamental Sweet Potato (*Ipomoea batatas L.*) Cultivars and Two Common Indoor Plants (*Hedera helix* L. and *Epipremnum aureum Lindl.* & *Andre*). *Horticulturae*, *8*(1), 26. https://doi.org/10.3390/horticulturae8010026

Lhotská, M., Zemanová, V., Pavlík, M., Pavlíková, D., Hnilička, F., & Popov, M. (2022). Leaf fitness and stress response after the application of contaminated soil dust particulate matter. *Scientific Reports*, *12*(1), 10046. https://doi.org/10.1038/s41598-022-13931-6

Li, Y., He, N., Hou, J., Xu, L., Liu, C., Zhang, J., Wang, Q., Zhang, X., & Wu, X. (2018). Factors Influencing Leaf Chlorophyll Content in Natural Forests at the Biome Scale. *Frontiers in Ecology and Evolution*, *6*, 64. https://doi.org/10.3389/fevo.2018.00064

Lichtenthaler, H. K., & Wellburn, A. R. (1983). Determinations of total carotenoids and chlorophylls *a* and *b* of leaf extracts in different solvents. *Biochemical Society Transactions*, *11*(5), 591–592. https://doi.org/10.1042/bst0110591

Lichtenthaler, H. K. (1987). [34] Chlorophylls and carotenoids: Pigments of photosynthetic biomembranes. In *Methods in Enzymology* (Vol. 148, pp. 350–382). Elsevier. https://doi.org/10.1016/0076-6879(87)48036-1

Lichtenthaler, H. K. (1996). Vegetation Stress: An Introduction to the Stress Concept in Plants. *Journal of Plant Physiology*, *148*(1–2), 4–14. https://doi.org/10.1016/S0176-1617(96)80287-2

Lichtenthaler, H. K., Buschmann, C., Döll, M., Fietz, H.-J., Bach, T., Kozel, U., Meier, D., & Rahmsdorf, U. (1981). Photosynthetic activity, chloroplast ultrastructure, and leaf characteristics of high-light and low-light plants and of sun and shade leaves. *Photosynthesis Research*, *2*(2), 115–141. https://doi.org/10.1007/BF00028752

Lobell, D. B., Di Tommaso, S., & Burney, J. A. (2022). Globally ubiquitous negative effects of nitrogen dioxide on crop growth. *Science Advances*, *8*(22), eabm9909. https://doi.org/10.1126/sciadv.abm9909

Loskot, J., Jezbera, D., Nalezinková, M., Šmejkalová, A. H., Fernandes, D., & Komárek, J. (2024). Impact of Saharan dust on particulate matter characteristics in an urban and a natural locality in Central Europe. *Scientific Reports*, *14*(1), 32002. https://doi.org/10.1038/s41598-024-83603-0

Lu, J., Sun, L., Jin, X., Islam, M. A., Guo, F., Tang, X., Zhao, K., Hao, H., Li, N., Zhang, W., Shi, Y., Wang, S., & Sun, D. (2022). Analysis of Physiological and Transcriptomic Differences between a Premature Senescence Mutant (GSm) and Its Wild-Type in Common Wheat (*Triticum aestivum* L.). *Biology*, *11*(6), 904. https://doi.org/10.3390/biology11060904

Łukowski, A., Popek, R., & Karolewski, P. (2020). Particulate matter on foliage of *Betula pendula*, *Quercus robur*, and *Tilia cordata*: Deposition and ecophysiology. *Environmental Science and Pollution Research*, *27*(10), 10296–10307. https://doi.org/10.1007/s11356-020-07672-0

Lyu, J., Chen, D., Zhang, X., Yan, J., Shen, G., & Yin, S. (2023). Coagulation effect of atmospheric submicron particles on plant leaves: Key functional characteristics and a comparison with dry deposition. *Science of The Total Environment*, *868*, 161582. https://doi.org/10.1016/j.scitotenv.2023.161582

Mansfield, T. A. (1998). Stomata and plant water relations: Does air pollution create problems? *Environmental Pollution*, *101*(1), 1–11. https://doi.org/10.1016/S0269-7491(98)00076-1

Massimi, L., Conti, M. E., Mele, G., Ristorini, M., Astolfi, M. L., & Canepari, S. (2019). Lichen transplants as indicators of atmospheric element concentrations: A high spatial resolution comparison with PM_{10} samples in a polluted area (Central Italy). *Ecological Indicators*, *101*, 759–769. https://doi.org/10.1016/j.ecolind.2018.12.051

Matile, P., Schellenberg, M., & Vicentini, F. (1987). Chlorophyll catabolism in senescing plant tissues: In vivo breakdown intermediates. Proceedings of the National Academy of Sciences, 84(7), 1901–1905. https://doi.org/10.1073/pnas.84.7.1901

Menser, H. A. (1964). Response of Plants to Air Pollutants. III. A Relation between Ascorbic Acid Levels and Ozone Susceptibility of Light-Preconditioned Tobacco Plants. *Plant Physiology*, *39*(4), 564–567. https://doi.org/10.1104/pp.39.4.564

Menut, L., Bessagnet, B., Siour, G., Mailler, S., Pennel, R., & Cholakian, A. (2020). Impact of lockdown measures to combat COVID-19 on air quality over Western Europe. *Science of the Total Environment*, *741*, 140426.

Meravi, N., Singh, P. K., & Prajapati, S. K. (2021). Seasonal variation of dust deposition on plant leaves and its impact on various photochemical yields of plants. *Environmental Challenges*, *4*, 100166. https://doi.org/10.1016/j.envc.2021.100166

Molnár, V. É., Simon, E., Tóthmérész, B., Ninsawat, S., & Szabó, S. (2020a). Air pollution induced vegetation stress – The Air Pollution Tolerance Index as a quick tool for city health evaluation. *Ecological Indicators*, *113*, 106234. https://doi.org/10.1016/j.ecolind.2020.106234

Molnár, V. É., Tőzsér, D., Szabó, S., Tóthmérész, B., & Simon, E. (2020b). Use of Leaves as Bioindicator to Assess Air Pollution Based on Composite Proxy Measure (APTI), Dust Amount and Elemental Concentration of Metals. *Plants*, *9*(12), 1743. https://doi.org/10.3390/plants9121743

Morais, M. C., Cabral, J. A., & Gonçalves, B. (2022). Seasonal Variation in Selected Biochemical Traits in the Leaves of Co-Occurring Invasive and Native Plant

Species under Mediterranean Conditions. *Plants*, *11*(9), 1171. https://doi.org/10.3390/plants11091171

Mota, L. M., Bravo, J. V. M., & Pereira, B. B. (2025). Urban environmental risk assessment through biomonitoring: A multivariate approach using Mangifera indica, lichens, and air pollutants. *Environmental Pollution*, *385*, 127102. https://doi.org/10.1016/j.envpol.2025.127102

Moura, B. B., Zammarchi, F., Manzini, J., Hoshika, Y., Brilli, L., Vagnoli, C., Gioli, B., Zaldei, A., Giordano, T., Martinelli, F., Paoletti, E., & Ferrini, F. (2024). Assessment of seasonal variations in particulate matter accumulation and elemental composition in urban tree species. *Environmental Research*, *252*, 118782. https://doi.org/10.1016/j.envres.2024.118782

Mukherjee, A., & Agrawal, M. (2016). Pollution Response Score of Tree Species in Relation to Ambient Air Quality in an Urban Area. *Bulletin of Environmental Contamination and Toxicology*, *96*(2), 197–202. https://doi.org/10.1007/s00128-015-1679-1

Mukhopadhyay, S., Dutta, R., & Das, P. (2024). Greenery planning for urban air pollution control based on biomonitoring potential: Explicit emphasis on foliar accumulation of particulate matter (PM) and polycyclic aromatic hydrocarbons (PAHs). *Journal of Environmental Management*, *355*, 120524. https://doi.org/10.1016/j.jenvman.2024.120524

Mulgrew, A., & Williams, P. (2000). Biomonitoring of air quality using plants (Air Hygiene Report No. 10). WHO Collaborating Centre for Air Quality Management and Air Pollution Control, Federal Environmental Agency. Berlin, Germany. 165 pp.

Nafula, W. S., Orlóci, L., Kisvarga, S., Boronkay, G., Tóthmérész, B., Ajele, S., Abriha-Molnár, V. É., & Simon, E. (2025). Rose cultivars for biomonitoring of air quality. *Heliyon*, *11*(3), e41978. https://doi.org/10.1016/j.heliyon.2025.e41978

Negi, C. S., & Varshney, C. K. (2003). Effect of air pollution on photosynthesis-A study of its effect on oxygen evolution. *Environment Conservation Journal*, *4*(1–3), 43–50. https://doi.org/10.36953/ECJ.2003.0412307

Niepsch, D., Clarke, L. J., Newton, J., Tzoulas, K., & Cavan, G. (2023). High spatial resolution assessment of air quality in urban centres using lichen carbon, nitrogen and sulfur contents and stable-isotope-ratio signatures. *Environmental Science and Pollution Research*, *30*(20), 58731–58754. https://doi.org/10.1007/s11356-023-26652-8

Nowak, D. J., Crane, D. E., & Stevens, J. C. (2006). Air pollution removal by urban trees and shrubs in the United States. *Urban Forestry & Urban Greening*, *4*(3), 115–123. https://doi.org/10.1016/j.ufug.2006.01.007

Ogunkunle, C. O., Suleiman, L. B., Oyedeji, S., Awotoye, O. O., & Fatoba, P. O. (2015). Assessing the air pollution tolerance index and anticipated performance index of some tree species for biomonitoring environmental health. *Agroforestry Systems*, *89*(3), 447–454. https://doi.org/10.1007/s10457-014-9781-7

Öncü, T., Yazman, M. M., Ustaoğlu, F., Hristova, E., & Yüksel, B. (2025). Source dynamics and environmental risk of street dust as a vector of human exposure

to potentially toxic elements in Istanbul, Türkiye. *Scientific Reports*, *15*(1), 30550. https://doi.org/10.1038/s41598-025-11472-2

Pandey, S., Kumar, S., & Nagar, P. K. (2003). Photosynthetic Performance of *Ginkgo biloba* L. Grown Under High and Low Irradiance. *Photosynthetica*, *41*(4), 505–511. https://doi.org/10.1023/B:PHOT.0000027514.56808.35

Paoli, L., Bandoni, E., & Sanità Di Toppi, L. (2023). Lichens and Mosses as Biomonitors of Indoor Pollution. *Biology*, *12*(9), 1248. https://doi.org/10.3390/biology12091248

Pásztor, L., Laborczi, A., Takács, K., Szatmári, G., Illés, G., Fodor, N., Négyesi, G., Bakacsi, Z., & Szabó, J. (2016). *Spatial distribution of selected soil features in Hajdú-Bihar county represented by digital soil maps*.

Patidar, S., Bafna, A., Batham, A. R., & Panwar, K. (2016). Impact of Urban Air Pollution on Photosynthetic Pigment and Proline Content of Plants Growing along the A.B road Indore City, India. *International Journal of Current Microbiology and Applied Sciences*, *5*(3), 107–113. https://doi.org/10.20546/ijcmas.2016.503.015

Peel, M. C., Finlayson, B. L., & McMahon, T. A. (2007). Updated world map of the Köppen-Geiger climate classification. *Hydrology and Earth System Sciences*, *11*(5), 1633–1644. https://doi.org/10.5194/hess-11-1633-2007

Pei, Z., Han, G., Ma, X., Su, H., & Gong, W. (2020). Response of major air pollutants to COVID-19 lockdowns in China. *Science of the Total Environment*, *743*, 140879.

Perri, G., Gargano, D., Randazzo, L., Calabrese, S., Brusca, L., Fuoco, I., Apollaro, C., & La Russa, M. F. (2024). Nature-Based Options for Improving Urban Environmental Quality: Using Black Poplar Trees for Monitoring Heavy Metals Pollution in Urbanized Contexts. *Resources*, *13*(6), 85. https://doi.org/10.3390/resources13060085

Piazzetta, K. D., Ramsdorf, W. A., & Maranho, L. T. (2019). Use of airplant Tillandsia recurvata L., Bromeliaceae, as biomonitor of urban air pollution. *Aerobiologia*, *35*(1), 125–137. https://doi.org/10.1007/s10453-018-9545-3

Pomponi, F., Li, M., Sun, Y.-Y., Malik, A., Lenzen, M., Fountas, G., D'Amico, B., Akizu-Gardoki, O., & Luque Anguita, M. (2021). A Novel Method for Estimating Emissions Reductions Caused by the Restriction of Mobility: The Case of the COVID-19 Pandemic. *Environmental Science & Technology Letters*, *8*(1), 46–52. https://doi.org/10.1021/acs.estlett.0c00764

Porter, B. W., Zhu, Y. J., Webb, D. T., & Christopher, D. A. (2009). Novel thigmomorphogenetic responses in *Carica papaya*: Touch decreases anthocyanin levels and stimulates petiole cork outgrowths. *Annals of Botany*, *103*(6), 847–858. https://doi.org/10.1093/aob/mcp009

Pozdniakova, S., Uchida, A., Fontal, A., Cañas, L., Santamaria, S., Hui, L. Y., Luhung, I., Schuster, S. C., Rodó, X., & Borràs, S. (2025). Integrating air microbiome for comprehensive air quality analysis. *iScience*, *28*(7), 113015. https://doi.org/10.1016/j.isci.2025.113015

Prusty, B. A. K., Mishra, P. C., & Azeez, P. A. (2005). Dust accumulation and leaf pigment content in vegetation near the national highway at Sambalpur,

Orissa, India. *Ecotoxicology and Environmental Safety*, *60*(2), 228–235. https://doi.org/10.1016/j.ecoenv.2003.12.013

Qor-El-Aine, A., Béres, A., & Géczi, G. (2022). Case Study of the Saharan Dust Effects on PM10 and $PM_{2.5}$ Concentrations in Budapest in March 2022. *Journal of Central European Green Innovation*, *10*(Suppl 1), 67–78. https://doi.org/10.33038/jcegi.3500

Rahman, M. M., Paul, K. C., Hossain, M. A., Ali, G. M. N., Rahman, M. S., & Thill, J.-C. (2021). Machine learning on the COVID-19 pandemic, human mobility and air quality: A review. *Ieee Access*, *9*, 72420–72450.

Rai, P. K. (2016). Impacts of particulate matter pollution on plants: Implications for environmental biomonitoring. *Ecotoxicology and Environmental Safety*, *129*, 120–136. https://doi.org/10.1016/j.ecoenv.2016.03.012

Rodríguez-Santamaría, K., Zafra-Mejía, C. A., & Rondón-Quintana, H. A. (2022). Macro-Morphological Traits of Leaves for Urban Tree Selection for Air Pollution Biomonitoring: A Review. *Biosensors*, *12*(10), 812. https://doi.org/10.3390/bios12100812

Ropkins, K., & Tate, J. E. (2021). Early observations on the impact of the COVID-19 lockdown on air quality trends across the UK. *Science of the Total Environment*, *754*, 142374.

Roy, A., Mandal, M., Das, S., Popek, R., Rakwal, R., Agrawal, G. K., Awasthi, A., & Sarkar, A. (2024). The cellular consequences of particulate matter pollutants in plants: Safeguarding the harmonious integration of structure and function. *Science of The Total Environment*, *914*, 169763. https://doi.org/10.1016/j.scitotenv.2023.169763

Sæbø, A., Popek, R., Nawrot, B., Hanslin, H. M., Gawronska, H., & Gawronski, S. W. (2012). Plant species differences in particulate matter accumulation on leaf surfaces. *Science of The Total Environment*, *427–428*, 347–354. https://doi.org/10.1016/j.scitotenv.2012.03.084

Sahu, C., Basti, S., & Sahu, S. K. (2020). Air pollution tolerance index (APTI) and expected performance index (EPI) of trees in sambalpur town of India. *SN Applied Sciences*, *2*(8), 1327. https://doi.org/10.1007/s42452-020-3120-6

Salma, I., Vörösmarty, M., Gyöngyösi, A. Z., Thén, W., & Weidinger, T. (2020). What can we learn about urban air quality from the first outbreak of COVID-19? A case study from central Europe. *Atmospheric Chemistry and Physics*, *20*(24), 15725–15742.

Sanusi, R., & Livesley, S. J. (2020). London Plane trees (*Platanus x acerifolia*) before, during and after a heatwave: Losing leaves means less cooling benefit. *Urban Forestry & Urban Greening*, *54*, 126746. https://doi.org/10.1016/j.ufug.2020.126746

Sarijeva, G., Knapp, M., & Lichtenthaler, H. K. (2007). Differences in photosynthetic activity, chlorophyll and carotenoid levels, and in chlorophyll fluorescence parameters in green sun and shade leaves of *Ginkgo* and *Fagus*. *Journal of Plant Physiology*, *164*(7), 950–955. https://doi.org/10.1016/j.jplph.2006.09.002

Schneider, R., Masselot, P., Vicedo-Cabrera, A. M., Sera, F., Blangiardo, M., Forlani, C., Douros, J., Jorba, O., Adani, M., & Kouznetsov, R. (2022). Differential

impact of government lockdown policies on reducing air pollution levels and related mortality in Europe. *Scientific Reports*, *12*(1), 726.

Sfetsas, T., Ghoghoberidze, S., Karnoutsos, P., Tziakas, V., Karagiovanidis, M., & Katsantonis, D. (2025). Urban Source Apportionment of Potentially Toxic Elements in Thessaloniki Using Syntrichia Moss Biomonitoring and PMF Modeling. *Environments*, *12*(6), 188. https://doi.org/10.3390/environments12060188

Shah, K., Amin, N. U., Ahmad, I., Ara, G., Ren, X., & Xing, L. (2019). Effects of Chronic Dust Load On Leaf Pigments of the Landscape Plant *Murraya Paniculata*. *Gesunde Pflanzen*, *71*(4), 249–258. https://doi.org/10.1007/s10343-019-00469-3

Shakoor, A., Chen, X., Farooq, T. H., Shahzad, U., Ashraf, F., Rehman, A., Sahar, N. E., & Yan, W. (2020). Fluctuations in environmental pollutants and air quality during the lockdown in the USA and China: Two sides of COVID-19 pandemic. *Air Quality, Atmosphere & Health*, *13*(11), 1335–1342. https://doi.org/10.1007/s11869-020-00888-6

Sheng, Q., & Zhu, Z. (2019). Physiological Response of European Hornbeam Leaves to Nitrogen Dioxide Stress and Self-recovery. *Journal of the American Society for Horticultural Science*, *144*(1), 23–30. https://doi.org/10.21273/JASHS04489-18

Shi, D., Wei, X., Chen, G., & Xu, Y. (2012). Changes in Photosynthetic Characteristics and Antioxidative Protection in Male and Female *Ginkgo* during Natural Senescence. *Journal of the American Society for Horticultural Science*, *137*(5), 349–360. https://doi.org/10.21273/JASHS.137.5.349

Shi, Z., Song, C., Liu, B., Lu, G., Xu, J., Van Vu, T., Elliott, R. J. R., Li, W., Bloss, W. J., & Harrison, R. M. (2021). Abrupt but smaller than expected changes in surface air quality attributable to COVID-19 lockdowns. *Science Advances*, *7*(3), eabd6696. https://doi.org/10.1126/sciadv.abd6696

Šic Žlabur, J., Radman, S., Fabek Uher, S., Opačić, N., Benko, B., Galić, A., Samirić, P., & Voća, S. (2021). Plant Response to Mechanically-Induced Stress: A Case Study on Specialized Metabolites of Leafy Vegetables. *Plants*, *10*(12), 2650. https://doi.org/10.3390/plants10122650

Simon, E., Braun, M., Vidic, A., Bogyó, D., Fábián, I., & Tóthmérész, B. (2011). Air pollution assessment based on elemental concentration of leaves tissue and foliage dust along an urbanization gradient in Vienna. *Environmental Pollution*, *159*(5), 1229–1233. https://doi.org/10.1016/j.envpol.2011.01.034

Simon, E., Molnár, V. É., Lajtos, D., Bibi, D., Tóthmérész, B., & Szabó, S. (2021). Usefulness of Tree Species as Urban Health Indicators. *Plants*, *10*(12), Article 12. https://doi.org/10.3390/plants10122797

Singh, S. K., Rao, D. N., Agrawal, M., Pandey, J., & Naryan, D. (1991b). Air pollution tolerance index of plants. *Journal of Environmental Management*, *32*(1), 45–55. https://doi.org/10.1016/S0301-4797(05)80080-5

Son, J., Kim, I., & Chang, H. (2022). Seasonal variations in accumulated particulate matter on leaves of four major tree species in Korea. *Forest Science and Technology*, *18*(3), 118–126. https://doi.org/10.1080/21580103.2022.2110164

Sonti, N. F., Hallett, R. A., Griffin, K. L., Trammell, T. L. E., & Sullivan, J. H. (2021). Chlorophyll fluorescence parameters, leaf traits and foliar chemistry of white oak and red maple trees in urban forest patches. *Tree Physiology*, *41*(2), 269–279. https://doi.org/10.1093/treephys/tpaa121

Srivastava, H. S., Jolliffe, P. A., & Runeckles, V. C. (1975). Inhibition of gas exchange in bean leaves by NO_2. *Canadian Journal of Botany*, *53*(5), 466–474. https://doi.org/10.1139/b75-057

Ștefănuț, S., Öllerer, K., Ion, M. C., Florescu, L. I., Constantin, M., Banciu, C., Onete, M., Manu, M., Vicol, I., Moldoveanu, M. M., Maican, S., Cobzaru, I., Nicoară, R. G., Mogîldea, E. D., Purice, D. M., Nicolae, C. D., Catană, R. D., Teodosiu, G., Dumitrache, C. A., … Manole, A. (2021). Country-scale complementary passive and active biomonitoring of airborne trace elements for environmental risk assessment. *Ecological Indicators*, *126*, 107357. https://doi.org/10.1016/j.ecolind.2021.107357

Steinparzer, M., Schaubmayr, J., Godbold, D. L., & Rewald, B. (2023). Particulate matter accumulation by tree foliage is driven by leaf habit types, urbanization- and pollution levels. *Environmental Pollution*, *335*, 122289. https://doi.org/10.1016/j.envpol.2023.122289

Sunyer, J., Spix, C., Quenel, P., Ponce-de-Leon, A., Pönka, A., Barumandzadeh, T., Touloumi, G., Bacharova, L., Wojtyniak, B., & Vonk, J. (1997). Urban air pollution and emergency admissions for asthma in four European cities: The APHEA Project. *Thorax*, *52*(9), 760–765.

Świsłowski, P., Nowak, A., & Rajfur, M. (2022). Comparison of Exposure Techniques and Vitality Assessment of Mosses in Active Biomonitoring for Their Suitability in Assessing Heavy Metal Pollution in Atmospheric Aerosol. *Environmental Toxicology and Chemistry*, *41*(6), 1429–1438. https://doi.org/10.1002/etc.5321

Świsłowski, P., Wacławek, S., Antos, V., Zinicovscaia, I., Rajfur, M., & Wacławek, M. (2024). One year of active moss biomonitoring in the identification of PAHs in an urbanized area—Prospects and implications. *Environmental Science and Pollution Research*, *31*(26), 38416–38427. https://doi.org/10.1007/s11356-024-33831-8

Szabó, V., Chen, H., Hrotkó, K., & Kohut, I. (2023). Investigation of Dust Deposition in Vegetation Period as an Ecological Service on Urban Trees in Budapest—A Case Study. *Pollutants*, *3*(4), 507–520. https://doi.org/10.3390/pollutants3040035

Szoboszlai, Z., Kertész, Zs., Szikszai, Z., Borbély-Kiss, I., & Koltay, E. (2009). Ion beam microanalysis of individual aerosol particles originating from Saharan dust episodes observed in Debrecen, Hungary. *Nuclear Instruments and Methods in Physics Research Section B: Beam Interactions with Materials and Atoms*, *267*(12–13), 2241–2244. https://doi.org/10.1016/j.nimb.2009.03.019

Talebzadeh, F., & Valeo, C. (2022). Evaluating the Effects of Environmental Stress on Leaf Chlorophyll Content as an Index for Tree Health. *IOP Conference Series: Earth and Environmental Science*, *1006*(1), 012007. https://doi.org/10.1088/1755-1315/1006/1/012007

Teng, K., Yue, Y., Zhang, H., Li, H., Xu, L., Han, C., Fan, X., & Wu, J. (2021). Functional Characterization of the Pheophytinase Gene, ZjPPH, From *Zoysia japonica* in Regulating Chlorophyll Degradation and Photosynthesis. *Frontiers in Plant Science*, *12*, 786570. https://doi.org/10.3389/fpls.2021.786570

Tripathi, D. P., & Nema, A. K. (2023). Seasonal variation of biochemical parameters and air pollution tolerance index (APTI) of selected plant species in Delhi city, and detailed meta-analysis from Indian metropolitan cities. *Atmospheric Environment*, *309*, 119862. https://doi.org/10.1016/j.atmosenv.2023.119862

Trueba, S., Pan, R., Scoffoni, C., John, G. P., Davis, S. D., & Sack, L. (2019). Thresholds for leaf damage due to dehydration: Declines of hydraulic function, stomatal conductance and cellular integrity precede those for photochemistry. *New Phytologist*, *223*(1), 134–149. https://doi.org/10.1111/nph.15779

Tsai, M.-Y., Hoek, G., Eeftens, M., De Hoogh, K., Beelen, R., Beregszászi, T., Cesaroni, G., Cirach, M., Cyrys, J., De Nazelle, A., De Vocht, F., Ducret-Stich, R., Eriksen, K., Galassi, C., Gražuleviciene, R., Gražulevicius, T., Grivas, G., Gryparis, A., Heinrich, J., … Brunekreef, B. (2015). Spatial variation of PM elemental composition between and within 20 European study areas—Results of the ESCAPE project. *Environment International*, *84*, 181–192. https://doi.org/10.1016/j.envint.2015.04.015

Varela, Z., Boquete, M. T., Fernández, J. A., Martínez-Abaigar, J., Núñez-Olivera, E., & Aboal, J. R. (2023). Mythbusters: Unravelling the pollutant uptake processes in mosses for air quality biomonitoring. *Ecological Indicators*, *148*, 110095. https://doi.org/10.1016/j.ecolind.2023.110095

Varga, G. (2020). Changing nature of Saharan dust deposition in the Carpathian Basin (Central Europe): 40 years of identified North African dust events (1979–2018). *Environment International*, *139*, 105712.

Varotsos, C., Christodoulakis, J., Kouremadas, G. A., & Fotaki, E.-F. (2021). The signature of the coronavirus lockdown in air pollution in Greece. *Water, Air, & Soil Pollution*, *232*, 1–12.

Vernon, L. P. (1960). Spectrophotometric Determination of Chlorophylls and Pheophytins in Plant Extracts. *Analytical Chemistry*, *32*(9), 1144–1150. https://doi.org/10.1021/ac60165a029

Volkov, A. G., & Ranatunga, D. R. A. (2006). Plants as Environmental Biosensors. *Plant Signaling & Behavior*, *1*(3), 105–115. https://doi.org/10.4161/psb.1.3.3000

Volta, M., Giostra, U., Guariso, G., Baldasano, J., Lutz, M., Kerschbaumer, A., Rauterberg-Wulff, A., Ferreira, F., Mendes, L., & Monjardino, J. (2022). The greatest air quality experiment ever. *PLoS ONE*, *17*. https://run.unl.pt/handle/10362/150631

Walker, B. J., Drewry, D. T., Slattery, R. A., VanLoocke, A., Cho, Y. B., & Ort, D. R. (2018). Chlorophyll Can Be Reduced in Crop Canopies with Little Penalty to Photosynthesis. *Plant Physiology*, *176*(2), 1215–1232. https://doi.org/10.1104/pp.17.01401

Wang, T., Li, L., Qin, Y., Lu, B., Xu, D., Zhuang, W., Shu, X., Zhang, F., Wang, N., & Wang, Z. (2023). Effects of Seasonal Changes on Chlorophyll Fluorescence and Physiological Characteristics in the Two Taxus Species. *Plants*, *12*(14), 2636. https://doi.org/10.3390/plants12142636

Weerakkody, U., Dover, J. W., Mitchell, P., & Reiling, K. (2017a). Particulate matter pollution capture by leaves of seventeen living wall species with special reference to rail-traffic at a metropolitan station. *Urban Forestry & Urban Greening*, *27*, 173–186. https://doi.org/10.1016/j.ufug.2017.07.005

Wellburn, A. R. (1994). The Spectral Determination of Chlorophylls a and b, as well as Total Carotenoids, Using Various Solvents with Spectrophotometers of Different Resolution. *Journal of Plant Physiology*, *144*(3), 307–313. https://doi.org/10.1016/S0176-1617(11)81192-2

Wu, Y., Guo, J., Wang, T., Cao, F., & Wang, G. (2020). Metabolomic and transcriptomic analyses of mutant yellow leaves provide insights into pigment synthesis and metabolism in *Ginkgo* biloba. *BMC Genomics*, *21*(1), 858. https://doi.org/10.1186/s12864-020-07259-6

Wykoff, D. D., Davies, J. P., Melis, A., & Grossman, A. R. (1998). The Regulation of Photosynthetic Electron Transport during Nutrient Deprivation in *Chlamydomonas reinhardtii* 1. *Plant Physiology*, *117*(1), 129–139. https://doi.org/10.1104/pp.117.1.129

Xie, X., He, Z., Chen, N., Tang, Z., Wang, Q., & Cai, Y. (2019). The Roles of Environmental Factors in Regulation of Oxidative Stress in Plant. *BioMed Research International*, *2019*, 1–11. https://doi.org/10.1155/2019/9732325

Xu, F., Cheng, S., Zhu, J., Zhang, W., & Wang, Y. (2011). Effects of 5-Aminolevulinic Acid on Chlorophyll, Photosynthesis, Soluble Sugar and Flavonoids of *Ginkgo* biloba. *Notulae Botanicae Horti Agrobotanici Cluj-Napoca*, *39*(1), 41–47. https://doi.org/10.15835/nbha3915880

Xu, L., Yan, Q., He, P., Zhen, Z., Jing, Y., Duan, Y., & Chen, X. (2022). Combined effects of different leaf traits on foliage dust-retention capacity and stability. *Air Quality, Atmosphere & Health*, *15*(7), 1263–1274. https://doi.org/10.1007/s11869-021-01141-4

Yabuki, K., & Miyagawa, H. (1970). Studies on the Effect of Wind Speed upon the Photosynthesis. *Journal of Agricultural Meteorology*, *26*(3), 137–141. https://doi.org/10.2480/agrmet.26.137

Yadav, R., & Pandey, P. (2020). Assessment of Air Pollution Tolerance Index (APTI) and Anticipated Performance Index (API) of Roadside Plants for the Development of Greenbelt in Urban Area of Bathinda City, Punjab, India. *Bulletin of Environmental Contamination and Toxicology*, *105*(6), 906–914. https://doi.org/10.1007/s00128-020-03027-0

Yang, X.-S., Chen, G.-X., Xie, K.-B., Wei, X.-D., Zhang, M.-P., Gao, Z.-P., & Han, B. (2010). Photosynthetic, biochemical, and ultra-structural changes in the chloroplasts of two *ginkgo* (*Ginkgo biloba* L.) cultivars during leaf development. *The Journal of Horticultural Science and Biotechnology*, *85*(4), 323–328. https://doi.org/10.1080/14620316.2010.11512675

Yayla, E. E., Sevik, H., & Isinkaralar, K. (2022). Detection of landscape species as a low-cost biomonitoring study: Cr, Mn, and Zn pollution in an urban air

quality. *Environmental Monitoring and Assessment*, *194*(10), 687. https://doi.org/10.1007/s10661-022-10356-6

Zangari, S., Hill, D. T., Charette, A. T., & Mirowsky, J. E. (2020). Air quality changes in New York City during the COVID-19 pandemic. *Science of the Total Environment*, *742*, 140496.

Zaręba, M., & Danek, T. (2022). Analysis of air pollution migration during COVID-19 lockdown in Krakow, Poland. *Aerosol and Air Quality Research*, *22*, 210275.

Zhang, L., Yang, L., Zohner, C. M., Crowther, T. W., Li, M., Shen, F., Guo, M., Qin, J., Yao, L., & Zhou, C. (2022). Direct and indirect impacts of urbanization on vegetation growth across the world's cities. *Science Advances*, *8*(27), eabo0095. https://doi.org/10.1126/sciadv.abo0095

Zheng, W., Li, X., Zhang, L., Zhang, Y., Lu, X., & Tian, J. (2015). Improved metabolites of pharmaceutical ingredient grade *Ginkgo biloba* and the correlated proteomics analysis. *PROTEOMICS*, *15*(11), 1868–1883. https://doi.org/10.1002/pmic.201400258

Zhou, Q., Mu, K., Xu, M., Ma, X., Ni, Z., Wang, J., & Xu, L. (2017). Variation in the Concentrations of Major Secondary Metabolites in *Ginkgo* Leaves from Different Geographical Populations. *Forests*, *8*(8), 266. https://doi.org/10.3390/f8080266

Zhu, J., & Xu, C. (2021). Intraspecific differences in plant functional traits are related to urban atmospheric particulate matter. *BMC Plant Biology*, *21*(1), 430. https://doi.org/10.1186/s12870-021-03207-y

Zhu, J., Xu, J., Cao, Y., Fu, J., Li, B., Sun, G., Zhang, X., & Xu, C. (2021). Leaf reflectance and functional traits as environmental indicators of urban dust deposition. *BMC Plant Biology*, *21*(1), 533. https://doi.org/10.1186/s12870-021-03308-8

Zhu, Y., Xie, J., Huang, F., & Cao, L. (2020). The mediating effect of air quality on the association between human mobility and COVID-19 infection in China. *Environmental Research*, *189*, 109911.

Ziernicka-Wojtaszek, A., Zuśka, Z., & Kopcińska, J. (2024). Assessment of the Effect of Meteorological Conditions on the Concentration of Suspended $PM_{2.5}$ Particulate Matter in Central Europe. *Sustainability*, *16*(11), 4797. https://doi.org/10.3390/su16114797

11. Appendix

Table 1. Results of concentrations of pigments (mean ± SE, mg g^{-1} fresh mass).

	Pigments			
Months	Chlorophyll-a	Chlorophyll -b	Total Chlorophyll	Carotenoids
July	0.54 ± 0.06	0.39 ± 0.04	0.94 ± 0.09	0.19 ± 0.01
August	0.49 ± 0.06	0.29 ± 0.03	0.78 ± 0.09	0.21 ± 0.02
September	0.49 ± 0.04	0.31 ± 0.02	0.81 ± 0.06	0.18 ± 0.01
October	0.41 ± 0.04	0.23 ± 0.02	0.64 ± 0.06	0.16 ± 0.01

	Pigments		
Months	Pheophytin-a	Pheophytin -b	Total Pheophytin
July	0.11 ± 0.01	0.21 ± 0.02	0.31 ± 0.02
August	0.06 ± 0.03	0.18 ± 0.02	0.24 ± 0.03
September	0.08 ± 0.01	0.16 ± 0.02	0.24 ± 0.03
October	0.03 ± 0.01	0.10 ± 0.01	0.13 ± 0.01

Table 2. Standard deviation values of biochemical parameters and pigments across zones, with mean differences relative to the control and temporal changes between 2023 and 2024

$$\Delta R \,\&\, \Delta D \; = \overline{X}2024 - \overline{X}2023$$

$$\text{Zone} - \text{Control} = \overline{X}\text{Zone} - \overline{X}\text{Control}$$

Parameter	R–Control (2023)	R–Control (2024)	ΔR (2024–2023)	D–Control (2023)	D–Control (2024)	ΔD (2024–2023)	F	P
APTI	3.9	3.99	0.09	2.64	3.28	0.63	3.12	0.003
Carotenoids	0.1	0.02	-0.08	0.15	0.05	-0.1	11.83	<0.001
Chl-*a*	0.25	0.05	-0.2	0.8	0.23	-0.57	9.29	<0.001
Chl-*b*	0.11	-0.03	-0.13	0.49	0.16	-0.33	5.55	<0.001
Total Chl	0.34	0.02	-0.32	1.29	0.39	-0.9	7.56	<0.001
Pheo-*a*	0.1	0.1	0.01	0.03	0.04	0.02	14.62	<0.001
Pheo-*b*	0.04	0.04	0.01	0.02	0.01	0	5.36	<0.001
Pheophytin	0.14	0.14	0	0.05	0.05	0	8.06	<0.001

Table 3. Mean (±SE) air pollutant concentrations and PIDR values across sampling sites and periods, July 2023, September 2023, and September 2024.

Sample	Month	CO (µg m^{-3})	NO_2 (µg m^{-3})	O_3 (µg m^{-3})	PM_{10} (µg m^{-3})	$PM_{2.5}$ (µg m^{-3})	SO_2 (µg m^{-3})	PIDR (Mean ± SE)
	Jul-23	58 ± 15	18 ± 1	38 ± 1	19 ± 1	8.2 ± 0.5	2.4 ± 0.1	0.871 ± 0.147
R	Sep-23	328 ± 26	28 ± 2	25 ± 1	25 ± 2	8.1 ± 0.7	2.6 ± 0.2	1.146 ± 0.427 †
	Sep-24	193 ± 17	13 ± 1	<LoD	11 ± 1	4.4 ± 0.5	25 ± 2	0.522 ± 0.058
	Jul-23	<LoD	14 ± 0.7	85 ± 2	13 ± 1	6.6 ± 0.4	<LoD	1.703 ± 0.318
Control	Sep-23	<LoD	19 ± 1	67 ± 3	19 ± 2	8.4 ± 0.6	<LoD	1.156 ± 0.393
	Sep-24	<LoD	4.9 ± 1.7	<LoD	17 ± 2	7.0 ± 0.6	<LoD	1.082 ± 0.330
	Jul-23	<LoD	24 ± 1	77 ± 2	19 ± 1	9.1 ± 0.7	4.9 ± 0.1	0.768 ± 0.088
D	Sep-23	209 ± 52	37 ± 2	51 ± 2	24 ± 2	6.4 ± 1.1	5.3 ± 0.3	2.507 ± 4.765 *
	Sep-24	63 ± 35	25 ± 2	<LoD	21 ± 3	8.8 ± 0.9	50 ± 5	0.109 ± 1.371

Table 4. Z-scores of significant air pollutants and PIDR throughout zones in different sites for three temporal intervals: July 2023, September 2023, and September 2024.

Sample	Month	Z CO	Z NO_2	Z O_3	Z PM_{10}	Z $PM_{2.5}$	Z SO_2	Z PIDR
	Jul-23	1.4	-0.1	-1.4	0.8	0.2	0.0	-0.6
R	Sep-23	-1.1	0.0	-1.3	0.9	0.5	0.0	0.9
	Sep-24	1.3	-0.2	0.0	-1.3	-1.3	0.0	-1.0
	Jul-23	-0.7	-1.1	0.9	-1.4	-1.3	-1.2	1.4
Control	Sep-23	-1.3	-1.2	1.1	-1.4	0.9	-1.2	-1.4
	Sep-24	-1.1	-1.1	0.0	0.2	0.1	-1.2	-0.3
	Jul-23	-0.7	1.3	0.5	0.6	1.1	1.2	-0.8
D	Sep-23	-1.5	1.2	0.2	0.5	-1.4	1.2	0.4
	Sep-24	-0.3	1.3	0.0	1.1	1.2	1.2	1.4

Note: Dust-load artefact: rainfall 2–3 Sep 2023 washed leaf surface dust - PIDR denominator reduced independently of biological stress signal. * Ratio artefact: Pheo-a ≈ 0.019 mg g^{-1} (<LoD) inflated PIDR numerator - excluded from quantitative interpretation. <LoD = below limit of detection.

Table 5. Results of two-way ANOVA based on the studied parameters of *H. helix* leaves compared to the studied sites and seasons.

Parameters		F	p
dust	correct model	5.851	<0.001
	sites	10.688	<0.001
	seasons	99.917	<0.001
Chlorophyll	correct model	7.199	<0.001
	sites	25.863	<0.001
	seasons	3.257	0.022
Carotenoids	correct model	4.606	<0.001
	sites	10.039	<0.001
	seasons	62.428	<0.001
Relative water content	correct model	1.371	0.012
	sites	1.697	<0.001
	seasons	20.506	<0.001
pH	correct model	0.802	0.935
	sites	0.653	0.939
	seasons	24.986	<0.001
Ascorbic acid	correct model	1.869	<0.001
	sites	2.331	<0.001
	seasons	31.207	<0.001

Table 6. Seasonal p-values of correlations between biochemical parameters and distance from the city center.

	Summer	Autumn	Winter	Spring
Dust	0.212	0.090	0.007	0.001
Chlorophyll	0.116	0.030	0.047	0.032
Carotenoid	0.249	0.048	0.069	0.038
Ascorbic acid	0.120	0.131	0.007	0.257

Table 7. Principal Component Analysis (PCA) loadings of plant physiological parameters in Summer.

Variables	PC1	PC2	PC3	PC4	PC5	PC6
Dust	0.256	-0.690	0.168	0.073	-0.649	-0.063
Chlorophyll	-0.519	-0.239	0.270	0.251	0.076	0.729
Carotenoid	-0.475	-0.231	0.520	-0.032	0.250	-0.622
Relative water content	0.237	0.550	0.630	0.404	-0.284	0.006
pH	-0.438	0.311	0.034	-0.619	-0.569	0.050
Ascorbic acid	0.437	-0.118	0.479	-0.620	0.325	0.274

Table 8. Principal Component Analysis (PCA) loadings of plant physiological parameters in Autumn.

Variables	PC1	PC2	PC3	PC4	PC5	PC6
Dust	0.089	-0.558	0.493	0.445	-0.346	-0.347
Chlorophyll	-0.644	-0.006	0.075	0.358	-0.225	0.633
Carotenoid	-0.653	-0.114	-0.043	0.068	0.547	-0.505
Relative water content	-0.202	-0.347	-0.691	-0.199	-0.529	-0.202
pH	-0.331	0.304	0.491	-0.583	-0.415	-0.210
Ascorbic acid	-0.003	-0.681	0.175	-0.538	0.279	0.373

Table 9. Principal Component Analysis (PCA) loadings of plant physiological parameters in Winter.

Variables	PC1	PC2	PC3	PC4	PC5	PC6
Dust	0.146	0.602	-0.418	-0.554	-0.367	0.014
Chlorophyll	0.597	-0.083	0.002	-0.090	0.264	0.748
Carotenoid	0.580	-0.031	0.119	-0.259	0.410	-0.643
Relative water content	0.066	0.433	0.869	-0.021	-0.218	0.068
pH	0.097	-0.664	0.175	-0.464	-0.551	-0.013
Ascorbic acid	-0.522	-0.030	0.159	-0.635	0.525	0.152

Table 10. Principal Component Analysis (PCA) loadings of plant physiological parameters in Spring.

Variables	PC1	PC2	PC3	PC4	PC5	PC6
Dust	0.204	-0.652	-0.002	-0.517	-0.513	0.057
Chlorophyll	0.642	-0.033	0.152	0.156	0.218	0.701
Carotenoid	0.625	-0.148	0.144	0.268	0.088	-0.698
Relative water content	-0.153	0.112	0.833	0.250	-0.453	0.050
pH	0.192	0.475	0.323	-0.755	0.217	-0.124
Ascorbic acid	-0.308	-0.560	0.397	-0.069	0.655	-0.019

Table 11. Concentration of air pollutants at Station 1 monitoring station.

Date	CO (μgm^{-3})	NO (μgm^{-3})	NO_2 (μgm^{-3})	NOx (μgm^{-3})	PM_{10} (μgm^{-3})	SO_2 (μgm^{-3})
2023-07	163 ± 46	n.d.	n.d.	n.d.	17 ± 5	67 ± 6
2023-08	322 ± 108	n.d.	n.d.	n.d.	18 ± 5	n.d.
2023-09	262 ± 124	n.d.	n.d.	n.d.	20 ± 9	n.d.
2023-10	427 ± 210	252 ± 119	298 ± 93	684 ± 256	20 ± 7	n.d.
2023-11	642 ± 211	288 ± 138	259 ± 80	701 ± 285	15 ± 5	n.d.
2023-12	924 ± 332	289 ± 170	251 ± 80	695 ± 332	20 ±9	n.d.
2024-01	657 ± 333	213 ± 196	248 ± 104	575 ± 393	23 ± 14	n.d.
2024-02	887 ± 234	224 ± 132	275 ± 106	618 ± 293	24 ± 12	n.d.
2024-03	864 ± 11	137 ± 96	234 ± 88	443 ± 225	21 ± 9	n.d.
2024-04	420 ± 125	n.d.	n.d.	n.d.	19 ± 13	n.d.
2024-05	447 ± 52	n.d.	n.d.	n.d.	15 ± 3	n.d.
2024-06	515 ± 62	87 ± 51	201 ± 89	334 ± 162	15 ± 5	8 ± 1

Table 12. Concentration of air pollutants at Station 2 monitoring station.

Date	CO (μgm^{-3})	NO (μgm^{-3})	NO_2 (μgm^{-3})	NO_x (μgm^{-3})	O_3 (μgm^{-3})	PM_{10} (μgm^{-3})	$PM_{2.5}$ (μgm^{-3})	SO_2 (μgm^{-3})
2023-06	313 ± 62	15 ± 2	76 ± 21	99 ± 23	69 ± 9	15 ± 5	10 ±3	10 ± 2
2023-07	410 ± 78	16 ± 2	69 ± 19	94 ± 21	77 ± 11	16 ± 5	10 ± 3	7 ± 5
2023-08	284 ± 146	19 ± 3	99 ± 31	128 ± 33	68 ± 12	19 ± 6	10 ± 3	11 ± 3
2023-09	425 ± 86	23 ± 6	122 ± 38	154 ± 44	61 ± 11	21 ± 9	10 ± 4	14 ± 6
2023-10	332 ± 100	29 ± 38	148 ± 54	192 ± 105	47 ± 12	21 ± 8	11 ± 4	18 ± 11
2023-11	406 ± 116	35 ± 32	136 ± 45	190 ± 83	36 ± 9	14 ± 5	10 ± 3	14 ± 3
2023-12	956 ± 184	81 ± 85	182 ± 52	306 ± 166	32 ± 14	19 ± 10	19 ± 9	18 ± 4
2024-01	610 ± 312	116 ±145	180 ± 72	327 ± 274	39 ± 10	n.d.	23 ± 15	23 ± 6
2024-02	457 ± 251	106 ± 113	152 ± 67	288 ± 225	41 ± 10	n.d.	21 ± 14	31 ± 9
2024-03	493 ± 90	n.d.	n.d.	n.d.	49 ± 12	n.d.	16 ± 8	22 ± 6
2024-04	576 ± 63	n.d.	n.d.	n.d.	62 ± 9	n.d.	11 ± 5	22 ± 5
2024-05	620 ± 52	9 ± 4	108 ± 26	121 ± 30	69 ± 8	n.d.	9 ± 3	21 ± 2

Table 13. Meteorological data obtained from the Debrecen Airport monitoring stations.

Date	Precipitation (mm)	Temperature (°C)	Wind speed (m/s)
2023-07	42.3	23.3 ± 1.9	2.7 ± 0.9
2023-08	80.0	23.3 ± 3.5	2.7 ± 0.9
2023-09	19.9	20.3 ± 1.6	2.9 ± 1.3
2023-10	38.1	14.2 ± 3.8	3.3 ± 1.6
2023-11	114.0	6.0 ± 4.0	3.6 ± 1.1
2023-12	57.0	2.9 ± 2.9	3.4 ± 1.6
2024-01	29.7	1.1 ± 4.1	3.9 ± 2.0
2024-02	8.8	8.1 ± 3.3	3.6 ± 2.0
2024-03	5.5	9.7 ± 3.4	3.1 ± 1.4
2024-04	44.6	13.8 ± 4.1	3.4 ± 1.4
2024-05	40.9	17.6 ± 2.1	3.0 ± 1.0
2024-06	50.0	21.9 ± 2.7	2.7 ± 1.2

Table 14. Results of earlier studies for concentrations of pigments

Reference	Year	Location (City, Country)	Chlorophyll *a* (mg g^{-1} dw)	Chlorophyll *b* (mg g^{-1} dw)	Total Chlorophylls (mg g^{-1} dw)	Total Carotenoids (mg g^{-1} dw)
Current research	2023	Debrecen, Hungary	1.93(fw)	0.93(fw)	3.17(fw)	19.55(fw)
Jurčevi & Šamec	2024	Koprivnica, Croatia (urban area)	0.7	0.2	3.6	0.1
Lichtenthaler et al.	2023	Karlsruhe-Durlach, Germany	9.7	2.8	12.5	2.6
Boateng	2022	N.A.	1.2	0.3	1.5	0.2
Zhang et al.	2021	Nanjing, China (Baima Experimental Base)	2.5	0.9	3.3	0.7
Kim et al.	2021	Seoul, South Korea	1.2	0.3	1.5	0.2
Lichtenthaler & Babani	2021	Karlsruhe (KIT), Germany	6.14	2.1	8.3	1.8
Wu et al.	2020	Jiujiang, China	1.4	0.4	1.8	0.2
Li et al.	2020	Yangzhou, China	1.3	0.3	1.6	0.2
Kinoshita et al.	2020	Kyoto, Japan	6	3	9	3
Wang et al.	2019	Beijing, China	1.42	0.4	1.8	0.3
Zhao et al.	2019	Xuzhou, China (*ginkgo* nursery)	1.4	0.4	1.8	0.2

Li et al.	2018	Yangzhou University, China	1.3	0.3	1.6	0.2
Zhou et al.	2017	Nanjing, China	1.5	0.4	1.8	0.2
Ji et al.	2017	Xuzhou, China	1.2	0.4	1.6	0.2
Huang et al.	2017	France	1.4	0.4	1.8	0.3
Beck & Stengel	2016	Berlin, Germany	1.5	0.4	1.9	0.2
Liu et al.	2016	Jiangsu Province, China	1.5	0.4	1.8	0.2
You et al.	2016	Seoul, South Korea	1.3	0.4	1.7	0.2
Zheng et al.	2015	N.A.	1.35	0.5	1.8	0.3
Wang et al.	2014	Nanjing, China	7.9	3.2	11.2	83.5
Shi et al.	2012	Nanjing, China	8	3.2	11.2	1.6
Yang et al.	2012	Jiangdu, China	7.2	2.9	10.1	1.1
Yang et al.	2010	Jiangdu, China	9.2	3.3	12.5	1.5
Xu et al.	2011	Hubei Province, China	1.2	0.35	1.5	0.2
Pavlovič et al.	2009	Bratislava, Slovakia	1.28	0.4	1.7	0.2
Sarijeva et al.	2007	Karlsruhe, Germany	1.3	0.4	1.6	0.2
Fu	2007	Shenyang, China	1.2	0.4	1.6	0.2
Pandey et al.	2003	Palampur, India	1.49	0.7	2.2	N.A